

# Engineering Nanoreactors for Catalytic Cascades In-flow

***Citation for published version (APA):***

De Martino, M. T. (2021). *Engineering Nanoreactors for Catalytic Cascades In-flow*. [Phd Thesis 1 (Research TU/e / Graduation TU/e), Chemical Engineering and Chemistry]. Technische Universiteit Eindhoven.

***Document status and date:***

Published: 03/05/2021

***Document Version:***

Publisher's PDF, also known as Version of Record (includes final page, issue and volume numbers)

***Please check the document version of this publication:***

- A submitted manuscript is the version of the article upon submission and before peer-review. There can be important differences between the submitted version and the official published version of record. People interested in the research are advised to contact the author for the final version of the publication, or visit the DOI to the publisher's website.
- The final author version and the galley proof are versions of the publication after peer review.
- The final published version features the final layout of the paper including the volume, issue and page numbers.

[Link to publication](#)

***General rights***

Copyright and moral rights for the publications made accessible in the public portal are retained by the authors and/or other copyright owners and it is a condition of accessing publications that users recognise and abide by the legal requirements associated with these rights.

- Users may download and print one copy of any publication from the public portal for the purpose of private study or research.
- You may not further distribute the material or use it for any profit-making activity or commercial gain
- You may freely distribute the URL identifying the publication in the public portal.

If the publication is distributed under the terms of Article 25fa of the Dutch Copyright Act, indicated by the "Taverne" license above, please follow below link for the End User Agreement:

[www.tue.nl/taverne](http://www.tue.nl/taverne)

***Take down policy***

If you believe that this document breaches copyright please contact us at:

[openaccess@tue.nl](mailto:openaccess@tue.nl)

providing details and we will investigate your claim.



Engineering Nanoreactors  
for Catalytic Cascades  
In-flow

M.Teresa De Martino



# Engineering Nanoreactors for Catalytic Cascades In-flow

PROEFSCHRIFT

ter verkrijging van de graad van doctor aan de Technische Universiteit Eindhoven,  
op gezag van de rector magnificus prof.dr.ir. F.P.T. Baaijens,  
voor een commissie aangewezen door het College voor Promoties, in het  
openbaar te verdedigen op mandag 3 mei 2021 om 1:30 uur

door

Maria Teresa De Martino

geboren Teano, Italië

Dit proefschrift is goedgekeurd door de promotoren en de samenstelling van de promotiecommissie is als volgt:

voorzitter: prof.dr.ir. R.A.J. Janssen

1<sup>e</sup> promotor: prof.dr.ir. J.C.M. Hest

copromotor(en): dr. L.K.E.A. Abdelmohsen

leden: prof. dr. R.P. Sijbesma

prof. dr. I.W.C.E. Arends (Utrecht University)

prof. dr. R.J.M. Nolte (Radboud University)

prof. dr. ir. A.R.A. Palmans

prof. dr. V. Hessel (The University of Adelaide)

*Het onderzoek of ontwerp dat in dit proefschrift wordt beschreven is uitgevoerd in overeenstemming met de TU/e Gedragscode Wetenschapsbeoefening.*

## Summary

### Engineering Nanoreactors for Catalytic Cascades In-flow

Catalysis is of great importance for a large number of chemical and industrial processes. Scientists from various disciplines seek to develop new catalytic platforms in order to optimize chemical reactions. Heterogeneous catalysis is most of the time the preferred method, as catalysts deposited on a solid support display good stability and can be easily recovered. However, often the support materials hamper the catalytic activity due to mass transfer limitations. In this thesis, we have investigated the use of polymeric nanoreactors as an alternative platform that overcomes the diffusional issues. The nanoreactors were equipped with both metal- and bio-catalysts. To further demonstrate their versatility and application potential they were employed to execute cascade reactions and were used in a flow device without the need for intermediate work-up procedures. Furthermore, the applicability of such polymeric nanoreactors for the preparation of pharmaceutically relevant compounds was explored.

In Chapter 1 we reviewed and discussed the use of different classes of catalytic nanoreactors as a tool for greener chemistry production. We focused on the applications of nanoreactors and critically assessed their utility for various chemical reactions.

In Chapter 2 cross-linked polymersomes and micelles were employed as nanoreactors for copper-based catalytic processes. We evaluated both nanoreactors by selecting a benchmark reaction; namely, the cyclopropanation of styrene with ethyldiazoacetate. This way, we shed light on the relationship between nanoreactors' morphology and their ability to catalyze chemical reactions. We performed the reactions either in aqueous or in a biphasic systems (Pickering emulsion with toluene). While micelles yielded a more stable and active system in water, polymersomes offered better yields and stability in Pickering emulsions. Interestingly, the morphology affected the type of emulsion (o/w for micelles and w/o for polymersomes). In-flow, polymersomes could be more easily recycled, with less leaching of the copper catalyst.

In Chapter 3 the polymersome nanoreactors introduced in the former chapter were used in a continuous multi-step synthesis of Rufinamide; an important biologically active compound for the pharmaceutical industry. This process was fine-tuned in terms of operational conditions, recyclability, and workup. The separation was simplified and the yields were much improved when compared to previously reported methodologies.

In Chapters 4 and 5 biocatalytic nanoreactors based on bowl-shaped polymersomes (stomatocytes) were reported. In Chapter 4 a novel platform nanoreactor was developed, which was coined "*compartmentalized- cross-linked-enzymes nano-aggregates*" (*c-CLEnAs*). This platform offered a new strategy for enzyme immobilization. Due to the enzyme preorganization and concentration in the cavity of the stomatocytes, cross-linking could be performed with substantially lower amounts of cross-linking agents, which was highly beneficial for the residual enzyme activity. Our strategy is generally applicable, as demonstrated by using two different cross-linkers (glutaraldehyde and genipin). Single or multiple enzymes were cross-linked, which allowed cascade reactions to be performed in one pot.

In Chapter 5 the application of *c-CLEnAs* in two different pharmaceutical processes was investigated. Firstly, the two enzymes 7 $\alpha$  and 7 $\beta$  hydroxysteroid hydrogenase, which catalyze the transformation of chenodeoxycholic acid to

ursodeoxycholic acid (UDCA) were compartmentalized. Both enzymes are known to be very sensitive and prone to deactivation. Creating *c-CLEnAs* using genipin as crosslinker maintained their activity, allowing the successful execution of the UDCA one pot cascade synthesis. As a second case study, the immobilization of a neuraminic acid aldolase in *c-CLEnA* particles was presented for usage in a microfluidic system. The optimized *c-CLEnA* was used to produce neuraminic acid, and demonstrated higher activity compared to previous reports.

Summary and Outlook describes an overview of the main findings of this work reporting the results per each chapter and proposes another application of *c-CLEnAs*, namely to perform catalytic processes that drive motion. Some preliminary experiments concerning *c-CLEnA* as nanomotors were also reported.

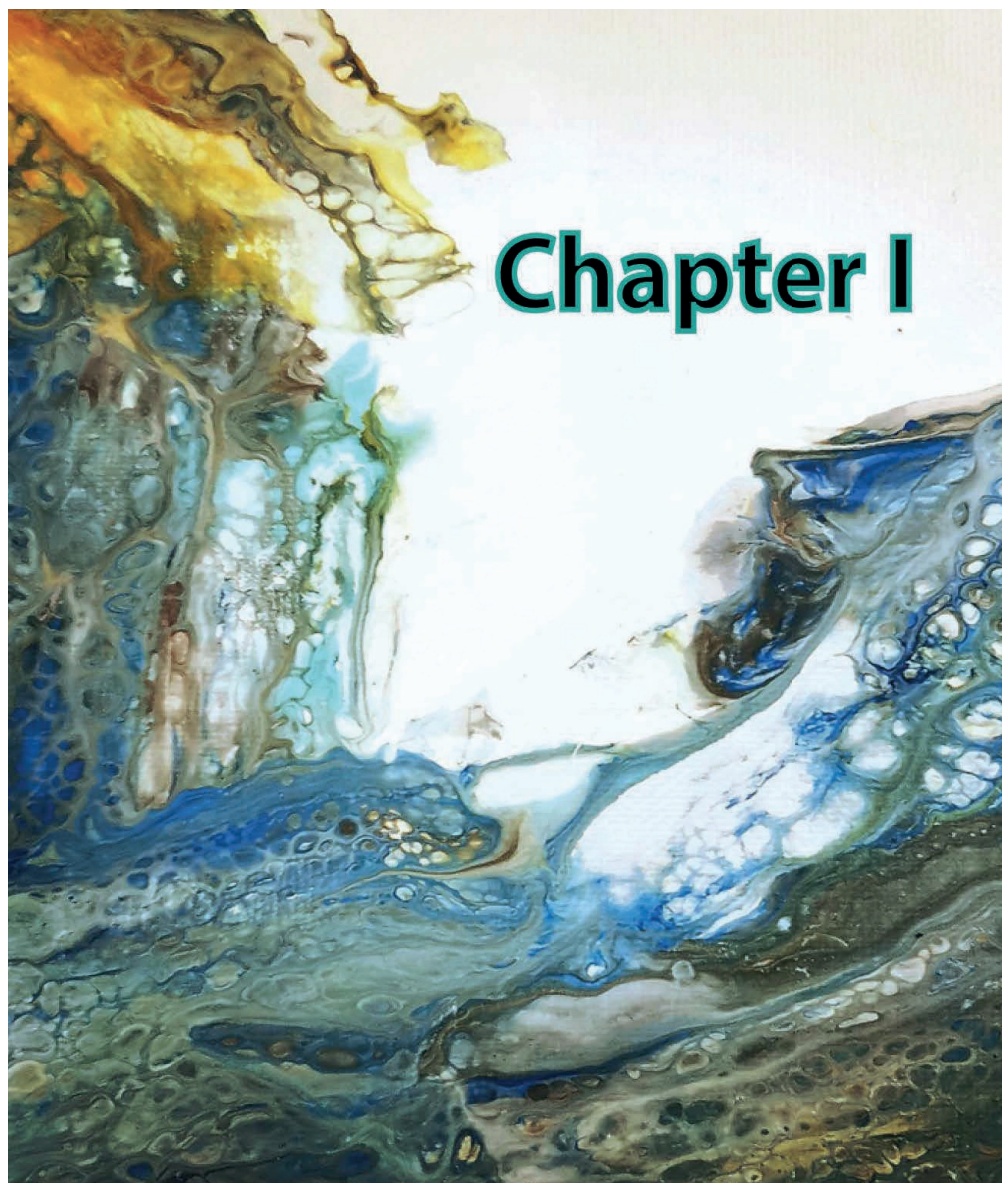
## Table of Contents

1. NANOREACTORS FOR GREEN CATALYSIS.....	6
1.1. INTRODUCTION .....	7
1.2. HOMOGENEOUS VS. HETEROGENEOUS CATALYSIS .....	9
1.3. SELF-ASSEMBLED NANOREACTORS.....	9
1.3.1. MICELLES.....	10
1.3.2. CATALYSIS IN MICELLES.....	11
1.3.3. POLYMERIC VESICLES.....	16
1.3.4. CATALYSIS IN POLYMERSOMES.....	16
1.4. COVALENT SYSTEMS.....	21
1.4.1. DENDRIMERS.....	21
1.4.2. CATALYSIS IN DENDRIMERS.....	22
1.4.3. NANOGELS.....	24
1.4.4. CATALYSIS IN NANOGELS.....	25
1.5. OUTLINE OF THE THESIS.....	26
REFERENCES.....	27
2. A COMPARATIVE STUDY OF ORGANOMETAL CATALYSIS IN MICELLAR AND VESICULAR COMPARTMENTS.....	32
2.1. INTRODUCTION .....	33
2.2. RESULTS AND DISCUSSION.....	35
2.3. CONCLUSIONS.....	32
2.4. EXPERIMENTAL SECTION.....	41
2.5. EXPERIMENTAL PROCEDURES.....	44
REFERENCES.....	45
2.6. SUPPLEMENTARY FIGURES AND TABLES.....	49
3. DESIGNED ONE-FLOW SYSTEM FOR THE SYNTHESIS OF RUFINAMIDE.....	56
3.1. INTRODUCTION.....	57
3.2. RESULTS AND DISCUSSION.....	59
3.3. CONCLUSIONS.....	69
3.4. EXPERIMENTAL SECTION.....	69
3.5. EXPERIMENTAL PROCEDURES.....	71
3.6. COSMO-RS.....	74
REFERENCES.....	74
3.7. SUPPORTING FIGURES AND TABLES.....	76
4. COMPARTMENTALIZED CROSS-LINKED ENZYME NANO-AGGREGATES (C-CLENA) FOR EFFICIENT IN-FLOW BIOCATALYSIS.....	78
4.1. INTRODUCTION.....	78
4.2. RESULTS AND DISCUSSION.....	79
4.3. CONCLUSIONS.....	87
4.4. EXPERIMENTAL SECTION.....	88
4.5. EXPERIMENTAL PROCEDURES.....	89



REFERENCES.....	95
4.6. SUPPLEMENTARY FIGURES AND TABLES.....	97
5. EXTENDING THE SCOPE OF C-CLENA: IN-FLOW ALDOL CONDENSATION TO NEU5Ac AND ONE- POT MULTI-STEP SYNTHESIS OF UDCA.....	104
5.1. INTRODUCTION.....	105
5.2. RESULTS AND DISCUSSION.....	107
5.3. CONCLUSIONS.....	113
5.4. EXPERIMENTAL SECTION.....	114
5.5. EXPERIMENTAL PROCEDURES.....	116
REFERENCES.....	118
5.6. SUPPLEMENTARY FIGURES AND TABLES.....	120
SUMMARY & CONCLUSIONS.....	126
OUTLOOK.....	130

A catalogue record is available from the Eindhoven University of Technology Library  
ISBN: 978-90-386-5271-9



# Chapter I

This Chapter is published as "Nanoreactors for Green Catalysis"

*Beilstein J. Org. Chem.* **2018**, *14*, 716–733. [doi:10.3762/bjoc.14.61](https://doi.org/10.3762/bjoc.14.61)

# Nanoreactors for Green Catalysis

## Abstract

Sustainable and environmentally benign production are key drivers for developments in the chemical industrial sector, as protecting our planet has become a significant element that should be considered for every industrial breakthrough or technological advancement. As a result, the concept of green chemistry has been recently defined to guide chemists towards minimizing any harmful outcome of chemical processes in either industry or research. Towards greener reactions, scientists have developed various approaches in order to decrease environmental risks while attaining chemical sustainability and elegance. Utilizing catalytic nanoreactors for greener reactions is a promising approach to reach these goals. This chapter describes the applications of some of the most used nanoreactors in catalysis, namely: (polymer) vesicles, micelles, dendrimers and nanogels. The ability and efficiency of catalytic nanoreactors to carry out organic reactions in water or their ability to be recycled will be discussed.

## 1.1. Introduction

It is widely acknowledged that “the best solvent is no solvent”; however, running a reaction under neat conditions is very challenging from the points of view of mass transfer and temperature gradients<sup>12</sup>. Therefore, sustainable chemical technologies are often related to the use of a green non-harmful solvent<sup>3</sup>, water. In principle, Green Chemistry refers to (1) the employment of raw material (substrates) in an efficient manner (2) decreasing the resulting waste or undesired by-products and (3) using cheap and environment friendly solvents (*i.e.* water). Generally, using water as a solvent is the choice for Green Chemistry<sup>4,5,6</sup>. Water is attractive from both economic and environmental points of view, and is not taken into account when the E-factor (defined as mass ratio of waste to desired product) for a chemical process is determined<sup>7,8</sup>. Unfortunately, most organic compounds and catalysts are not soluble in water, limiting its utility for most reactions<sup>9,10</sup>. For this reason, scientists across academia and industry have proposed many solutions in order to maximize the outcome of reactions (*i.e.* yields, enantioselectivities, etc.) in water. The abovementioned issues are particularly relevant in the field of asymmetric catalysis, which besides overcoming catalyst compatibility also has to deal with cost issues<sup>11,12</sup>. Research on asymmetric catalysis has been mainly focused on performing catalytic reactions with high enantioselectivity and efficiency<sup>13,14</sup>. As a result, a wide range of chiral catalysts have been established<sup>15,16</sup>. Chiral catalysts are, however, not only incompatible with aqueous solutions, but also expensive due to the structural complexity of the ligands used and the usage of transition metals. Finding an approach to utilize chiral catalysts in water while minimizing their cost (*i.e.* recycling) is still a big challenge. In order to accomplish this, various strategies have been proposed and applied<sup>17,18,19</sup>. One significant, well-established and widely used strategy, is the use of site-isolated techniques, *i.e.* creating a separate micro environment<sup>20,21,22</sup> for catalysts to (1) allow their use in incompatible media, (2) to reduce their costs by recycling them and (3) avoid any unfavorable environmental influences that might affect

reaction yield and output<sup>23,24</sup>. Indeed, such a strategy has proven to be advantageous for performing reactions in water and minimizing both reaction waste and cost<sup>25,26</sup>.

Attempts to support homogeneous metal complexes onto organic or inorganic surfaces to facilitate their removal/extraction from the reaction mixture has proven to be successful<sup>27,28</sup>. In fact, the utility of catalytic supports has been fundamental to the concept of entrapping catalysts in organic nanodomains and bringing the notion of catalytic nanoreactors to light<sup>29,30</sup>. In recent years the use of nanocontainers/reactors wherein catalysts are entrapped and physically separated in an isolated compartment has appeared to be a facile approach to enhance performance of reactions in water<sup>31,32, 33,34</sup>. Pioneering examples in this field include small molecule host-guest containers such as cavitands<sup>35,36,37</sup> and calixarenes<sup>38,39</sup>. Besides these supramolecular cage structures compartmentalization can also be achieved in macromolecular nanoreactors. The advantage of employing these polymeric structures is their improved robustness and loading capacity, which makes recycling and efficient usage of catalytic species more achievable. Nanocompartments such as polymersomes<sup>40</sup>, micelles<sup>41</sup>, dendrimers<sup>42</sup>, and nanogels<sup>43,44</sup> represent smart and compact devices to carry out reactions in aqueous media. Besides, their facile recyclability makes them very suitable as nanoreactors for a multitude of applications in synthetic chemistry<sup>24,31</sup>. In a recent study the E-factors for different traditional coupling reactions used in the pharmaceutical industry were reported and compared to those achieved in micellar nanoreactors<sup>45</sup>, showing for the latter a decrease of at least an order of magnitude, which underlines their considerable potential in green catalysis (Table 1).

**Table 1:** Representative comparison of E-Factors (including the aqueous workup), of a pharmaceutically relevant synthesis, carried out via a traditional and a micellar process<sup>45</sup>.

Reaction	E-factors	
	In traditional process	In Micelles
Heck Coupling (300g Scale)	136	7.6
Suzuki-Miyaura (302g Scale)	83	8.3
Sonogashira Coupling (57Kg Scale)	37.9	7.0

In this chapter we will describe the application of polymeric nanoreactors in green catalysis by highlighting their structure and ability to encapsulate and shield catalysts. Four different types of nanoreactors will be discussed, namely micelles, polymersomes, dendrimers and nanogels. The choice of discussing these nanoreactors stems from their accredited relevance in the field of catalysis and the significant number of examples published in literature. The advantageous aspects of these four classes of nanoreactors over non-supported homogeneous systems include:

(1) the site isolation of reactive components (enabling cascade reactions), (2) the ability to convert hydrophobic substrates in water (under green conditions), and (3) the facile catalyst recovery. Moreover, in this chapter we have not attempted to be comprehensive, but we rather want to show the application potential of these nanoreactors with some illustrative examples of the most relevant classes of organic reactions (performed in water).

## 1.2. Homogeneous vs. heterogeneous catalysis

Catalysis, in general, is divided into two major types, homogenous and heterogeneous. In homogeneous catalysis catalyst and substrates are both present and molecularly dissolved in the same phase (typically a liquid phase)<sup>46</sup>. Homogeneous catalysis involves the use of biocatalysts (enzymes), organocatalysts and metal catalysts<sup>47</sup>. Catalysis is defined as heterogeneous when catalysts are in an aggregated state, and are thus in a different phase than the reactants<sup>27,48</sup>. Heterogeneous catalysts typically consist of a solid carrier, the so called “support”, on which catalytic sites are dispersed<sup>49,50</sup>. Homogeneous catalysis is generally performed under milder operative conditions than heterogeneous catalysis<sup>51</sup>. In fact, heterogeneous catalysts generally possess very high decomposition temperatures (above 100 °C)<sup>52</sup>. The presence of a solid phase often results in the formation of temperature gradients when using high temperatures, which leads to an increase in reactant diffusion and a consequent hampering of mass transfer<sup>53</sup>. Furthermore, the catalytic sites in heterogeneous catalysis are often not as well-defined as in homogeneous catalysis. Therefore, homogeneous catalysis usually results in better selectivity and fewer by-products<sup>54</sup>.

Although homogenous catalysis ensures high selectivity and a better reaction outcome, yet it is expensive (catalyst recycling is not an option) and it requires the utility of harmful solvents, yielding high E-factors<sup>55</sup>. A strategy to overcome this problem is the inclusion and confinement of the homogeneous catalysts into a host nano-architecture<sup>56</sup>. Compartmentalization enables catalyst segregation and shielding, and ensures its facile removal from the reaction mixture after the reaction has taken place<sup>34</sup>. Moreover, shielding and segregation of catalysts in a nanoreactor facilitates one pot tandem reactions that, in most cases, require two or more incompatible catalysts<sup>57,22</sup>. Catalyst confinement leads to a high local concentration of the substrate at the active site, which results in higher reaction rates and better conversion<sup>9</sup>. In the next sections we will discuss some typical nanoreactors that are used to accommodate homogeneous catalysts, holding promise in green organic synthesis. A division will be made between self-assembled nanoreactors, section 1.3, and covalent systems, section 1.4.

## 1.3. Self-assembled nanoreactors

Self-assembled nanoreactors are macromolecular architectures that are non-covalently assembled from their constituent building units<sup>58,59</sup>. Such nanoreactors allow for physical confinement of catalysts, shielding them from their surroundings<sup>58,60</sup>. Compartmentalization of catalysts in supramolecular nanoreactors is advantageous from kinetic (faster catalytic process)<sup>61</sup> and thermodynamic (lower transition state of reaction)<sup>9</sup> points of view. Segregation and isolation of catalysts inside nanoreactors guarantee, in most cases, a valuable platform for catalyst recycling<sup>30,59,62</sup>.

### 1.3.1. Micelles

Micelles are supramolecular architectures that are assembled of amphiphilic molecules<sup>41</sup>. Above the critical micellar concentration (CMC), surfactants with the appropriately designed hydrophilic head (neutral, anionic or cationic) and hydrophobic chain organize themselves in micelles<sup>31</sup>. Micelles have been extensively studied<sup>32,9</sup> and their utility as nanoreactors is well-established<sup>60,41</sup>. Various micellar morphologies can be obtained depending on the 'packing parameter'<sup>61,62,63</sup>, which is defined as  $p = v/a_0 l_c$ , where  $v$  is the volume,  $l_c$  is the length of the hydrophobic chain and  $a_0$  is the area of the head groups<sup>64</sup>. As a general rule, if  $p \leq 1/3$  spherical micelles are obtained, while cylindrical micelles, or the so-called worm-like micelles, form when  $1/3 \leq p \leq 1/2$ . A typical micelle acquires a hydrophobic core that is able to accommodate hydrophobic catalysts, providing thermodynamic and kinetic control over chemical reactions<sup>31</sup>. Moreover, carrying out reactions in such a hydrophobic core leads to a concentration effect for hydrophobic substrates, which ensures higher reaction rates than those performed in bulk<sup>65</sup>. Besides, the structure of any micellar catalytic environment is governed by the arrangement of the amphiphilic molecules, creating, in many cases, a regioselective environment (Figure 1) that affects the outcome of some reactions<sup>29</sup>.

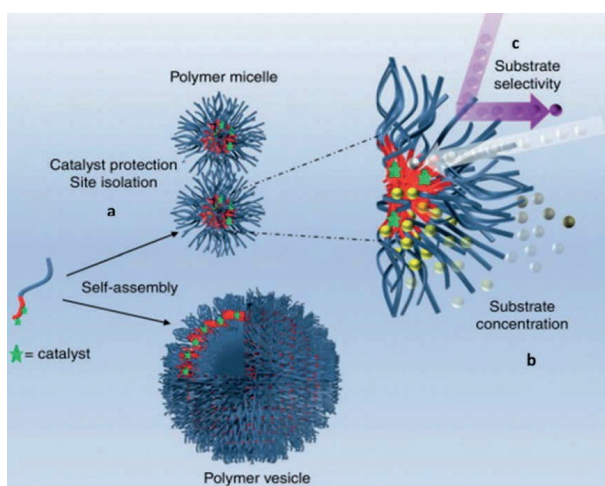


**Figure 1-** Assembly of catalyst-functionalized amphiphilic block copolymers into polymer micelles and vesicles. Characteristics of a nanoreactor system are shown for the polymer micelles, including **(a)** the catalysts are protected and isolated from each other by the micellar shell, **(b)** substrates are effectively sequestered by the core from the surrounding environment, creating a highly concentrated environment for confined catalysis, **(c)** the nanostructure shell may regulate the access of substrates to the catalyst-containing micelle core. Reprinted with permission from reference 29.

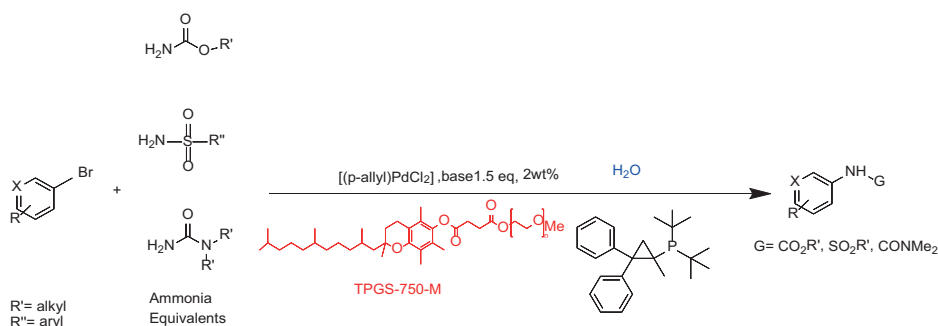
Non-spherical, high aspect ratio micelles are preferred for catalysis as such structures provide large surface areas where reactions could take place<sup>66</sup>. Indeed, this has proven to be beneficial for some reactions<sup>66</sup> such as dehydration

reactions<sup>24</sup> in which case the high surface to volume ratio, in combination with the hydrophobic effect, led to an accelerated product formation, as water can diffuse quickly away from the reaction center<sup>40</sup>.

### 1.3.2. Catalysis in micelles

Micelles as nanoreactors have been extensively used in organic synthesis<sup>31</sup>, allowing reactions in water<sup>67</sup> with better yields and easier catalyst recovery<sup>26</sup> than traditional processes.

Lipshutz et al. have successfully exploited micelles not only as nanoreactors, but as an outstanding platform for achieving greener organic reactions<sup>26,67,68</sup>. They have shown, for example, C-N cross-coupling reactions between heteroaryl bromides, chlorides or iodides and carbamate, sulfonamide or urea derivatives to be successfully realized in water using palladium-loaded TPGS-750-M (dl- $\alpha$ -tocopherol methoxypolyethylene glycol succinate) micelles (Scheme 1). Moreover, this micellar catalytic system allowed for catalyst recycling, minimizing the amount of the used organic solvent and generated waste<sup>69</sup>.

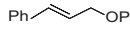
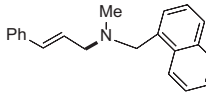
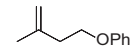
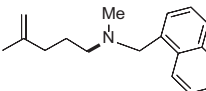
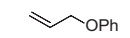
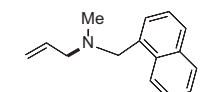
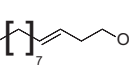
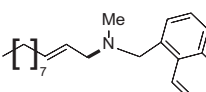
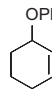
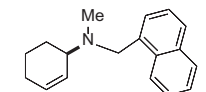


**Scheme 1:** C-N bond formation under micellar catalyst conditions, no organic solvent involved. Adapted from reference <sup>69</sup>.

The same group reported another interesting catalytic micelle system, which is based on PTS (polyoxyethanyl  $\alpha$ -tocopheryl sebacate)<sup>70</sup>. Using PTS-based micelles, they showed the amination of allylic ethers in water (Table 2). The reaction of different ethers with naphthylmethylamine resulted in excellent yields. Comparable yields were obtained when different amines reacted with *trans*-cinnamyl phenyl ether (data not reported here). In both of the cases micelles were used to protect the very sensitive and unstable  $[\text{Pd}(\text{allyl})\text{Cl}]_2$  intermediate from air.

**Table 2:** Reactions of allylic ethers (**1a-1e**) with naphthylmethylamine<sup>a</sup>.

Run	Ether	Time (min)	Product	Yield(%)
-----	-------	------------	---------	----------

1	 <b>1a</b>	20		98
2	 <b>1b</b>	60		81
3	 <b>1c</b>	5		91
4	 <b>1d</b>	190	 E:Z → 25:1	90
5	 <b>1e</b>	300		80

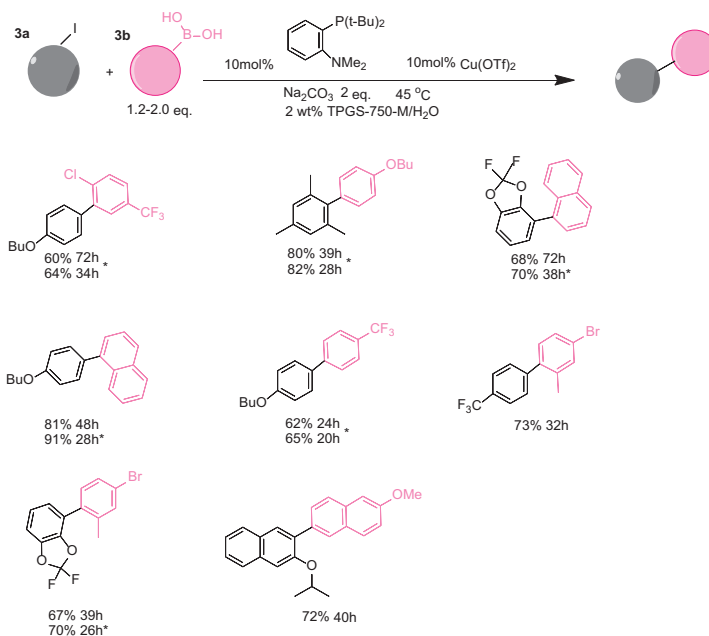
<sup>a</sup>Reactions were carried out under air at RT in 2wt% PTS-water in the presence of [Pd(allyl)Cl]<sub>2</sub> (0.5 mol%), bis[[2-diphenylphosphino)phenyl] ether (DPEphos) (1 mol%), ether (1 eq.), naphthylmethylamine (1.5 eq.), K<sub>2</sub>CO<sub>3</sub> (1.5 eq.) and HCO<sub>2</sub>Me (4 eq.). Adapted from reference <sup>70</sup>.

Micelles were also used to perform cross-coupling reactions between benzylic and aryl halides in water<sup>67</sup>. This reaction is known to result in very limited yields due to the undesired homo-coupling reaction between electron-rich and electron poor benzyl bromides<sup>71</sup>. This draw-back has been circumvented by using Pd-catalytic micelles, which were assembled in water using TMEDA (tetramethyl ethylene diamine) as additive. TMEDA was used to stabilize the Pd catalyst by chelation and indeed, presence of TMEDA resulted in higher yields.<sup>67</sup> High catalytic efficiency of these Pd-catalytic micelles was also achieved while catalyzing reactions involving less reactive or sterically hindered species.

Handa *et al.* described a self-assembled TPGS-750M micelle (shown in Scheme 1), that allowed for copper catalyzed Suzuki-Miyaura coupling of aryl iodides (Scheme 2)<sup>72</sup>. When the reaction was conducted in inert atmosphere, no product was formed. However, the reaction was performed successfully in presence of air, suggesting that the actual mechanistic pathway involved the formation of a P-(O)-N- species on the ligand. The presence of traces of Pd was also beneficial in this process, as 200 ppm of Pd(OAc)<sub>2</sub> worked like a co-catalyst improving the reaction rate and the yields. Furthermore, the recyclability of the catalyst was improved and the experiments could be repeated up to 5 runs with yields >90%. Contrary to the results obtained in bulk, the usage of micelles resulted in higher yields even after catalyst recycling, providing a promising catalytic platform for these coupling reactions<sup>72</sup>.



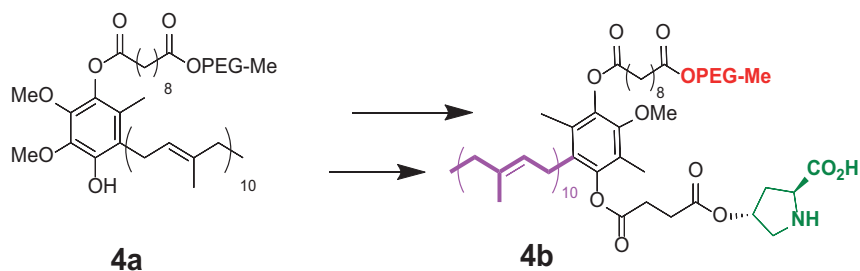
**Scheme 2:** Suzuki–Miyaura couplings with, or without, ppm Pd.<sup>a</sup>



<sup>a</sup>Conditions: ArI 0.5 mmol (**3a**), Ar'B(OH)<sub>2</sub> (0.75-1.00 mmol, 1.5-2.0 eq.) (**3b**), \*with 200 ppm of Pd(OAc)<sub>2</sub>. Adapted from reference <sup>72</sup>.

Lee *et al.* described an approach to perform catalysis in micelles based on rod-coil block copolymers<sup>73</sup>. Micelles were assembled from hydrophilic poly(ethylene oxide) (PEO) and hexa-*p*-phenylene, providing a platform for Suzuki reactions with the hydrophobic core acting as a suitable pocket for apolar aromatic guests<sup>73,74</sup>. With such a platform, full conversion was achieved at room temperature in water. Almost quantitative yields were observed when aryl chloride coupling was performed with aryl boronic acids. This is indeed remarkable as aryl chlorides are generally not as reactive as aryl bromides or aryl iodides.

Lipshutz and Ghorai developed a micellar system called PQS to perform aldol reactions in water<sup>26</sup>. As depicted in Figure 2, PQS has an OH-moiety (**4a**) which allows for its linkage to the organo catalyst proline (**4b**). Also, PQS has a lipophilic component that acts as a reaction solvent for hydrophobic dienes. The latter feature allows aldol reactions to take place efficiently in water.

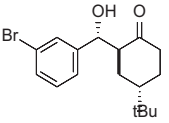
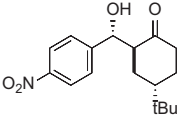
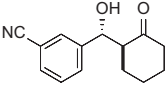
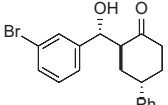
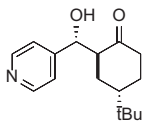
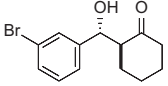
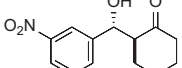


**Figure 2:** PQS (**4a**), PQS attached proline catalyst (**4b**). Adapted from reference 26.

The aldol reaction between cyclohexanone and *p*-nitrobenzaldehyde was chosen to verify the performance of this nanoreactor. PQS-proline and the analogous mixed diester derivative of 4-hydroxyproline were prepared and tested in this process. The aldol product was achievable only by using the proline compound **4b**, therefore different substrates were subsequently tested using 10 mol% of this catalyst in water at room temperature. The achievement of this study was not only on the stereoselectivity of the catalysts, but also on the substrate selectivity (Table 3): the preferred substrates are water-insoluble, suggesting that the reaction occurs in the lipophilic pocket and not in water. The authors also demonstrated the ability of the PQS system to be recycled up to 10 times without loss in its catalytic activity.

**Table 3:** Representative PQS-proline (**4b**)-catalyzed reactions<sup>a</sup>:

Entry	Product	Time (h)	Yield <sup>b</sup> (%)	anti:syn <sup>c</sup>	ee <sup>d</sup> (%)
1		30	88	82:18	90
2		18	90	90:10	90
3		48	74	86:14	92

4		36	80	83:17	91
5		18	85	85:15	79
6		30	80	90:10	97
7		36	82	68:32	86
8		18	85	89:11	75
9		36	82	84:16	86
10		24	90	90:10	91

<sup>a</sup>The reactions were performed with aldehyde (0.01 mmol), ketone (0.5 mmol), and catalyst **4b** (0.01 mmol) at RT. <sup>b</sup>Combined yield of isolated diastereomers. <sup>c</sup>Determined by <sup>1</sup>H NMR of the crude product. <sup>d</sup>Determined by chiral-phase HPLC analysis for *anti*-products. Adapted from reference 26.

Catalytic micelles were also prepared by O'Reilly *et al.* by self-assembly of a novel amphiphilic Sulfur-Carbon-Sulfur (SCS) pincer Pd catalyst together with a PAA (poly(acrylic acid)) based polymer in water<sup>32</sup>. The catalytic activity of the nanostructures was compared to the results achieved with the small molecule analogues of the pincer Pd complex, in a Suzuki-Miyaura coupling. When the reaction of vinyl epoxide with phenyl boronic acid was realized with 2% of pincer catalyst, the rate was 100 times higher for the water-based micellar system compared to the same reaction in organic solvent with the unsupported Pd-complex. A 100 times lower amount of catalyst was also loaded (0.02%), and still the reaction rate achieved was higher than the ones in organic media. This remarkable kinetic effect was attributed to two factors: 1) the small particle radius which increased the nanoreactor's surface area and 2) the

creation of a more hydrophobic local pocket, as the catalyst was facing directly the hydrophobic membrane. Furthermore, the nanosystem also facilitated catalyst recycling by regular extraction.

### 1.3.3. Polymeric vesicles

Polymeric vesicles or polymersomes are synthetic bilayered hollow architectures that are self-assembled from amphiphilic block copolymers<sup>75</sup>. The synthetic nature of polymersomes allows for facile tuning of their properties such as size<sup>76</sup>, membrane permeability<sup>77</sup> and stability<sup>78</sup>. Various copolymers have been reported for polymersome formation such as poly (ethylene glycol)-*b*-polystyrene (PEG-*b*-PS)<sup>79</sup>, polystyrene-*b*-polyisocyanopeptide (PS-*b*-PIAT)<sup>21,22</sup>, and poly(N-isopropylacrylamide) –*b*-poly(ethylene oxide) (PNIPAM-*b*-PEO)<sup>80</sup>. The term “polymersomes” is derived from liposomes because of the structural resemblance. Compared to liposomes, polymersomes are mechanically robust vesicles and therefore considered to be highly attractive for nanoreactor applications<sup>40,24</sup>. Polymersomes comprise an aqueous lumen and hydrophobic membrane. Such hydrophilic and hydrophobic compartments are capable of accommodating hydrophilic (e.g. enzymes) or hydrophobic catalysts (e.g. metal catalysts) in their lumen or bilayer, respectively<sup>81,28</sup>. In aqueous environment the hydrophobic membrane attracts hydrophobic substrates and brings them in proximity to the membrane-bound catalyst, leading to faster reaction rates. The presence of multicompartment in one system is interesting from a catalysis point of view as multi-step cascades using incompatible catalysts can be achieved in one polymersome nanoreactor<sup>22</sup>. The compositional versatility of polymersomes thus allows for several applications in catalysis by encapsulating in or tethering catalysts to their compartments<sup>82,33</sup>. Polymersomes preserve and protect catalysts in their compartments improving, most of the time, catalytic activity and their performance in incompatible solvents such as water<sup>21,24</sup>.

### 1.3.4. Catalysis in polymersomes

Polymersomes have been most often used as biocatalytic nanoreactors<sup>22,84</sup>, and have in this respect also been employed in Pickering emulsions<sup>83</sup>. Pickering emulsions are emulsions stabilized by colloidal particles that adsorb at the water-oil interface. They are more stable than classical emulsions and do not require the usage of small molecule surfactants. This is a big advantage in downstream processing and product and catalyst recovery. The enzyme *Candida Antarctica* lipase B (CalB) was encapsulated in the lumen of the polymersomes or in the Pickering emulsion water droplet. The esterification reaction of 1-hexanol and hexanoic acid was used to evaluate the catalytic performance of the CalB-loaded Pickering emulsions. Higher enzymatic activity was observed when CalB was encapsulated and the best results were achieved when the enzyme was in the lumen (Figure 3b), highlighting the advantage of enzyme compartmentalization and shielding. The explanation for this improved performance is the enlarged contact area between (hydrophobic) substrate and (water soluble) enzyme. Moreover, the system was recycled for at least 9 times without any loss in enzymatic activity.

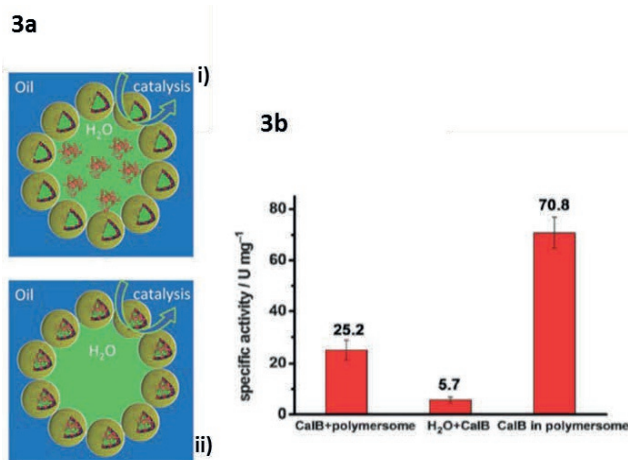
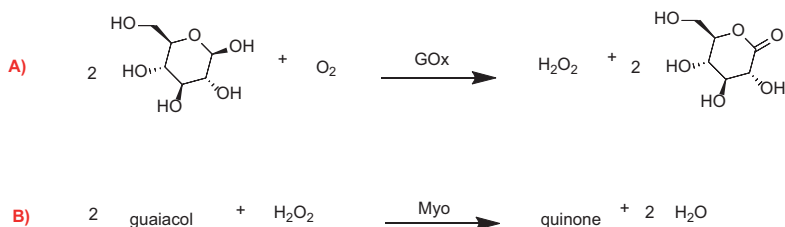


**Figure 3.** **3a**) Schematic representation of a Pickering emulsion with the enzyme in the water phase (**i**), or with the enzyme inside the polymersome lumen (**ii**). **3b**) Chart of the specific activities of CalB dissolved in the water phase of the polymersome Pickering emulsion (left), CalB in a biphasic water/ toluene system (middle,) and CalB encapsulated in the lumen of the polymersome Pickering emulsion (right). Adapted with permission from <sup>81</sup>.

Polymersomes have proven to be very useful for the performance of multistep catalytic conversions, in particular with enzymes<sup>83,88</sup>. Voit *et al.* studied the use of cross-linked pH sensitive polymersomes for the conversion of glucose in a tandem reaction<sup>84</sup>. The hydrophilic block of their polymersomes was PEG, and the hydrophobic block contained both poly(diethyl aminoethyl methacrylate) (PDEAEM) which is pH responsive, and poly(3,4-dimethyl maleic imido butyl methacrylate) (PDMIBM) as cross-linker. The activity of glucose oxidase (GOx) to convert glucose into D-glucono- $\delta$ -lactone and hydrogen peroxide was the first step of the reaction (Scheme 3A); subsequently, myoglobin (Myo) employed the hydrogen peroxide produced to oxidize guaiacol to quinone and water (Scheme 3B).

**Scheme 3:** Cascade reaction with GOx and Myo. Adapted from reference <sup>84</sup>.



When the pH was below 7, the permeability of the cross-linked membrane allowed for substrate/product diffusion, but at basic pH the membrane collapsed and prevented any transport of small molecules. Two different activity tests

were performed: 1) GOx and Myo were both entrapped inside the polymersome lumen; 2) GOx and Myo were individually incorporated into the polymersomes and mixed together in solution; in both of the cases the final product formation was monitored by UV-vis spectroscopy. The control over the pH allowed the regulation of the enzymatic cascade (no product was observed at pH 8 in both of the reactive systems), as the diffusion through the membrane was not possible. Moreover, the crosslinking enabled stabilization of the enzymes, which remained active also after 10 days.

Polymersome nanoreactors have also been used to perform many types of non-enzymatic catalytic reactions, such as the proline-catalyzed asymmetric aldol reaction of cyclohexanone and 4-nitrobenzaldehyde<sup>85</sup>. Cross-linked polymersome nanoreactors were also used to perform asymmetric cyclopropanation reactions in water<sup>15</sup>. These products are highly desired intermediates in the preparation of agrochemicals and pharmaceuticals<sup>86,87,88</sup>. To perform cyclopropanation reactions in polymersomes, the membrane was cross-linked with bisoxazoline (BOX) ligands complexing the copper catalyst. Cyclopropanation reactions were efficiently performed in water, resulting in high yields and enantioselectivities, comparable to those when the reaction was carried out in organic solvent<sup>82</sup> (Figure 4).

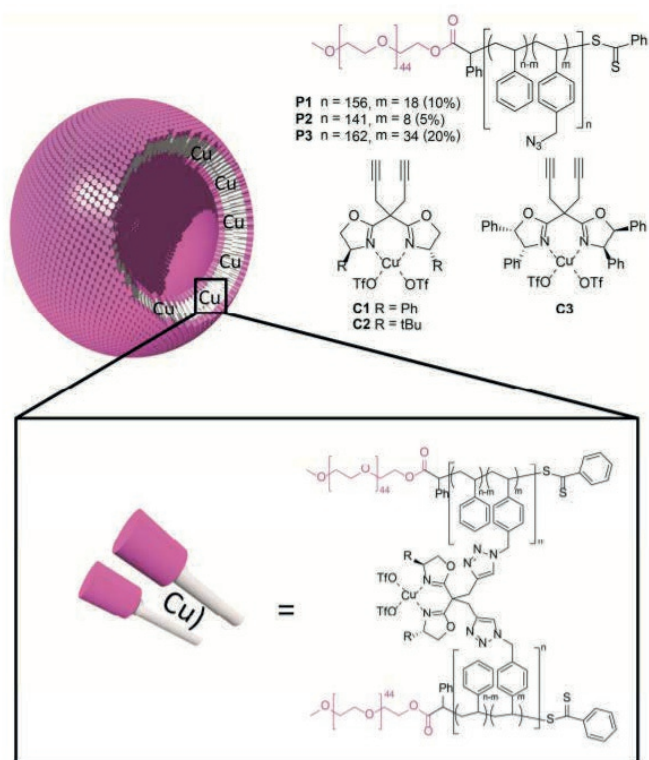
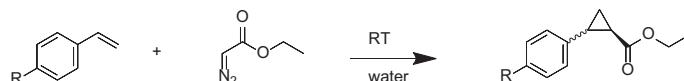


**Figure 4:** Cross-linked polymersomes with  $\text{Cu}(\text{OTf})_2$  catalyst. Reprinted with permission from 15.

As depicted in Table 4, substrate selectivity was observed when catalytic polymersomes were used, reasonably ascribed to a concentration effect, with more hydrophobic substrates leading to an increased local concentration around the catalyst in the hydrophobic membrane and as a consequence a higher reaction rate.

**Table 4:** Asymmetric cyclopropanation reaction of styrene derivatives and ethyl diazoacetate<sup>a</sup>.



Entry	R	Time (min)	Load <sup>b</sup> (%)	Catalyst	Conversion <sup>c,d</sup> (%)	Trans/Cis <sup>d</sup>	ee trans <sup>e</sup> (%)
1	H	120	10	C1	50 <sup>f</sup>	73/27	60
2	H	10	10	C1	54	74/26	60
3	H	10	2	C1	12	72/28	60
4	H	10	0	-	0	-	-
5	H	10	10	C3	39	68/32	84
6	H	10	10	C2	43	59/41	34 <sup>g</sup>
7	OMe	10	10	C2	93 <sup>i</sup>	68/32	59 <sup>h</sup>
8	Cl	10	10	C2	32 <sup>i</sup>	75/25	53 <sup>h</sup>
9	tBu	10	10	C2	67 <sup>i</sup>	67/33	71

<sup>a</sup>Reactions carried out in 3.0 mL of MilliQ water with 5.0 eq of styrene and 1.0 eq. of ethyl diazoacetate. <sup>b</sup>Catalyst loading in mol%. <sup>c</sup>Conversion of ethyl diazoacetate into cyclopropane product. <sup>d</sup>Determined by <sup>1</sup>H-NMR using triethylene glycol dimethyl ether as an internal standard. <sup>e</sup>Determined by chiral GC. <sup>f</sup>Polymersomes started to precipitate after 15min. <sup>g</sup>Configuration of the product was (1*S*,2*S*). <sup>h</sup>Determined by chiral HPLC. <sup>i</sup>Isolated yields. Adapted from reference 15.

Sergey *et al.* reported on the design of a porous polymeric nanoreactor with a lipid bilayer for coupling reactions<sup>89</sup>. These nanocapsules were loaded with palladium catalysts and successfully used in Suzuki, Sonogashira and Heck cross-coupling reactions. Catalytic activity was compared to the activity of the freshly prepared free catalyst, and the palladium entrapment did not affect either the conversion or the yields of the reaction<sup>28</sup>. The catalyst immobilization also allowed facile Pd removal from the final product and catalyst recycling.

Polymeric nanoreactors were also used to perform ring opening polymerization (ROP) in water. Nallani *et al.* reported on the enzymatic polymerization of lactones using CalB, which was immobilized in both the polymersome

lumen and bi-layer<sup>21</sup>. Nanoreactors for ROP were prepared from polystyrene-polyisocyanopeptide (PS-PIAT) (figure 5).

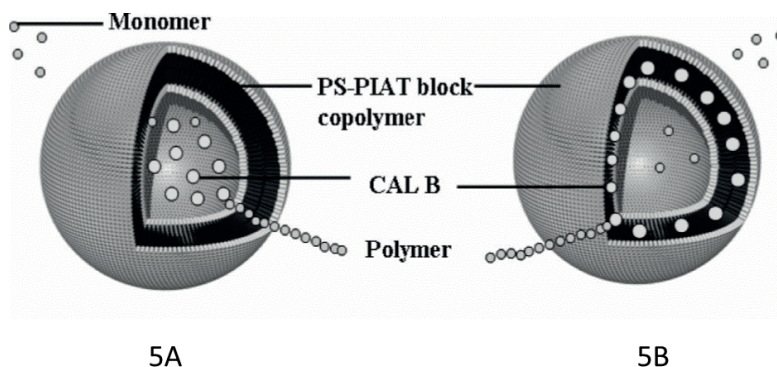


**Figure 5:** Schematic representation of enzymatic polymerization in polymersomes. (5A) CalB in the aqueous compartment (5B) CalB embedded in the bilayer. Reprinted with permission from 21.

ROP of lactones is usually performed in organic solvents so that hydrolysis reactions can be avoided<sup>17</sup>. However, when nanoreactors were used, polymerization proceeded efficiently in water and without formation of any undesired products, providing a platform for aqueous ROP<sup>21</sup>.

As shown in this section, polymersomes have been applied as a platform towards greener reactions<sup>22,90</sup>, either by allowing reactions to be performed in water<sup>85,21</sup> or by providing a recyclable catalytic system<sup>82</sup>. As they contain both hydrophobic and aqueous compartments, they are especially useful for the immobilization of different catalysts, such as organocatalysts and enzymes that require different microenvironments for their optimal performance.

## 1.4. Covalent systems

### 1.4.1. Dendrimers

Dendrimers are a class of highly branched molecules with high degree of symmetry<sup>91</sup>. They consist of different generations in which every generation is twice the molecular weight of the previous one. Dendritic architectures comprise three regions: a core, inner shell and outer shell<sup>92</sup>. The properties of dendrimers such as hydrophobicity can be tuned by varying their initial molecular components or the number of generations they possess<sup>93,94</sup>. They can assemble in a spherical shape, and within the three dimensional structure, an interior void is present wherein to accommodate other molecules<sup>95</sup>.

### 1.4.2. Catalysis in Dendrimers

The controlled synthesis of dendrimers and their applications as nanoreactors and catalyst carriers have been extensively studied over the last decades<sup>96,97,98</sup>. Fan and coworkers incorporated a bis(oxazoline)-copper (II) complex



in the hydrophobic core of a polyether dendrimer<sup>11</sup>. The copper catalytic complex was used to carry out asymmetric Mukaiyama aldol reactions. Although this system did not result in any substantial improvements in yields or enantioselectivities, it allowed for facile catalyst recovery and recycling.

Dendrimers were also used to encapsulate bimetallic catalysts to attain highly selective reactions<sup>97,99</sup>. The first successful attempt was reported by Chung and Rhee, in which they showed the encapsulation of a bimetallic Pt-Pd catalyst in a highly branched PMAM-OH dendrimer corona<sup>95</sup>. These catalytic dendrimers were employed in partial hydrogenation of 1,3-cyclooctadiene into cyclooctene. The utility of these dendrimers in hydrogenation reactions resulted in efficient reactions that proceeded with unprecedented selectivity of 99%. Moreover, this system is one of the first of bimetallic catalytic systems to be used for hydrogenation reactions in water.

Water soluble dendrimer-stabilized nanoparticles (DSN) have been shown to be highly efficient in the catalysis of olefin hydrogenation and in Suzuki coupling reactions<sup>100,101</sup>. Ornelas *et al.* cloaked a palladium catalytic nanoparticle with dendrimers containing triazole groups (Figure 6)<sup>102</sup>.

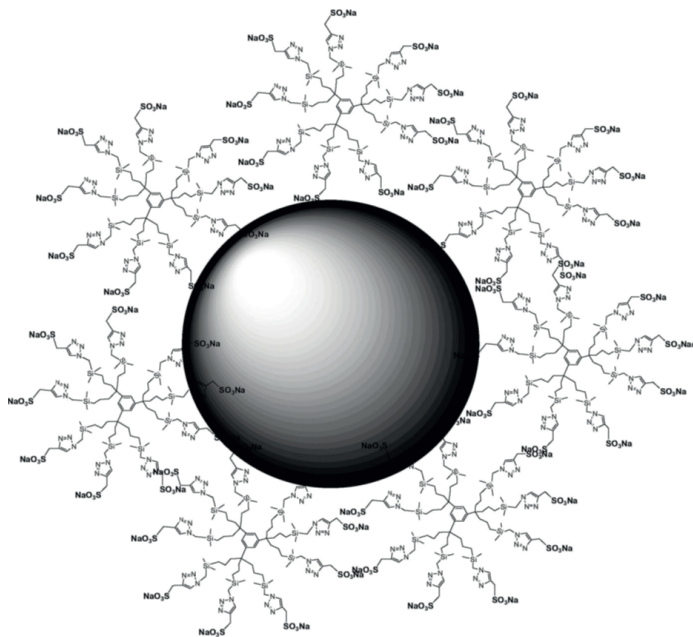


**Figure 6:** Representation of DSN-G0. Reprinted with permission from<sup>102</sup>.

The aim here was to provide a platform to perform hydrogenation in water. By using only 0.01% of palladium at room temperature, the hydrogenation of allyl alcohol was realized<sup>103</sup>. DSNs were recycled for up to 10 times without

loss in activity. DSN nanoreactors were later shown to be utilized for catalysing Suzuki coupling reactions between  $\text{PhB(OH)}_2$  and  $\text{PhX}$  ( $X = \text{I}$  or  $\text{Br}$ ) in water<sup>102</sup>.

Other examples of water-soluble dendrimers are peptide- and glycol-based dendrimers<sup>104,105</sup>. As a result of their compositional versatility, they have been reported in many applications for biomedical engineering (e.g. glycopeptide dendrimers for drug delivery<sup>106</sup>).

The ability of peptide dendrimers to perform catalysis in an aqueous environment has also been investigated<sup>107</sup>. Many different libraries of peptide dendrimers have been used for biocatalytic applications, such as hydrolysis and aldolase reactions<sup>107,108,109,110</sup>, showing their potential in green catalysis. Reymond *et al.* synthesized a series of peptide dendrimers including aspartate, histidine and serine as catalytic esterase triad, and the activity was successfully demonstrated using fluorogenic 8-acyloxyppyrene-1,3,6-trisulfonates as substrate (Figure 7) at the pH optimum of 5.5<sup>109</sup>.

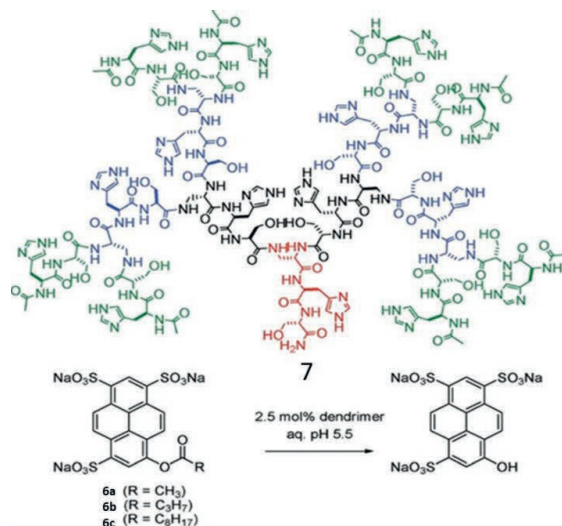


**Figure 7-** The multivalent esterase dendrimer (7) catalyzes the hydrolysis of 8-acyloxyppyrene 1,3,6-trisulfonates 6a–c. Reprinted with permission from<sup>107</sup>.

A noticeable rate enhancement was observed, related to a large apparent reactivity increase per catalytic site. This can be explained by different factors: 1) the more effective binding of the hydrophobic acyl group; 2) the double role of the histidine side chains, acting as both catalytic groups in their base form and as electrostatic substrate binding sites in their acidic form.

### 1.4.3. Nanogels

Nanogels are composed of hydrophilic homopolymer or copolymer networks which can swell in the presence of water<sup>111</sup>. Chemical cross-links or physical junctions (e.g. secondary forces, crystallite formation, chain

entanglements) provide the nanogels' unique swelling behavior and three-dimensional structure<sup>43,112</sup>. They have been a topic of extensive research in the past decades and their properties as for example their high water content and the possible control over the swelling kinetics make them very attractive for biomedical applications<sup>113</sup>. Nanogels show promise as nanoreactors as they not only display the convenience of easy dispersion in water but also can be obtained with a large variety of compositions. They can also be used as templates for metal nanoparticles: the size and morphology of the resulting metal nanoparticles depend on the nanogel template<sup>56,114</sup>. For example, metal nanoparticle cores can be covered by polymeric brushes, the length and the grafting are important factors which can affect the reaction, as discussed in the following paragraph, and the easy manufacturing of metal nanoparticles makes the preparation of these core-brushes nano systems suitable for many applications<sup>115,116,117</sup>.

#### 1.4.4. Catalysis in Nanogels

Nanogels have intrinsic properties that make them well suited for green chemistry<sup>118,119</sup>. Water-compatible gels are usually based on poly(*N*-isopropylacrylamide) (PNIPAM), poly(*N*-vinylcaprolactam) (PVCL) or other water-soluble polymers<sup>111</sup>. For instance, PNIPAM is a thermo-responsive polymer, which has an LCST of 32 °C. Above the LCST, individual polymer chains switch from a swollen coil configuration to a collapsed globular one, providing a nano environment that is suitable for either hydrophobic or hydrophilic substrates<sup>114</sup>. Water forces PNIPAM brushes to become hydrophobic, acting as a suitable environment for most organic reactions<sup>120</sup>; it allows hydrophobic substrates to diffuse towards the encapsulated catalysts, leading to a concentration effect that directly contributes to an efficient aqueous reaction<sup>121</sup>.

The preparation of catalytic nano-composite hydrogels has been widely reviewed<sup>56,116</sup>. Several examples showing their utility as nanoreactors for various reactions such as coupling, oxidation and reduction reactions have been reported<sup>43,116,120</sup>. Wei *et al.* described a nanogel composed of poly (*N*-isopropylacrylamide) brushes grafted on Pd-NPs (Pd@PNIPAM) to carry out coupling reactions in water under mild conditions<sup>122</sup>. They showed highly efficient coupling of several hydrophobic aryl halides with phenylboronic acid, which in all cases resulted in yields above 70%. Moreover, the Pd@PNIPAM nanoreactors could be easily recycled thanks to the reversible phase-transition of the polymeric brushes<sup>114</sup>.

Que *et al.* reported the synthesis of gold nanoparticles (Au NPs) sheltered in PEG-PS nanogels for the reduction of 4-nitrophenol (4NP)<sup>123</sup>. Thiol-functionalized PEG blocks were immobilized on Au NPs. PS segments improved the stability of the system and provided the necessary hydrophobic environment that is required to undertake the reduction reaction in water. The outcome of using Au@PEG-PS as nanoreactors was compared to those resulting from using both uncoated and PEG-coated Au-NPs. While Au@PEG-PS resulted in quantitative conversions for 5 subsequent cycles, both uncoated and PEG<sub>45</sub> coated Au-NPs resulted in full and 61 % conversions only for the first cycle, respectively. Recycling of uncoated and PEG<sub>45</sub> coated Au-NPs was not possible, highlighting the significance of the nanoreactor design (figure 8).

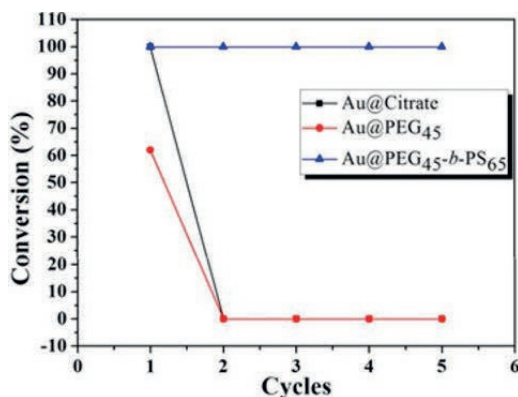


**Figure 8:** Conversion of 4-NP in five successive cycles of reduction, catalyzed by Au@citrate, Au@PEG and Au@PEG<sub>45</sub>-*b*-PS<sub>65</sub>."Reprinted with permission from 121. Copyright (2015) American Chemical Society.

Au@PEG-*b*-PS showed excellent catalytic activity in the reduction reaction of 4-nitrophenol into 4-aminophenol, and the catalytic activity increased with the decrease in the chain length of the PS block. In addition, the high stability imparted by the PS layer endowed Au@PEG-*b*-PS with good reusability in catalysis without the loss of catalytic activity, and prevented from electrolyte-induced aggregation, making the system very attractive as nanoreactor. Following on the previous work, He *et al.* synthesized cross-linked nanogels that were based on poly(acrylamide-co-acryl acid) (poly(AAm-co-AAc))<sup>119</sup>. These nanogels were transformed into their catalytic counter parts by growing silver nanoparticles (Ag NPs) inside the cross-linked polymeric network. These catalytic nanogels were also used to catalyse the reduction of 4-nitrophenol to 4-aminophenol in water. The activity of these nanoreactors was tuned by varying the Ag NPs loading and the cross-linking density; higher activities were achieved by increasing the amount of Ag NPs loaded and decreasing the degree of polymer cross-linking. Such conditions facilitated the diffusion of water and substrates through the hydrogels and increased the probability of the reactant to be in contact with the catalyst (Ag NPs).

### 1.5. Outline of the thesis

In this chapter, we have discussed the utility of supramolecular polymersomes, micelles, dendrimers and nanogels in catalysis. Over the past decades, many groups have demonstrated the specific features which make these nanoreactors an advantageous choice for chemical synthesis, we only focused on few classes of polymeric nanoreactors but there are many others interesting type, for example single-chain polymeric nanoparticle (SCPN) which were not discussed in the chapter but are well established platforms for the compartmentalization of metal catalysts which also have a great ability to be recycled. Nanoreactors combine a high active surface area with good dispersion in

solution and therefore are ideal structures for facile diffusion of reactants. Furthermore, the compartments protect the catalyst from undesired interactions with the environment, which can be either the solvent, specifically water, or other catalytic species. As a result, they allow reactions to proceed in water and often at room temperature, with excellent yields and selectivities, which traditionally can only be achieved by performing catalysed reactions in organic media. Moreover, although they are homogeneously dispersed in the solvent, the nanoreactors are still large enough to be separated from the reaction mixture using standard filtration protocols. Therefore, they enable a facile purification and catalyst reuse.

This latter feature has potentially both an economic and environmental impact, deriving from a lower consumption of organic solvents, as lowering the E-factor in a process is a must for the modern chemical industry. Despite these many advantages, nanoreactors have not yet found widespread use in industry. A number of reasons can account for this. First of all, the construction of the nanoreactors is not always a cost-efficient process. Scalability and reproducibility in nanoreactor production also are key factors that have to be addressed. The recyclability and cost price should be improved to allow competition with existing heterogeneous and homogeneous processes. Furthermore, in most cases only model reactions have been studied. The improvement of a process that is highly relevant for industry would aid in a further acceptance of this technology by the end-users. Another issue is that the specific characteristics of nanoreactors should be employed more effectively. Physical protection and separation of catalytic species will allow the performance of multistep conversions in one pot reactors. This would then enable continuous flow processing, as intermediate work up steps and solvent switching procedures can be prevented. Flow chemistry has been over the years an innovative strategy to implement safer, faster and more efficient reactions. The use of fluidic, or micro-fluidic devices to allow a chemical transformation is becoming crucial for the optimization of chemical processes and often for their scaling-up.

This thesis is based on the introduction of the ONE-FLOW concept as a new platform that brings together a variety of technologies (e.g. compartmentalization methods, software for automatization of the processes, functional solvents) for the enhancement of chemical transformations with a special interest in cascade reactions in a continuous process. Functional solvent and nanoparticle combinations are developed in the ONE-FLOW scope to provide a compartmentalized flow reactor/separator system with 'horizontal hierarchy' – as opposed to the 'vertical hierarchy' of common multi-step flow syntheses (or batches) with their consecutive reactors-separators. The final aim of ONE-FLOW is a greener, faster and automated production of pharmaceutical ingredients which are normally tedious to be produced and highly priced (*i.e.* Rufinamide, UDCA). Key factors to reach this goal are: to avoid separation steps and laborious workups; reducing the usage of many solvents; and still obtaining the best yield of the final product. In this scenario, nanoreactors offer potentially a good solution to solve the problem of separation and compatibilization of catalytic species under different reaction conditions. To implement nanoreactors in the ONE FLOW concept they were equipped with both metal- and bio-catalysts. To further demonstrate their versatility and application potential they were employed to execute cascade reactions, and were used in a flow device without

need for intermediate work-up procedures. Furthermore, the applicability of such polymeric nanoreactors for the preparation of pharmaceutically relevant compounds was explored.

A general description on some examples of polymeric nanoreactors and their application in catalysis was given in this chapter. In **Chapter 2** cross-linked polymersomes and micelles were employed as nanoreactors for copper-based catalytic processes. We evaluated both nanoreactors by selecting a benchmark reaction; namely, the cyclopropanation of styrene with ethyldiazoacetate. This way, we shed light on the relationship between nanoreactor morphology and the ability to catalyze chemical reactions. We performed the reactions either in aqueous or in biphasic systems (Pickering emulsion with toluene). While micelles yielded a more stable and active system in water, polymersomes offered better yields and stability in Pickering emulsions. Interestingly, the morphology affected the type of emulsion (*o/w* for micelles and *w/o* for polymersomes). In-flow, polymersomes could be more easily recaptured and recycled, with less leaching of the copper catalyst.

In **Chapter 3** cross-linked polymersomes similar to those introduced in the former chapter, were used in a continuous multi-step synthesis of Rufinamide; an important biologically active compound for the pharmaceutical industry. This process was fine-tuned in terms of operational conditions, recyclability, and workup. The separation was simplified and the yields were much improved when compared to previously reported methodologies.

In **Chapters 4** and **5** biocatalytic nanoreactors based on bowl-shaped polymersomes (stomatocytes) were reported. In **Chapter 4** a novel platform nanoreactor was developed, which was coined a “*compartmentalized- cross-linked-enzymes nano-aggregate*” (*c-CLEnA*). This platform offered a new strategy for enzyme immobilization. Due to the enzyme preorganization and concentration in the cavity of the stomatocytes, cross-linking could be performed with substantially lower amounts of cross-linking agents, which was highly beneficial for the residual enzyme activity. Our strategy is generally applicable, as demonstrated by using two different cross-linkers (glutaraldehyde and genipin). Single or multiple enzymes were cross-linked, which allowed cascade reactions to be performed in one pot.

In **Chapter 5** the application of *c-CLEnAs* in two different pharmaceutical processes was investigated. Firstly, the two enzymes  $7\alpha$  and  $7\beta$  hydroxysteroid hydrogenase, which catalyze the transformation of chenodeoxycholic acid (CDCA) to ursodeoxycholic acid (UDCA) were compartmentalized. Both enzymes are known to be very sensitive and prone to deactivation. Creating *c-CLEnAs* using genipin as crosslinker maintained their activity, allowing the successful execution of the UDCA one pot cascade synthesis. As a second case study, the immobilization of a neuraminic acid aldolase in *c-CLEnA* particles was presented for usage in a microfluidic system. The optimized *c-CLEnA* was used to produce neuraminic acid, and demonstrated higher activity compared to previous reports.

Finally, we provided a **Summary & Outlook** section, with general conclusions about this work and recommendations for future investigations.

## References

- 1 R. a. Sheldon, *Green Chem.*, 2005, **7**, 267.
- 2 M.-O. Simon and C.-J. Li, *Chem. Soc. Rev.*, 2012, **41**, 1415–1427.
- 3 R. D. Rogers, *Science (80-. )*, 2003, **302**, 792–793.
- 4 J. H. Clark, 1999, 1–8.
- 5 M. J. Mulvihill, E. S. Beach, J. B. Zimmerman and P. T. Anastas, *Annu. Rev. Environ. Resour.*, 2011, **36**, 271–293.
- 6 J. H. Clark and S. J. Tavener, *Org. Process Res. Dev.*, 2007, **11**, 149–155.
- 7 R. A. Sheldon, *Green Chem.*, 2007, **9**, 1273.
- 8 J. Sperry and J. García-Álvarez, *Molecules*, 2016, **21**, 10–12.
- 9 B. H. Lipshutz, S. Ghorai, W. W. Y. Leong, B. R. Taft and D. V. Krogstad, *J. Org. Chem.*, 2011, **76**, 5061–5073.
- 10 J. Lu, M. J. Lazzaroni, J. P. Hallett, A. S. Bommarius, C. L. Liotta and C. a. Eckert, *Ind. Eng. Chem. Res.*, 2004, **43**, 1586–1590.
- 11 B.-Y. Yang, X.-M. Chen, G.-J. Deng, Y.-L. Zhang and Q.-H. Fan, *Tetrahedron Lett.*, 2003, **44**, 3535–3538.
- 12 L. Canali and D. C. Sherrington, 1999, 85–93.
- 13 N. Mase, Y. Nakai, N. Ohara, H. Yoda, K. Takabe, F. Tanaka and C. F. Barbas, *J. Am. Chem. Soc.*, 2006, **128**, 734–735.
- 14 T. Okino and Y. Takemoto, *Org. Lett.*, 2001, **3**, 1515–1517.
- 15 M. C. M. van Oers, L. K. E. A. Abdelmohsen, F. P. J. T. Rutjes and J. C. M. van Hest, *Chem. Commun.*, 2014, **50**, 4040–4043.
- 16 Y. Wu, Y. Zhang, M. Yu, G. Zhao and S. Wang, *Org. Lett.*, 2006, **8**, 4417–4420.
- 17 J. W. Peeters, O. Van Leeuwen, A. R. A. Palmans and E. W. Meijer, *Macromolecules*, 2005, **38**, 5587–5592.
- 18 J. Lee, S. M. Kim and I. S. Lee, *Nano Today*, 2014, **9**, 631–667.
- 19 A. Küchler, M. Yoshimoto, S. Luginbühl, F. Mavelli and P. Walde, *Nat. Nanotechnol.*, 2016, **11**, 409–420.
- 20 A. W. Kleij and J. N. H. Reek, *Chem. - A Eur. J.*, 2006, **12**, 4218–4227.
- 21 M. Nallani, H. P. M. de Hoog, J. J. L. M. Cornelissen, A. R. A. Palmans, J. C. M. van Hest and R. J. M. Nolte, *Biomacromolecules*, 2007, **8**, 3723–3728.
- 22 R. J. R. W. Peters, M. Marguet, S. Marais, M. W. Fraaije, J. C. M. van Hest and S. Lecommandoux, *Angew. Chem. Int. Ed.*, 2014, **53**, 146–150.
- 23 R. Poli, *Fundamental and Applied Catalysis Effects of Nanoconfinement on Catalysis*, .
- 24 L. Schoonen and J. C. M. van Hest, *Adv. Mater.*, 2016, **28**, 1109–1128.
- 25 Y. Tu, F. Peng, A. Adawy, Y. Men, L. K. E. A. Abdelmohsen and D. A. Wilson, *Chem. Rev.*, 2016, **116**, 2023–2078.
- 26 B. H. Lipshutz and S. Ghorai, *Org. Lett.*, 2012, **14**, 422–425.
- 27 D. J. Cole-Hamilton, *Science (80-. )*, 2003, **299**, 1702–1706.
- 28 S. A. Dergunov, A. T. Khabiyeu, S. N. Shmakov, M. D. Kim, N. Ehterami, M. C. Weiss, V. B. Birman and E.

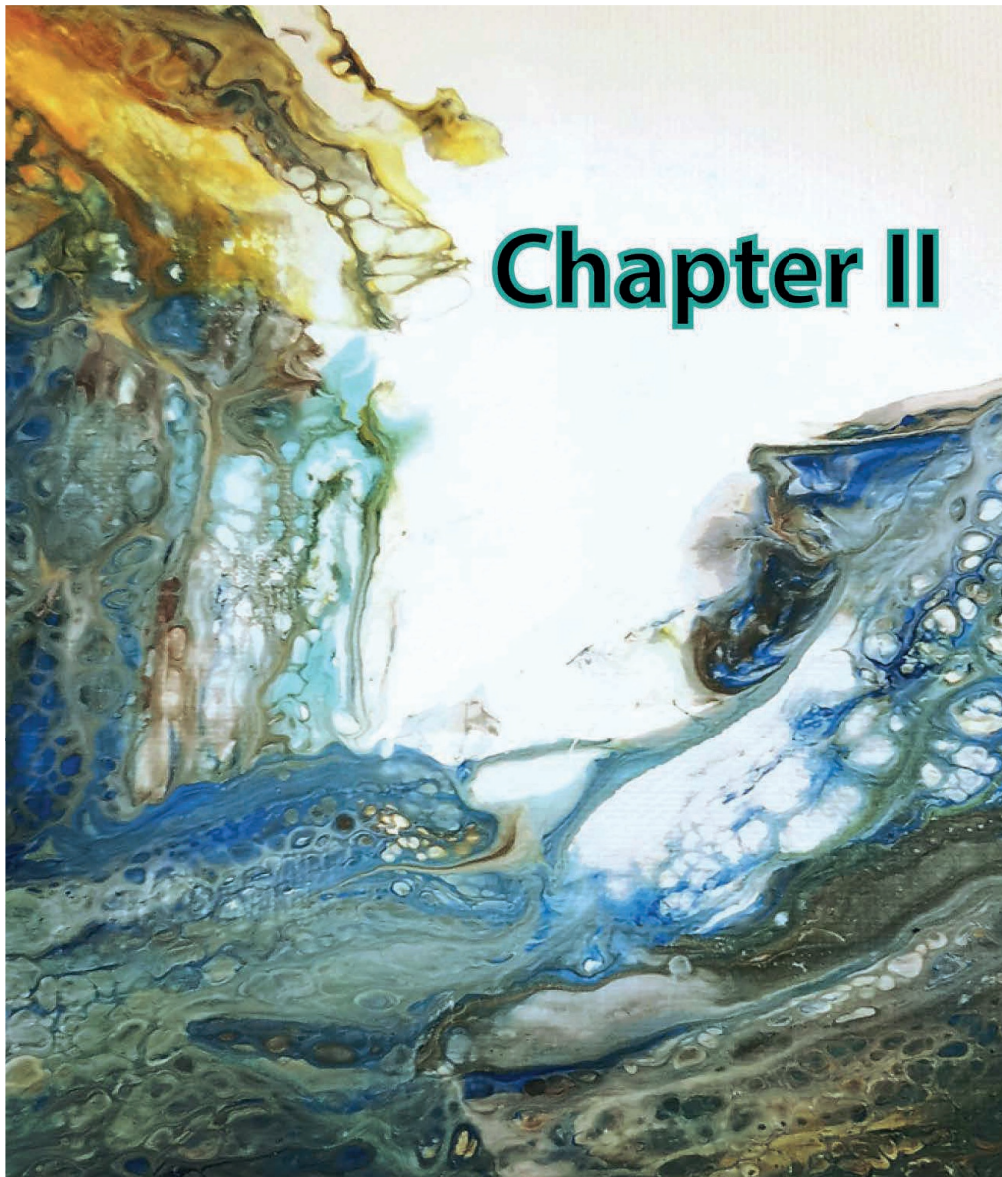
- Pinkhassik, *ACS Nano*, 2016, **10**, 11397–11406.
- 29 A. Lu and R. K. O'Reilly, *Curr. Opin. Biotechnol.*, 2013, **24**, 639–645.
- 30 D. J. (University of S. A. Cole-Hamilton and S. Tooze, Robert P. (Sasol Technology, St. Andrews Fife, in *Catalyst Separation, Recovery and Recycling*, Springer, Dordrecht, 2006, pp. 1–247.
- 31 T. Dwars, E. Paetzold and G. Oehme, *Angew. Chem. Int. Ed.*, 2005, **44**, 7174–7199.
- 32 J. P. Patterson, P. Cotanda, E. G. Kelley, A. O. Moughton, A. Lu, I. I. I. T. H. Epps and R. K. O'Reilly, *Polym. Chem.*, 2013, **4**, 2033–2039.
- 33 K. T. Kim, S. A. Meeuwissen, R. J. M. Nolte and J. C. M. van Hest, *Nanoscale*, 2010, **2**, 844.
- 34 S. H. A. M. Leenders, R. Gramage-Doria, B. de Bruin and J. N. H. Reek, *Chem. Soc. Rev.*, 2015, **44**, 433–448.
- 35 H. Abe, Y. Mawatari, H. Teraoka, K. Fujimoto and M. Inouye, *J. Org. Chem.*, 2004, **69**, 495–504.
- 36 M. G. Zolotukhin, M. D. C. G. Hernández, A. M. Lopez, L. Fomina, G. Cedillo, A. Nogales, T. Ezquerra, D. Rueda, H. M. Colquhoun, K. M. Fromm, A. Ruiz-Treviño and M. Ree, *Macromolecules*, 2006, **39**, 4696–4703.
- 37 K. E. Djernes, O. Moshe, M. Mettry, D. D. Richards and R. J. Hooley, *Org. Lett.*, 2012, **14**, 788–791.
- 38 S. Shimizu, S. Shirakawa, T. Suzuki and Y. Sasaki, *Tetrahedron*, 2001, **57**, 6169–6173.
- 39 C. D. Gutsche and I. Alam, *Tetrahedron*, 1988, **44**, 4689–4694.
- 40 H. Che and J. C. M. van Hest, *J. Mater. Chem. B*, 2016, **4**, 4632–4647.
- 41 P. Khullar, V. Singh, A. Mahal, H. Kumar, G. Kaur and M. S. Bakshi, *J. Phys. Chem. B*, 2013, **117**, 3028–3039.
- 42 D. M. Vriezema, M. Comellas Aragonès, J. A. A. W. Elemans, J. J. L. M. Cornelissen, A. E. Rowan and R. J. M. Nolte, *Chem. Rev.*, 2005, **105**, 1445–1490.
- 43 V. Thomas, M. Namdeo, Y. M. Mohan, S. K. Bajpai and M. Bajpai, *J. Macromol. Sci. Part A*, 2007, **45**, 107–119.
- 44 P. McMorn and G. J. Hutchings, *Chem. Soc. Rev.*, 2004, **33**, 108.
- 45 B. H. Lipshutz, N. A. Isley, J. C. Fennewald and E. D. Slack, *Angew. Chem. Int. Ed.*, 2013, **52**, 10952–10958.
- 46 M. Tariq, S. Ali and N. Khalid, *Renew. Sustain. Energy Rev.*, 2012, **16**, 6303–6316.
- 47 J. R. H. Ross, *Heterog. Catal.*, 2012, 1–15.
- 48 M. Campanati, G. Fornasari and A. Vaccari, *Catal. Today*, 2003, **77**, 299–314.
- 49 R. G. Rao, R. Blume, T. W. Hansen, E. Fuentes, K. Dreyer, S. Moldovan, O. Ersen, D. D. Hibbitts, Y. J. Chabal, R. Schlögl and J.-P. Tessonnier, *Nat. Commun.*, 2017, **8**, 340.
- 50 I. L. C. Buurmans and B. M. Weckhuysen, *Nat. Chem.*, 2012, **4**, 873–886.
- 51 J. Pritchard, G. A. Filonenko, R. van Putten, E. J. M. Hensen and E. A. Pidko, *Chem. Soc. Rev.*, 2015, **44**, 3808–3833.
- 52 A. Mortreux and F. Petit, in *Industrial Applications of homogeneous catalysis*, eds. R. (University of M. Ugo and B. R. (Universit. of B. C. James, 1988, pp. 1–347.
- 53 F. H. M. Dekker, A. Blik, F. Kapteijn and J. a. Moulijn, *Chem. Eng. Sci.*, 1995, **50**, 3573–3580.
- 54 C. Copéret, M. Chabanas, R. Petroff Saint-Arroman and J.-M. Basset, *Angew. Chem. Int. Ed.*, 2003, **42**, 156–



- 181.
- 55 M. Pagliaro, V. Pandarus, R. Ciriminna, F. Béland and P. DemmaCarà, *ChemCatChem*, 2012, **4**, 432–445.
- 56 Y. Lu, P. Spyra, Y. Mei, M. Ballauff and A. Pich, *Macromol. Chem. Phys.*, 2007, **208**, 254–261.
- 57 M. van Oers, F. Rutjes and J. van Hest, *Curr. Opin. Biotechnol.*, 2014, **28**, 10–16.
- 58 T.-L. Nghiem, D. Coban, S. Tjaberings and A. H. Gröschel, *Polymers (Basel)*, 2020, **12**, 2190.
- 59 F. Cuomo, A. Ceglie, A. De Leonardis and F. Lopez, *Catalysts*, 2019, **9**, 1–18.
- 60 V. Kapishon, R. A. Whitney, P. Champagne, M. F. Cunningham and R. J. Neufeld, *Biomacromolecules*, 2015, **16**, 2040–2048.
- 61 J. van Herrikhuyzen, G. Portale, J. C. Gielen, P. C. M. Christianen, N. a J. M. Sommerdijk, S. C. J. Meskers and A. P. H. J. Schenning, *Chem. Commun.*, 2008, 697–699.
- 62 R. Erhardt, A. Böker, H. Zettl, H. Kaya, W. Pyckhout-Hintzen, G. Krausch, V. Abetz and A. H. E. Müller, *Macromolecules*, 2001, **34**, 1069–1075.
- 63 S. Jain, F.S. Bates, *Science* 2003, **300**, 460–464.
- 64 A. Blanazs, S. P. Armes and A. J. Ryan, *Macromol. Rapid Commun.*, 2009, **30**, 267–277.
- 65 L. M. Wang, N. Jiao, J. Qiu, J. J. Yu, J. Q. Liu, F. Lou Guo and Y. Liu, *Tetrahedron*, 2010, **66**, 339–343.
- 66 S. R. K. Minkler, N. A. Isley, D. J. Lippincott, N. Krause and B. H. Lipshutz, *Org. Lett.*, 2014, **16**, 724–726.
- 67 C. Duplais, A. Krasovskiy, A. Wattenberg and B. H. Lipshutz, *Chem. Commun. (Camb)*, 2010, **46**, 562–564.
- 68 B. H. Lipshutz, S. Ghorai, A. R. Abela, R. Moser, T. Nishikata, C. Duplais, A. Krasovskiy, R. D. Gaston and R. C. Gadwood, *J. Org. Chem.*, 2011, **76**, 4379–4391.
- 69 N. A. Isley, S. Dobarco and B. H. Lipshutz, *Green Chem.*, 2014, **16**, 1480–1488.
- 70 T. Nishikata and B. H. Lipshutz, *Org. Lett.*, 2009, **11**, 2377–2379.
- 71 W. De Graaf, J. Bowsma and G. Van Koten, *Organometallics*, 1990, **9**, 1479–1484.
- 72 S. Handa, J. D. Smith, M. S. Hageman, M. Gonzalez and B. H. Lipshutz, *ACS Catal.*, 2016, **6**, 8179–8183.
- 73 M. Lee, C.-J. Jang and J.-H. Ryu, *J. Am. Chem. Soc.*, 2004, **126**, 8082–8083.
- 74 M. Lee, B.-K. Cho and W.-C. Zin, *Chem. Rev.*, 2001, **101**, 3869–3892.
- 75 B.M. Discher, Y.-Y. Won, D.S. Ege, J.C.-M. Lee, F.S. Bates, D.E. Discher, D.A. Hammer, *Science* 1999, **284**, 1143–1146.
- 76 C. Sanson, C. Schatz, J. F. Le Meins, A. Brûlet, A. Soum and S. Lecommandoux, *Langmuir*, 2010, **26**, 2751–2760.
- 77 K. T. Kim, J. J. L. M. Cornelissen, R. J. M. Nolte and J. C. M. Van Hest, *Adv. Mater.*, 2009, **21**, 2787–2791.
- 78 R. J. Hickey, J. Koski, X. Meng, R. A. Riggelman, P. Zhang and S.-J. Park, *ACS Nano*, 2014, **8**, 495–502.
- 79 C. Gao, J. Wu, H. Zhou, Y. Qu, B. Li and W. Zhang, *Macromolecules*, 2016, **49**, 4490–4500.
- 80 C. Y. Hong, Y. E. Z. I. You and C. Y. Pan, *J. Polym. Sci. Part A Polym. Chem.*, 2004, **42**, 4873–4881.
- 81 Z. Wang, M. C. M. van Oers, F. P. J. T. Rutjes and J. C. M. van Hest, *Angew. Chem. Int. Ed.*, 2012, **51**, 10746–10750.

- 82 M. C. M. van Oers, Randboud Universiteit Nijmegen, 2015.
- 83 S. M. Kuiper, M. Nallani, D. M. Vriezema, J. J. L. M. Cornelissen, J. C. M. van Hest, R. J. M. Nolte and A. E. Rowan, *Org. Biomol. Chem.*, 2008, **6**, 4315.
- 84 D. Gräfe, J. Gaitzsch, D. Appelhans and B. Voit, *Nanoscale*, 2014, **6**, 10752–10761.
- 85 M. C. M. van Oers, W. S. Veldmate, J. C. M. van Hest and F. P. J. T. Rutjes, *Polym. Chem.*, 2015, **6**, 5358–5361.
- 86 M. Alcón, *J. Mol. Catal. A Chem.*, 1999, **144**, 337–346.
- 87 V. B. Sharma, S. L. Jain and B. Sain, 2004, **94**, 57–59.
- 88 H. M. Lee, C. Bianchini, G. Jia and P. Barbaro, *Organometallics*, 1999, **18**, 1961–1966.
- 89 S. A. Dergunov, K. Kesterson, W. Li, Z. Wang and E. Pinkhassik, *Macromolecules*, 2010, **43**, 7785–7792.
- 90 S. F. M. Van Dongen, M. Nallani, J. J. L. M. Cornelissen, R. J. M. Nolte and J. C. M. Van Hest, *Chem. - A Eur. J.*, 2009, **15**, 1107–1114.
- 91 D. A. Tomalia and J. M. Fréchet, *Prog. Polym. Sci.*, 2005, **30**, 217–219.
- 92 L. M. Bronstein and Z. B. Shifrina, *Nanotechnologies Russ.*, 2009, **4**, 576–608.
- 93 D. a. Tomalia and I. Majoros, *J. Macromol. Sci. Part C Polym. Rev.*, 2003, **43**, 411–477.
- 94 Y. Cheng, L. Zhao, Y. Li and T. Xu, *Chem. Soc. Rev.*, 2011, **40**, 2673–2703.
- 95 Y. M. Chung and H. K. Rhee, *Catal. Letters*, 2003, **85**, 159–164.
- 96 X. Peng, Q. Pan and G. L. Rempel, *Chem. Soc. Rev.*, 2008, **37**, 1619.
- 97 R. W. J. Scott, O. M. Wilson, S.-K. Oh, E. A. Kenik and R. M. Crooks, *J. Am. Chem. Soc.*, 2004, **126**, 15583–15591.
- 98 R. W. J. Scott, C. Sivadinarayana, O. M. Wilson, Z. Yan, D. W. Goodman and R. M. Crooks, *J. Am. Chem. Soc.*, 2005, **127**, 1380–1381.
- 99 H. Lang, S. Maldonado, K. J. Stevenson and B. D. Chandler, *J. Am. Chem. Soc.*, 2004, **126**, 12949–12956.
- 100 C. Ornelas, J. R. Aranzaes, L. Salmon and D. Astruc, *Chem. - A Eur. J.*, 2008, **14**, 50–64.
- 101 C. Ornelas, L. Salmon, J. Ruiz Aranzaes and D. Astruc, *Chem. Commun.*, 2007, **3**, 4946.
- 102 C. Ornelas, J. Ruiz, L. Salmon and D. Astruc, *Adv. Synth. Catal.*, 2008, **350**, 837–845.
- 103 O. M. Wilson, M. R. Knecht, J. C. Garcia-Martinez and R. M. Crooks, *J. Am. Chem. Soc.*, 2006, **128**, 4510–4511.
- 104 J. Lim and E. E. Simanek, *Org. Lett.*, 2008, **10**, 201–204.
- 105 P. Agrawal, U. Gupta and N. K. Jain, *Biomaterials*, 2007, **28**, 3349–3359.
- 106 D. C. Dewey, C. a Strulson, D. N. Cacace, P. C. Bevilacqua and C. D. Keating, *Nat. Commun.*, 2014, **5**, 4670.
- 107 J.-L. Reymond and T. Darbre, *Org. Biomol. Chem.*, 2012, **10**, 1483.
- 108 P. Sommer, N. A. Uhlich, J.-L. Reymond and T. Darbre, *ChemBioChem*, 2008, **9**, 689–693.
- 109 R. Biswas, N. Maillard, J. Kofoed and J.-L. Reymond, *Chem. Commun.*, 2010, **46**, 8746.
- 110 A. Clouet, T. Darbre and J.-L. Reymond, *Angew. Chem. Int. Ed.*, 2004, **43**, 4612–4615.
- 111 L. Klouda, *Eur. J. Pharm. Biopharm.*, 2015, **97**, 338–349.
- 112 D. Seliktar, *Science*, 2012, **336**, 1124–1128.

- 113 B.D. Ratner, B. D.; A.S. Hoffman, *ACS Symp. Ser.* 1976, **31**, 1–36.
- 114 S. Varma , L. Bureau, D. Débarre, *Langmuir* 2016, **32**, 3152–3163.
- 115 I. Neamtu, A. G. Rusu, A. Diaconu, L. E. Nita and A. P. Chiriac, *Drug Deliv.*, 2017, **24**, 539–557.
- 116 M. Molina, M. Asadian-Birjand, J. Balach, J. Bergueiro, E. Miceli and M. Calderon, *Chem. Soc. Rev.*, 2015, **44**, 6161–6186.
- 117 Y. Sasaki and K. Akiyoshi, *Chem. Rec.*, 2010, **10**, 366–376.
- 118 A. Lu, T. P. Smart, T. H. Epps, D. A. Longbottom and R. K. O'Reilly, *Macromolecules*, 2011, **44**, 7233–7241.
- 119 Y. He, G. Huang, Z. Pan, Y. Liu, Q. Gong, C. Yao and J. Gao, *Mater. Res. Bull.*, 2015, **70**, 263–271.
- 120 J. Zhang, M. Zhang, K. Tang, F. Verpoort and T. Sun, *Small*, 2014, **10**, 32–46.
- 121 I. Tokareva, S. Minko, J. H. Fendler and E. Hutter, *J. Am. Chem. Soc.*, 2004, **126**, 15950–15951.
- 122 G. Wei, W. Zhang, F. Wen, Y. Wang and M. Zhang, *J. Phys. Chem. C*, 2008, **112**, 10827–10832.
- 123 Y. Que, C. Feng, S. Zhang and X. Huang, *J. Phys. Chem. C*, 2015, **119**, 1960–1970.



Dr. Ana Maria Bago Rodriguez, Dr. Shoupeng Cao, Dr. Jingxin Shao and Paul van der Ven are kindly acknowledged for their contribution to this chapter

# A comparative study of organometal catalysis in micellar and vesicular compartments.

## Abstract

A systematic investigation on the effect of spatial organization of metal catalysts in polymeric nanoreactors, namely, polymersomes and micelles, is reported in this chapter. The performance of both platforms was assessed in the asymmetric cyclopropanation of styrene with ethyl diazoacetate, with a focus on their capacity for substrate conversion and catalyst retention. While the catalytic performance of both nanoreactors was compared in batch in aqueous media and biphasic systems, their ability to retain catalytic species was assessed in-flow with leaching experiments. We demonstrate that the overall conversion is not much affected by the type of carrier employed. However, during reaction in aqueous medium, micellar systems show better colloidal stability than polymersomes. Moreover, the positioning of the catalyst within the core of the micelles or the bilayer of polymersomes has direct consequences on catalyst retention and its use for in-flow processes.

## 2.1. Introduction

Asymmetric catalysis is a key process in the field of synthetic chemistry. It is affected by a range of obvious aspects such the choice of (a)chiral ligands<sup>1</sup>, and operative reaction conditions (temperature, reaction time, initial concentration), but also more subtle effects have to be taken into account, such as the order of reagents added<sup>2</sup> to improve the outcome of the reaction<sup>3</sup>. In most cases asymmetric catalysis is performed under homogeneous conditions in organic solvents to provide sufficient and unhindered accessibility to the catalytic species and prevent undesired interactions with water. However, this makes recycling of the expensive catalysts more challenging and introduces a larger environmental burden. To provide a solution to these bottlenecks smart compartmentalization strategies have been developed over the years involving the use of nanoreactors as robust platforms for the catalysis of organic reactions in water, which is a favorable solvent for green chemistry<sup>4</sup>. Nanoreactors typically are block copolymer-derived nanoparticles such as micelles<sup>5</sup>, nanospheres<sup>6</sup>, nanocapsules<sup>7</sup>, and polymer vesicles<sup>6</sup>.

Micelles are self-assembled structures, in which the hydrophobic domains of the amphiphilic molecules position themselves in such a way that an internal core is formed, surrounded by hydrophilic tails. In general, micelles are characterized by diameters ranging from 10 to 100 nm<sup>6</sup>. Vesicles are comprised of an aqueous inner compartment surrounded by a bilayer of amphiphilic molecules, of which the inner part of the bilayer accommodates the hydrophobic blocks of the amphiphiles. Both micelles and vesicles can be composed of small surfactants or polymeric amphiphiles<sup>4,5</sup>. Polymeric vesicles are furthermore also named polymersomes, in analogy to the low molecular weight liposome counterparts. Polymersomes are relatively larger than micelles, with sizes ranging from 50 nm – 5 μm<sup>6</sup>. Because of their stability and ability to shield hydrophobic catalysts, both micelles and polymersomes have been presented as powerful tools to carry out reactions in aqueous media. As nanoreactors, they are easily

recycled, they can be quickly recovered with in-flask separations (*e.g.* extraction methods), further highlighting their potential in green chemistry and environmental-factor (E-factor) improvement<sup>5,8</sup>. They have been shown to be effective in shielding the catalytic species from unwanted interactions and minimizing by-product formation while facilitating catalyst recovery<sup>8</sup>. They allow metallic or bi-metallic catalyzed-reactions that would normally require organic solvents<sup>9</sup> to be effectively executed in water. This approach can also be extended to organocatalyzed reactions. For example, the L-proline-catalysed asymmetric aldol reaction of 4-nitrobenzaldehyde with ketone donors normally results in poor yields and selectivity when water is added to the reaction mixture<sup>10</sup>. It was reported that when polymersome nanoreactors were employed, the corresponding  $\beta$ -hydroxyketones were obtained in quantitative yields and with high enantio- and diastereoselectivities. This way, not only the selectivity issue was solved but it was proven that the catalytic L-proline-polymersomes could be recycled up to five times without any loss in activity or selectivity<sup>11</sup>. Lipshutz *et. al.* reported the use of micelles to perform cross-coupling reactions between benzylic and aryl halides in water<sup>12</sup>, which normally results in very limited yields due to the undesired homo-coupling reaction<sup>13</sup>. In a recent study, different coupling reactions with relevance for the production of pharmaceutical intermediates were performed using free and immobilized catalysts in batch and micellar nanoreactors, respectively, and the E-factor was compared in both cases<sup>14</sup>. Strikingly, the E-factors reported for reactions performed using micellar nanoreactors were at least an order of magnitude lower than those reported from batch reactions, demonstrating their great potential to facilitate greener reactions. Although polymersomes and micelles both have been used to accommodate asymmetric catalysis in an aqueous environment<sup>15</sup>, a direct comparison between these two nanoreactors with different topologies has not been made yet. These particles vary in their surface area and organization of their hydrophobic domain, which could lead to differences in substrate accessibility, protection against water and catalyst leaching.

To systematically investigate these effects, polymersomes and micelles were assembled using the same type of block copolymer, namely, poly(ethylene glycol)<sub>44</sub>-block-poly(styrene-4-vinyl benzyl azide) PEG<sub>44</sub>-*b*-P(S-4-VBA). Specifically, two building blocks with different hydrophobic chain lengths, PEG<sub>44</sub>-*b*-P(S<sub>115</sub>-4-VBA<sub>18</sub>) and PEG<sub>44</sub>-*b*-P(S<sub>70</sub>-4-VBA<sub>11</sub>), were formed and used for the preparation of polymersomes and micelles, respectively (Figure 1).

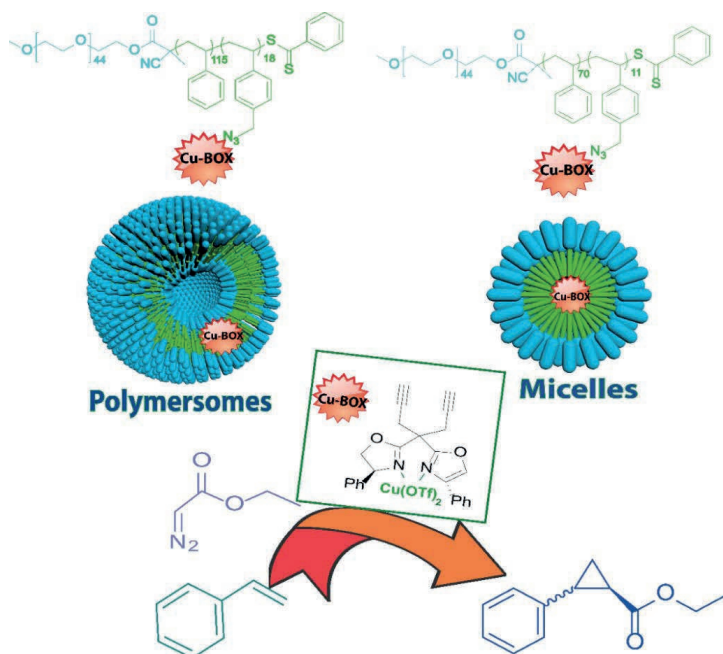


**Figure 1-** Schematic formation of polymersomes and micelles starting from PEG<sub>44</sub>-b-P(S<sub>115</sub>-4-VBA<sub>18</sub>) and PEG<sub>44</sub>-b-P(S<sub>70</sub>-4-VBA<sub>11</sub>), respectively. The different positioning of the Cu-BOX catalyst, immobilized via a CuAAC reaction in the hydrophobic domain of both of the structures is depicted. The resulting nanoreactors are used in the asymmetric cyclopropanation of styrene with ethyl diazoacetate.

The micellar core and polymersome membrane resulted in a different spatial organization of the chiral copper triflate catalyst [(4*S*,4'*S*)-2,2'-(hepta-1,6-diyne-4,4-diyl)bis(4-phenyl-4,5-dihydrooxazole)]-copper(II)triflate (Cu-BOX), which was conjugated to the azide residues in the hydrophobic block via a Cu-mediated Azide-Alkyne Cycloaddition (CuAAC) reaction. The activity of both nanoreactors was subsequently evaluated in the aqueous cyclopropanation of styrene with ethyl diazoacetate (EDA).

## 2.2. Results and discussion

Following a previously reported procedure, block copolymers comprising poly(ethylene glycol), and a copolymer of styrene and vinyl benzyl azide were synthesized using reversible addition-fragmentation chain-transfer (RAFT) polymerization. The self-assembly of PEG<sub>44</sub>-b-P(S<sub>70</sub>-4-VBA<sub>11</sub>) and PEG<sub>44</sub>-b-P(S<sub>115</sub>-4-VBA<sub>18</sub>) using the solvent switch methodology resulted in micelles and polymersomes, respectively – as confirmed by transmission electron microscopy (TEM), scanning electron microscopy (SEM) and light scattering techniques (Figure 2a,2b,2c,2d, and S2-S3-S4).

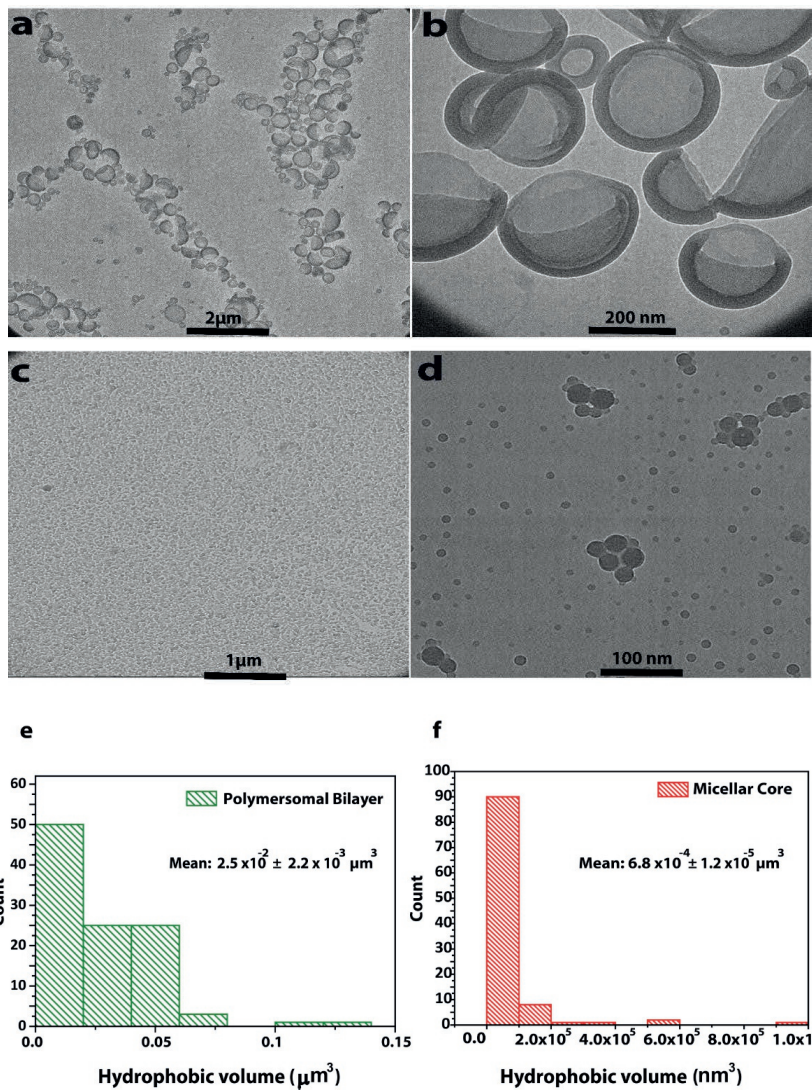


**Figure 2-** TEM images showing a) b) polymersomes; c) d) micelles. The two histograms show the distribution of hydrophobic volumes extracted from the TEM images: e) Hydrophobic volume distribution in polymersomes, mean value is  $2.5 \cdot 10^{-2} \mu\text{m}^3$  f) Hydrophobic volume distribution in micelles, mean value is  $6.8 \cdot 10^{-4} \mu\text{m}^3$ .

Using a combination of static and dynamic light scattering indicated that micellar and polymersomal structures were formed with average sizes of 120 (micelles) and 340 nm (polymersomes), with condensed ( $Rg/Rh = ca. 0.8$ ) and



empty cores ( $R_g/R_h = ca. 1$ ), respectively (Figure S3, S4). These results were corroborated by TEM analysis. Interestingly, in the micellar structures the presence of two population of micelles could be observed (Figure 2d). The larger micelle population was determined to be 30% of the total sample formed, by isolating the two fractions using either spin filtration (membrane pore size 0.1  $\mu\text{m}$ , 5 min at 3000 rpm) or size exclusion chromatography (SEC) and then weighting the two individual fractions after freeze-drying. This bimodal distribution explains the high value for the average size of the micelles, as determined by DLS. However, the effect on the PDI was limited. Further analysis of the images from TEM on 100 particles indicated a hydrophobic volume of  $6.8 \cdot 10^{-5} \pm 1.2 \cdot 10^{-4} \mu\text{m}^3$  and  $2.5 \cdot 10^{-2} \pm 1.2 \cdot 10^{-3} \mu\text{m}^3$  for the micelles and polymersomes, respectively. Per particle, the average volume of the hydrophobic domain of the polymersomes was *ca.* 350 and the surface area *ca.* 35 times larger, respectively, than that of the micelles (Figure 2a-2b).

A chiral copper triflate bisoxazoline (Cu-BOX) catalyst was incorporated in the hydrophobic domains of both the micelles and polymersomes via a CuAAC click reaction. This contributed to the overall stability of the assemblies and allowed the immobilization of the catalysts in the hydrophobic domain of the nanoreactors<sup>17</sup>. The successful incorporation of the BOX ligands was confirmed using Fourier transform infrared (FTIR) analysis, which indicated the complete disappearance of the azide band (Figure S5). Copper loading was quantified using Inductively Coupled Plasma Mass Spectrometry (ICP-MS); this was determined to be *ca.* 0.45 mM per 10 mg mL<sup>-1</sup> of polymer, with a small deviation between the two nanoreactor types (Figure S6A). It is worth to mention that in principle each BOX ligand is cross-linked to two azides; therefore, control over catalyst loading was achieved by controlling the percentage of azides in both the micelles and polymersomes. Indeed, in control experiments, conjugating a fluorescent probe (Cy3) to both micelles and polymersomes with equal azide content resulted in equal fluorescence (Figure S6B).

Having confirmed the structural integrity of both the micelle and polymersome nanoreactors, we set out to investigate and compare their catalytic performance in a single phase (water) and in a biphasic Pickering emulsion system (toluene and water). In both cases, the asymmetric cyclopropanation of styrene with EDA was chosen as a benchmark reaction for our study. The results obtained using both nanoreactors were compared to those obtained using free catalysts in dichloromethane (as reference). Following our previously published work<sup>4</sup>, either catalytic micelles or polymersomes (10 mg mL<sup>-1</sup>) were mixed with EDA and styrene under stirring for 10 min at room temperature.

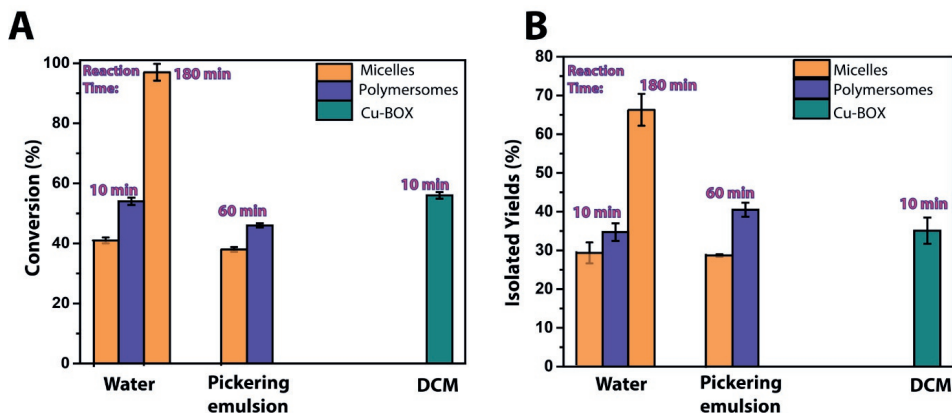


**Figure 3-** Comparative bar plots showing: **A)** conversion of EDA to ethyl 2-phenyl cyclopropane carboxylate employing micelles and polymersomes in water (for 10 or 180 min) and in a biphasic water/toluene Pickering emulsion (for 60 min). The results with the free Cu-BOX catalyst (10 min reaction) in DCM are reported as reference. **B)** Isolated yields of the product obtained from the reaction in water and in Pickering emulsion, compared with the free Cu-BOX catalyst in DCM. No differences were observed in the stereochemistry of the product when using different nanosystems.

It is worth to mention that these reaction conditions were previously optimized for the aqueous asymmetric cyclopropanation reaction in polymersomes<sup>4</sup>, and therefore might not be ideal for the micelles. After 10 min, the polymersome nanoreactors aggregated and precipitated out of solution – in line with our previous findings<sup>4</sup>. Such aggregation is hypothesized to be a result of continuous accumulation of the formed cyclopropane in the polystyrene bilayer. Micelles, on the other hand, remained stable - even after 7h. The conversion during the 10 min time frame was ~20% higher when polymersomes were used, compared to the micellar system. However, after 3h, an almost full conversion was reached using the micelle nanoreactors (Figure 3A). This is mainly a result of the long term colloidal stability of the micelles, which is suggested to be a consequence of their small size and their better ability to shield the hydrophobic domain from the environment, even when swollen with product.

To further investigate the effects of the spatial organization of catalysts in a biphasic system, a Pickering emulsion of an aqueous dispersion containing either micelle or polymersome nanoreactors (polymer concentration = 10 mg mL<sup>-1</sup>) and toluene as oil phase was formed. Pickering emulsions are known to be beneficial when the substrate and the catalyst are soluble in different phases. When the reactant is solubilized in the oil phase and the catalyst in the water phase, the formation of the emulsion drastically increases the interfacial area, improving the contact between the substrate and the catalyst, leading to a faster reaction<sup>18</sup>. As was previously demonstrated<sup>19,20</sup>, both nanoreactors served as the surface-active components that stabilized the emulsion droplets, and as such no extra emulsifiers were added. The biphasic system was formed by mixing equal volumes (2 mL) of the two phases with an ultrasonic probe for 1 min. During emulsification, the temperature was kept low at 4 °C by using an ice-bath, to prevent temperature variations that might affect the catalytic activity. The organic phase of the emulsion that was stabilized with micelle

nanoreactors contained 100  $\mu\text{L}$  of styrene (0.87 mmol) and 25  $\mu\text{L}$  of EDA (0.2 mmol). In the case of the emulsion stabilized with polymersome nanoreactors, styrene was dispersed in toluene and EDA was added after emulsification to start the reaction. The emulsion type varied depending on the emulsifier used; while micelle nanoreactors formed an oil in water (o/w) emulsion, polymersomes stabilized a water in oil (w/o) system. The emulsion type was confirmed through fluorescence microscopy images (figure 4).

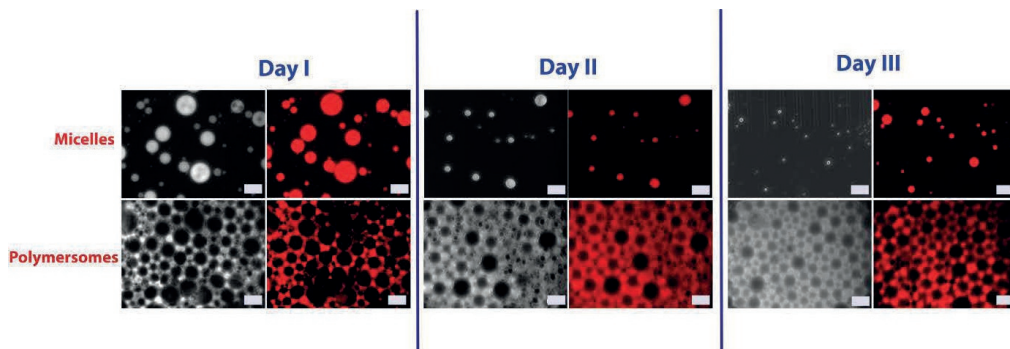


**Figure 4-** Optical microscope images of Pickering emulsions stabilized by micelles and polymersomes taken at different times (as indicated). The emulsion type was confirmed through fluorescence microscopy (Rhodamine dye/Tetramethyl rhodamine Isothiocyanate (TRITC) filter), scale bar is 50  $\mu\text{m}$ . The organic phase was dyed with Nile red. 6  $\mu\text{L}$  of a  $1 \cdot 10^{-4}$  M Nile red solution in acetone was added to the toluene phase prior to homogenization.

The differences in the emulsion type could be attributed to the difference in the degree of hydrophobicity of both entities, given by the different length of the polystyrene chain. The outer composition of both nanoreactors is similar, however, it is known that the wettability and the contact angle of amphiphilic particles might be affected by the hydrophobic surface area<sup>21</sup> which is considerably different in the nanosystems we designed (higher for the polymersomes).

In terms of emulsion stability, the w/o polymersome-stabilized emulsion was stable and sedimentation was not observed (Figure S7) - it did not coalesce even after 30 min, as no aqueous phase was resolved. On the other hand, the o/w micelle-stabilized emulsion was stable to creaming but not to coalescence, as there was a layer of oil released after the same period (Figure S7). The mean droplet diameter of both micelle- and polymersome-stabilized emulsions was calculated from at least fifty individual droplets on digital micrographs. The average droplet diameter of polymersome- and micelle-stabilized emulsions was  $37.7 \pm 11.1 \mu\text{m}$  and  $32.8 \pm 15.1 \mu\text{m}$ , respectively. While the size of the polymersome-stabilized droplets remained stable for at least 3 days, that of the micelle-stabilized emulsions showed a considerable decrease in time, with 51 % decrease in 3 days (Figure S8). This makes the micelle-stabilized Pickering emulsions less suitable for long-term catalytic experiments. In terms of catalytic performance, polymersome- and micelle-stabilized emulsions resulted in similar conversions, albeit that the isolated yield of the final product was higher for the polymersome-based system within all the experiments performed (Figure 3). Remarkably, no aggregation was observed after 1h of reaction time as was the case when using polymersomes in a

single-phase reaction, which can be ascribed to the diffusion of product out of the polymersome to the organic phase; both polymersomes and micelles preserved their morphological integrity (Figure S9).

Finally, in order to investigate the leaching and the recyclability of the Cu-catalysts in polymersomes and micelles while considering continuous processes, we set out to perform in-flow experiments using a microtubular membrane reactor ( $V_{\text{tot}}=1.5$  mL, membrane size 10 kDa). Both nanoreactors were injected in the membrane inlet and then water was flowed through the system at different flow rates (from  $0.2 \text{ mL min}^{-1}$  to  $1 \text{ mL min}^{-1}$ )<sup>22</sup>. The outflow was recollected at the outlet of the system and the Cu concentration (leached from the nanoreactors) was determined using ICP-MS (Figure 5).

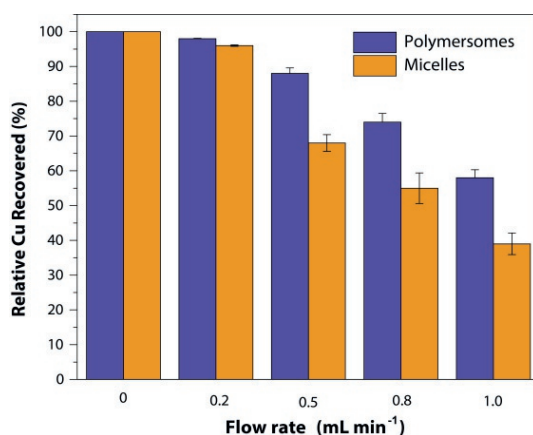


**Figure 5-** Relative amount of Cu recovered in the leaching experiments in the flow setup. Cross-linked micelles or polymersomes ( $10 \text{ mg mL}^{-1}$ ) were tested at different flow rates, the bar plot reports the relative Cu amount retrieved in the samples after 30 minutes measured by ICP-MS. The error bars are based on the average of three repetitions of the experiment using the same sample. ICP-MS is measured on  $100 \mu\text{L}$  of each sample at the end of the experiment.

In both cases, it was clear that the leaching increased as the flow rate increased. At  $1 \text{ mL min}^{-1}$ , polymersomes showed 40% of leaching while micelles only retained 35% of the Cu loaded. For the moderate flow rate of  $0.2 \text{ mL min}^{-1}$ , the leaching observed in both nanoreactors was comparable (less than 10% of Cu loss). At intermediate rates ( $0.5$  and  $0.8 \text{ mL min}^{-1}$ ), polymersomes retained more catalyst than micelles. Thus, the embedding of the catalyst in the polymeric bilayer of the polymersomes offers higher retention during in-flow processes, where micelles might deactivate earlier due to loss of the catalytic material.

### 2.3. Conclusions

In summary, micelles and polymersomes with a similar composition were prepared and cross-linked with a chiral Cu-BOX catalyst. We investigated their catalytic performance using cyclopropanation of styrene in water (single-phase) and in a Pickering emulsion (toluene/water) as biphasic system and we tested the effect of the spatial organization on the Cu-leaching in flow experiments. The spatial distribution of the catalyst in the hydrophobic domain has no significant impact in terms of catalytic efficiency; in fact, conversions and isolated yields are comparable between micelles and polymersomes in both the single-phase and the emulsion reactions. However, the spatial organization can have other implications: when the reaction was performed in water, polymersomes aggregated after 10 minutes of reaction while micelles could be used for longer reaction times and therefore reached a higher conversion. Reasonably, accumulation of product in the polymersomes could cause this aggregation of polymersomes. In the biphasic system, the different nature of polymersomes and micelles interestingly led to the stabilization of different types of Pickering emulsions (i.e., water-in-oil droplets for the polymersomes and oil-in-water droplets for the micelles). In contrast to single-phase experiments, the polymersome stability was not compromised and both nanoreactors showed similar conversions.

Finally, we studied the catalyst retention ability and recyclability of the nanoreactors in flow processes. While catalyst leaching was negligible for both nanoreactors at low rates, it increased at higher rates. In terms of catalyst retention polymersomes performed better than micelles.

Overall, these experiments have proven that the choice for polymersomes or micelles as nanoreactor has minimal effect on the catalytic performance of this specific reaction. Nonetheless, other features such as colloidal stability, emulsification features and protection against catalyst leaching should be taken into account when applying these nanoreactors in a specific experimental setup. Future studies related to other types of reactions and flow operations under more stringent conditions (*e.g.* higher temperature, solvent, etc.) could be an interesting extension of this research.

## **2.4. Experimental Section**

### **2.4.1 Methods and Materials**

All chemicals were used as received unless otherwise stated. For the block copolymer synthesis, poly(ethylene glycol) 4-cyano-4-(phenylcarbonothioylthio)pentanoate ( $\sim M_n = 2\text{kDa}$ ) was purchased from Sigma Aldrich, and used as RAFT macro-initiator. 2,2'-Azobis(2-methylpropanitrile) (AIBN) by Sigma Aldrich was used as a radical initiator. Styrene, vinyl benzyl chloride (4VBC), and sodium azide were obtained from Sigma Aldrich. Cyanine3 (Cy3) alkyne dye was purchased from Lumiprobe; Ultra-pure MilliQ water obtained from a Labconco Water Pro PS purification system (18.2 M $\Omega$ ) was used for the self-assembly and dialysis of both polymersomes and micelles. Dialysis membranes MWCO 3000 g mol<sup>-1</sup> Spectra/Por<sup>®</sup> were used to remove the excess of organic solvent or copper catalyst after cross-linking. For the spin filtration, Amicon Ultra-0.5 mL Centrifugal Filters Unit 10 kDa were purchased from Millipore.

For the ligand and catalyst preparation: *n*-buthyllithium, propargyl bromide and copper(II) trifluoromethanesulfonate (Cu(OTf)<sub>2</sub>) were obtained from Sigma Aldrich.

For the cross-linking: CuSO<sub>4</sub>·5H<sub>2</sub>O, sodium ascorbate and bathophenanthroline, sulfonated sodium salt were purchased from Sigma Aldrich. For the cyclopropanation reaction, styrene and ethyl diazoacetate (85% solution in dichloromethane) were obtained from Sigma Aldrich. Triethylene glycol dimethyl ether, methanol, dichloromethane (DCM), and all other solvents used were obtained from Biosolve Chemie. For the Pickering emulsions, toluene was purchased from Biosolve Chemie and Nile Red from Sigma Aldrich.

**Proton nuclear resonance (<sup>1</sup>H- and <sup>13</sup>C-NMR) spectroscopy:** <sup>1</sup>H- and <sup>13</sup>C-NMR spectra were recorded on a Varian Inova 400 spectrometer with CDCl<sub>3</sub> as a solvent and TMS as an internal standard.

**Gel permeation chromatography (GPC):** GPC was used to determine the molecular weights of the block copolymers. A Shimadzu Prominence GPC system equipped with a PL gel 5 μm mixed D column (Polymer Laboratories) and differential refractive index and UV (254 nm) detectors was used. THF was used as eluent with a flow rate of 1 mL min<sup>-1</sup>.

**Fourier Transform Infra-Red (FTIR) spectroscopy:** Infra-red emission of the liquid solution was measured using a Mettler Toledo FTIR equipped with a diamond probe. The occurrence of the cross-linking reaction was determined by observing the disappearance of the N<sub>3</sub> band (2094 cm<sup>-1</sup>).

**Transmission Electron Microscopy (TEM):** TEM images were recorded on a FEI Tecnai 20 (type Sphera) at 200 kV. 5 μL of the sample was dropped onto a carbon-coated copper grid (200 mesh, EM science). Samples were dried at ambient conditions overnight.

**Scanning Electron Microscopy (SEM):** SEM images were obtained using a Quanta 3D FEG (FEI, The Netherlands) with a field emission electron gun at 15 kV. All samples were diluted ten times with MilliQ. 5 μL of the diluted sample solution was drop-cast on a silicon wafer, which was previously washed in 70% EtOH and dried at room temperature overnight. Prior measurement, all samples were coated with gold via sputtering for 30 s at 60 mA using an EMITECH 575K coater.

**Dynamic Light Scattering (DLS):** DLS measurements were performed on a Malvern instrument Zetasizer (model Nano ZSP). Zetasizer software was used to process and analyse the data. The results are given as an average of 6 repetitions.

**Size Exclusion Chromatography (SEC):** For a more efficient separation of the different size micelles, a Shimadzu Prominence SEC system equipped with a Superose™ 6 column and a UV detector (220 nm) was used. The separation was performed using filtered PBS buffer at 0.6 mL min<sup>-1</sup>.

**Asymmetric flow field flow fractionation – light scattering (AF4-LS):** The AF4-LS experiments were performed on a Wyatt Eclipse AF4 instrument connected to Shimadzu LC-20A Prominence system with Shimadzu CTO20A injector.

The AF4 was further connected to the following detectors: a Shimadzu SPD20A UV detector, a Wyatt DAWN HELEOS II light scattering detector (MALS) installed at different angles (12.9 °, 20.6 °, 29.6 °, 37.4 °, 44.8 °, 53.0 °, 61.1 °, 70.1 °, 80.1 °, 90.0 °, 99.9 °, 109.9 °, 120.1 °, 130.5 °, 149.1 °, and 157.8 °) using a laser operating at 664.5 nm, a Wyatt Optilab Rex refractive index detector and a Quels detector installed at angle of 140.1°. The detectors were normalized using bovine serum albumin protein. The AF4 channel was pre-washed with a running solution of PBS, which was also used for the separation. The processing and analysis of the LS data and hydrodynamic radii calculations were performed using the Astra 7.1.2 software. All AF4 separations were performed on an AF4 short channel equipped with regenerated cellulose (RC) 10 kDa membrane (Millipore) and spacer of 350 µm. The method for the AF4 fractionation is described in Table S11<sup>23</sup>.

**Inductively Coupled Plasma Mass-Spectrometry (ICP-MS):** ICP-MS measurements were performed on a Thermo Fisher Scientific Xseries I quadrupole machine using 10.0 mL tubes containing 0.49 mg L<sup>-1</sup> InCl<sub>3</sub> solutions as an internal standard. 100 µL of polymersomes/ micelles were used in each measurement.

**Fluorescence measurements:** The fluorescence measurements were performed using 384-black well flat bottom microplates (Thermo Fisher Scientific-Nunclon) and a Tecan Spark 10M Multidetector Microplate Reader equipped with a 537 nm excitation filter and a 584 nm emission filter, bandwidth 20 nm, integration time 40 µs. For the determination of the Cy3 loading a calibration curve was used.

**Gas Chromatography (GC):** The measurements were performed on a Shimadzu GC2010+, containing an Agilent CP-Chiralsil-DEX CB column (25m, 0.32 mm ID, 0.25 µm DF) and equipped with an FID detector.

**Sonicators used for the emulsions:** For the cyclopropanation in Pickering emulsions, a Qsonica Sonicator Q500 (Qsonica Misonix, USA) was employed. All the controls and preliminary experiments were performed using an ultrasonic probe Jencons scientific LTD, Sonics & Materials.

**Optical Microscopy:** Optical images were acquired using an Olympus BX-51 microscope fitted with a DP70 digital camera.

**In-flow setup for leaching experiments:** A tubular reactor with a filter module: ID 0.5 mm, pore size 10 kDa, effective length 20.0 cm, total length 23.0 cm, surface area 28.0 cm<sup>2</sup> was purchased from Spectrum Lab<sup>®</sup> and used in the Cu-catalyst leaching test. The inlet was equipped with a peek ferrule (VWR<sup>®</sup>) to facilitate the syringe attachment to the tubular module.

## 2.5. Experimental procedures

### 2.5.1. Synthesis of PEG<sub>44</sub>-b-P(S<sub>115</sub>-4-VBA<sub>22</sub>) and PEG<sub>44</sub>-b-P(S<sub>70</sub>-4-VBA<sub>11</sub>) via RAFT polymerization

Both polymers were synthesized following a previously reported procedure<sup>4</sup>. For PEG<sub>44</sub>-b-P(S<sub>115</sub>-4-VBA<sub>22</sub>): in a flame dried Schlenk flask equipped with a magnetic stirrer, poly(ethylene glycol) 4-cyano-4-(phenylcarbonothioylthio) pentanoate (137 mg, 0.06 mmol, 1.0 equiv) was added with AIBN (2 mg, 0.012 mmol, 0.2 equiv), styrene (1.8 g, 17.3

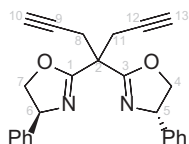
mmol, 288 equiv) and 4-VBC (326 mg, 1.92 mmol, 32 equiv). After addition of the reactants, the flask was capped with a rubber septum. The reaction mixture was degassed for 30 min using argon. Subsequently, the flask was transferred into a hot oil (80 °C) bath, and the reaction was allowed to stir for 32 h. The conversion was monitored using <sup>1</sup>H-NMR spectroscopy. The reaction was quenched by adding DCM (7 mL) and the product was precipitated by addition of cold methanol (50 mL) and subsequently filtered over a glass filter. 350 mg of the polymer was obtained after vacuum overnight. The final products were allowed to react with an excess of NaN<sub>3</sub> (666 mg, 10.2 mmol, 488 equiv) in DMF (2.5 mL) at room temperature for 3 days. At the end of the substitution reactions, the mixture was diluted with DCM (3 mL) and precipitated in cold methanol. The final product was analyzed by <sup>1</sup>H-NMR spectroscopy and GPC ( $M_n=16.7 \text{ kg mol}^{-1}$ ,  $\bar{D}=1.13$ ).

For the PEG<sub>44</sub>-*b*-P(S<sub>70</sub>-4-VBA<sub>11</sub>) the same procedure was used, 320 mg of the product was obtained after 24h reaction. The final product was analyzed by <sup>1</sup>H-NMR spectroscopy and GPC ( $M_n=10.9 \text{ kg mol}^{-1}$ ,  $\bar{D}=1.08$ ).

## 2.5.2. Preparation of polymersomes and micelles *via* solvent switch method

Polymersomes were prepared via the solvent switch methodology<sup>4</sup>. A 15 mL vial was equipped with a magnetic stirrer and PEG<sub>44</sub>-*b*-P(S<sub>115</sub>-4-VBA<sub>22</sub>) (20 mg) was dissolved in THF (2 mL) before capping the vial with a rubber septum. After 30 min under vigorous stirring (700 rpm) MilliQ water (2 mL) was added via a syringe pump (1 mL h<sup>-1</sup>)<sup>4</sup>. The preparation of micelles followed the same procedure as for the polymersomes, in this case the PEG<sub>44</sub>PS<sub>70</sub>VBA<sub>11</sub> polymer (20 mg) was used.

## 2.5.3. (4*S*,4'*S*)-2,2'-(Hepta-1,6-diyne-4,4-diyl)bis(4-phenyl-4,5-dihydrooxazole) (-BOX)



A solution of 2,2'-methylenebis[(4*S*)-4-phenyl-2-oxazoline] (2.03 g, 6.62 mmol) in dry THF (66 mL) was cooled to -60 °C and stirred vigorously. *n*-Buthyllithium (14.6 mmol, 9.10 mL of 1.6 M solution in hexanes, 2.2 equiv) was added dropwise over 15 min using a dropping funnel. After addition, the mixture was stirred for 1 h at -60 °C after which propargyl bromide (2.17 g, 14.6 mmol, 80 wt% solution in toluene, 2.2 equiv) was added dropwise using a dropping funnel. The reaction mixture was subsequently stirred for 4 h at -10 °C. After the reaction was quenched with sat aq. NH<sub>4</sub>Cl (50 mL), the product was extracted with Et<sub>2</sub>O (3 × 20 mL). The organic layers were combined, dried using MgSO<sub>4</sub> and concentrated *in vacuo*. Column chromatography (EtOAc/*n*-heptane, 0→30%, v/v) afforded compound BOX as a yellow solidified oil (1.89 g, 75%) **TLC** (EtOAc/*n*-heptane, 1:1, v/v):  $R_f = 0.56$ . **<sup>1</sup>H-NMR** (400 MHz, CDCl<sub>3</sub>)  $\delta$  7.44 – 7.25 (m, 10H), 5.30 (dd,  $J = 10.2, 8.1 \text{ Hz}$ , 2H), 4.74 (dd,  $J = 10.2, 8.4 \text{ Hz}$ , 2H), 4.20 (t,  $J = 8.3 \text{ Hz}$ , 2H), 3.30 (dd,  $J = 5.6, 2.7 \text{ Hz}$ , 4H), 2.13 (t,  $J = 2.6 \text{ Hz}$ , 2H). **<sup>13</sup>C-NMR** (101 MHz, CDCl<sub>3</sub>)  $\delta$  166.06, 141.78, 128.65, 127.72, 126.92, 79.23, 75.87, 71.60, 69.88, 45.15, 23.75. Data correspond to literature<sup>4</sup>.



#### 2.5.4. [(4S,4'S)-2,2'-(hepta-1,6-diyne-4,4-diyl)bis(4-phenyl-4,5-dihydrooxazole)]-copper(II) triflate (Cu-BOX)

BOX (50.0 mg, 0.13 mmol, 1.0 equiv) was added to a solution of Cu(OTf)<sub>2</sub> (47.3 mg, 0.13 mmol, 1.0 equiv) in anhydrous methanol (1.5 mL). After stirring for 24 h, the resulting product was separated by filtration, washed with methanol and dried under vacuum overnight to afford Cu-BOX (79 mg, 81.6%) as a green oil<sup>4</sup>.

#### 2.5.5. Cu-BOX cross-linking in polymersomes and micelles via CuAAC click chemistry

Following a previously reported procedure, polymersomes and micelles were crosslinked. A solution of Cu-BOX catalyst (100  $\mu$ L of a 12 mg mL<sup>-1</sup> solution in THF) was added to either a solution of polymersomes or micelles (10 mg mg<sup>-1</sup>). The cross-linking reaction was subsequently initiated by adding a solution containing CuSO<sub>4</sub>·5H<sub>2</sub>O (2.7 mg, 0.011 mmol), bathophenanthroline, sulfonated sodium salt (5.6 mg, 0.011 mmol) and sodium ascorbate (4.3 mg, 0.022 mmol) in MilliQ (200  $\mu$ L) to both reaction mixtures. The final solutions were then stirred (400 rpm) for three days at room temperature. To remove the excess of uncross-linked catalyst, both the solution of cross-linked polymersomes and micelles were dialysed in 1L MilliQ for 2 days (dialysis membrane MW 3000 g mol<sup>-1</sup>). The MilliQ was refreshed after 1h, and after 1 day. After dialysis, the final concentration of the cross-linked polymersomes or micelles was adjusted to be 10 mg mL<sup>-1</sup> by spin filtration (10kDa filters, 15 mins at 10000 rpm).

#### 2.5.6. Cy3-dye conjugation via CuAAC click chemistry

Pre-assembled polymersomes and micelles were first redispersed in a mixture of 50% vol THF and water. To the polymersome solution (250  $\mu$ L, 10 mg mL<sup>-1</sup>) or micelle solution (250  $\mu$ L, 10 mg mL<sup>-1</sup>), alkyne-functional Cy3-dye in THF (200  $\mu$ L of a 150  $\mu$ M solution in water) was added to the mixture. Thereafter, sodium ascorbate (200  $\mu$ L of a 0.5 mM solution in water) and CuSO<sub>4</sub>·5H<sub>2</sub>O (200  $\mu$ L of a 0.5 mM solution in water) were added to the mixture and the solution was left to stir (700 rpm) for 4 h. The excess of dye was removed by dialyzing for 2 days in 1L MilliQ(dialysis membrane MW 3000 g mol<sup>-1</sup>). MilliQ was refreshed after 1h and after 1 day. After dialysis, the final concentration of functionalized polymersomes or micelles was adjusted to be 10 mg mL<sup>-1</sup> by spin filtration (10kDa filters, 15 mins at 10000 rpm).

#### 2.5.7. Hydrophobic volume and surface area determination

The hydrophobic volume and surface area of the core of the micelles were calculated according to the volume and surface area of a sphere:  $V_{\text{hydrophobic}}=(4/3 \pi R^3)$  (1) and  $S_{\text{hydrophobic}}=(4 \pi R^2)$  (2). In (1) and (2) R is the radius of the hydrophobic portion. Using ImageJ®, the radius of 100 spherical cores was measured from analysis of TEM images and used in (1) and (2). As for the polymersomes, the hydrophobic volume corresponds to the volume of the entire

polymersome, of which the volume of the hydrophilic lumen is subtracted,  $V_{\text{hydrophobic}} = (4/3 \pi R_{\text{tot}}^3) - (4/3 \pi R_i^3)$  (3), with  $R_i = R_{\text{tot}} - R_{\text{membrane}}$ . By using ImageJ®, the radius of the total polymersome sphere ( $R_{\text{tot}}$ ) and the radius of the inner lumen ( $R_i$ ) were determined of 100 particles from analysis of TEM images. For the surface area calculation equation (2) was used.

### 2.5.8. Cyclopropanation reaction and workup (in single phase)

Catalytic polymersomes and micelles (1 mL sample  $10 \text{ mg mL}^{-1}$ ) were transferred to a 15 mL vial equipped with a stirring bar. Styrene (49.5 mg, 0.475 mmol, 5.0 equiv) was added, followed by ethyl diazoacetate (10.8 mg, 11.8  $\mu\text{L}$  of 85% solution in DCM, 0.095 mmol, 1.0 equiv). The reaction mixture was stirred for 10 min, after which the product was extracted with DCM. The resulting organic fraction was dried using sodium sulfate and concentrated *in vacuo*. The conversion of the reaction was measured using  $^1\text{H-NMR}$  after addition of 0.095 mmol of triethylene glycol dimethyl ether as the internal standard. (R)-Ethyl 2-phenyl cyclopropane carboxylate was isolated by column chromatography (EtOAc/heptane, 1→20%, v/v) and analyzed with  $^1\text{H-NMR}$  spectroscopy and by Chiral GC. The isolated yields reported in Figure 3 of the main text are for the mixture of *trans* and *cis* isomers.

### 2.5.9. Leaching and recycling experiments in flow

For the flow experiment a tubular reactor with a filter module: ID 0.5 mm, pore size 10 kDa, EL 20.0 cm, TL 23.0 cm, surface area  $28.0 \text{ cm}^2$  supplied by Spectrum Lab® was used. To facilitate the introduction of the particles in the membrane, the inlet was equipped with a peek ferrule (VWR®). A syringe pump was connected to the module, and water was flowed through the reactor length at different flow rates for 30 min. In each entry, 0.5 mL of the sample (either micelles or polymersomes) were loaded in the membrane reactor<sup>22</sup>. The samples were recollected using a syringe, and concentrated to the initial amount ( $10 \text{ mg mL}^{-1}$ ) via spin filtration (Amicon Ultra-0.5 mL Centrifugal Filter Unit 10 kDa). The samples were finally analysed using ICP-MS for the quantification of the retained copper.

### 2.5.10. Pickering Emulsion preparation and control emulsions

Control emulsions were prepared without polymersomes or micelles ( $10 \text{ mg mL}^{-1}$ ) by ultrasonication ( $t = 1 \text{ min}$ ,  $A = 40$ , pulse = 2 s) at different times of mixtures of water and toluene, water, toluene and styrene, and water, toluene and ethyl diazoacetate. The fraction of oil in the emulsion ( $\phi^o$ ) was 0.5 in all cases. The volumes of each compound used in the emulsions are given in Table S2. Clear phase separation was obtained one day after preparation in all cases indicating that neither of the reagents can stabilise the emulsion.

### 2.5.11. Cyclopropanation reaction and workup (in Pickering emulsion)

The reaction in Pickering emulsion was performed as described in the main text. The biphasic system was formed by mixing equal volumes of the two phases with an ultrasonic probe Qsonica Sonicator Q500 (Qsonica Misonix, USA) for 1 min in a 15 mL glass vial. The organic phase of the emulsion that was stabilized with micelle nanoreactors (1 mL of 10 mg mL<sup>-1</sup> solutions) contained 100 µL of styrene (0.872 mmol) and 25 µL of EDA (0.2 mmol) in toluene. In the case of the emulsion stabilized with polymersome nanoreactors, styrene (0.872 mmol) was dispersed in toluene and EDA (0.2 mmol) was added after emulsification to start the reaction. In both cases the glass vial was kept in an ice bath during sonication.

After the reaction, the emulsion was broken via centrifugation (3000 rpm, 5 min). The conversion of the reaction was measured using <sup>1</sup>H-NMR, with triethylene glycol dimethyl ether (0.2 mmol) as an internal standard. (R)-Ethyl 2-phenyl cyclopropane carboxylate was isolated using column chromatography (EtOAc/heptane, 1→20%, v/v) and analyzed with <sup>1</sup>H-NMR spectroscopy and Chiral GC<sup>4</sup>. The isolated yields reported in Figure 3 of the main text are for the mixture of *trans* and *cis* isomers.

### 2.5.12. Emulsion type validation

The emulsion type was confirmed through fluorescence microscope images (Rhodamine dye/Tetramethylrhodamine Isothiocyanate (TRITC)) filter) of the emulsion, in which the organic phase was dyed with Nile red. 6 µL of a 1·10<sup>-4</sup> M Nile Red solution in acetone was added to the toluene phase prior to homogenisation. Nile Red has a maximum excitation wavelength of 552 nm and a maximum emission wavelength of 636 nm in DMSO and methanol. The Rhodamine/TRITC filter has an excitation wavelength = 530-554 nm and an emission wavelength = 570 – 613 nm<sup>21</sup>.

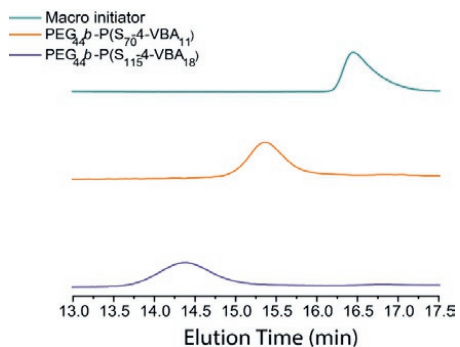
For the emulsion stability the amount of oil and water released was observed visually after 3 days and images of the vials were taken with a camera (Figure S7). The average droplet diameter was measured from optical microscope images taken at different times by measuring the diameter of at least fifty droplets with ImageJ (Figure S8).

## References

- 1 T. J. Davis, J. Balsells, P. J. Carroll and P. J. Walsh, *Org. Lett.*, 2001, **3**, 2161–2164.
- 2 S. E. Denmark, B. L. Christenson, D. M. Coe and S. P. O'Connor, *Tetrahedron Lett.*, 1995, **36**, 2215–2218.
- 3 Z. Fu, X. Li, Z. Wang, Z. Li, X. Liu, X. Wu, J. Zhao, X. Ding, X. Wan, F. Zhong, D. Wang, X. Luo, K. Chen, H. Liu, J. Wang, H. Jiang and M. Zheng, 2020, 2269–2277.
- 4 M. C. M. M. van Oers, L. K. E. A. E. A. Abdelmohsen, F. P. J. T. J. T. Rutjes and J. C. M. Van Hest, *Chem. Commun.*, 2014, **50**, 4040–4043.
- 5 T. Dwars, E. Paetzold and G. Oehme, *Angew. Chem. Int. Ed.*, 2005, **44**, 7174–7199.
- 6 K. Letchford and H. Burt, *Eur. J. Pharm. Biopharm.*, 2007, **65**, 259–269.
- 7 S. A. Dergunov, K. Kesterson, W. Li, Z. Wang and E. Pinkhassik, *Macromolecules*, 2010, **43**, 7785–7792.
- 8 L. Schoonen and J. C. M. van Hest, *Adv. Mater.*, 2016, **28**, 1109–1128.

- 9 Y. M. Chung and H. K. Rhee, *Catal. Letters*, 2003, **85**, 159–164.
- 10 N. Mase, Y. Nakai, N. Ohara, H. Yoda, K. Takabe, F. Tanaka and C. F. Barbas, *J. Am. Chem. Soc.*, 2006, **128**, 734
- 11 M. C. M. van Oers, W. S. Veldmate, J. C. M. van Hest and F. P. J. T. Rutjes *Polym. Chem.*, 2015, **6**, 5358
- 12 C. Duplais, A. Krasovskiy, A. Wattenberg and B. H. Lipshutz, *Chem. Commun. (Camb.)*, 2010, **46**, 562–564.
- 13 W. De Graaf, J. Bowsma and G. Van Koten, *Organometallics*, 1990, **9**, 1479–1484.
- 14 B. H. Lipshutz, N. A. Isley, J. C. Fennewald and E. D. Slack, *Angew. Chem. Int. Ed.*, 2013, **52**, 10952–10958.
- 15 D. E. Discher and A. Eisenberg, *Science (80-. )*, 2002, **297**, 967–973.
- 16 L. K. E. A. E. A. Abdelmohsen, M. Nijemeisland, G. M. Pawar, G.-J. A. J. A. Janssen, R. J. M. M. Nolte, J. C. M. M. van Hest and D. A. Wilson, *ACS Nano*, 2016, **10**, 2652–2660.
- 17 P. Song and H. Wang, *Adv. Mater.*, 2020, **32**, 1901244.
- 18 A. M. B. Rodriguez and B. P. Binks, *Soft Matter*, 2020, **16**, 10221–10243.
- 19 Z. Wang, M. C. M. van Oers, F. P. J. T. Rutjes and J. C. M. van Hest, *Angew. Chem. Int. Ed.*, 2012, **51**, 10746–10750.
- 20 K. Hu, J. Tang, S. Cao, Q. Zhang, J. Wang and Z. Ye, *J. Phys. Chem. C*, 2019, **123**, 9066–9073.
- 21 B. P. Binks and S. O. Lumsdon, *Langmuir*, 2000, **16**, 8622–8631.
- 22 M. T. De Martino, F. Tonin, N. A. Yewdall, M. Abdelghani, D. S. Williams, U. Hanefeld, F. P. J. T. Rutjes, L. K. E. A. Abdelmohsen and J. C. M. Van Hest, *Chem. Sci.*, 2020, **11**, 2765–2769.
- 23 J. Gigault, J. M. Pettibone, C. Schmitt and V. A. Hackley, *Anal. Chim. Acta*, 2014, **809**, 9–24.

## 2.6. Supplementary Figures and Tables



	N <sub>3</sub> %	Đ
PEG <sub>44</sub> b-P(S <sub>70</sub> -4-VBA <sub>11</sub> )	13.6	1.08
PEG <sub>44</sub> b-P(S <sub>115</sub> -4-VBA <sub>18</sub> )	13.5	1.13

**Figure S1:** : GPC traces of the PEG<sub>44</sub> macroinitiator (green), PEG<sub>44</sub>b-P(S<sub>70</sub>-4-VBA<sub>11</sub>) (orange), and PEG<sub>44</sub>b-P(S<sub>115</sub>-4-VBA<sub>18</sub>) (purple), respectively. On the right, the table displays the content of azide and the dispersity.

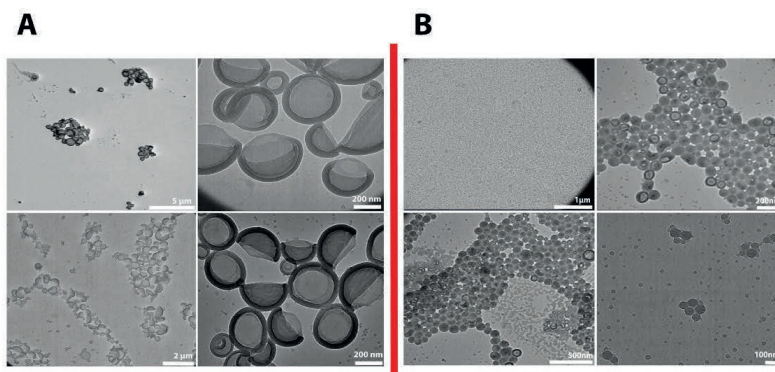


**Figure S2:** TEM images of cross-linked polymersomes **A)** and cross-linked micelles **B)** at different magnifications.

## Mean shape factors of micelles and polymersomes

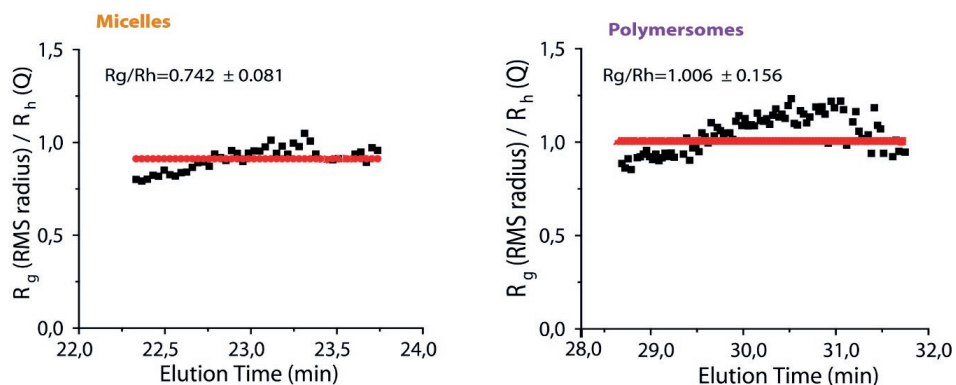


**Figure S3:** (Left) The ratio of the radius of gyration ( $R_g$ ) and the hydrodynamic radius ( $R_h$ ) of micelles. The red line represents the mean value of these ratios. (Right) The ratio of the radius of gyration ( $R_g$ ) and the hydrodynamic radius ( $R_h$ ) of polymersomes. The red line represents the mean value of these ratios.

**Table S1:** General methods for the AF4 analysis of nanoparticles. The flow conditions applied were the following: 1.2  $\text{mL min}^{-1}$  detector flow, 1.50  $\text{mL min}^{-1}$  focus flow and 0.20  $\text{mL min}^{-1}$  injection flow.

### Micelles:

Start time (min)	End time(min)	Mode	Crossflow start ( $\text{mL min}^{-1}$ )	Crossflow end ( $\text{mL min}^{-1}$ )
0	1	Elution	0.50	0.50
1	2	Focus	-	-
2	3	Focus + inject	-	-
3	4	Focus	-	-
4	19	Elution	0.50	0.50
19	22	Elution	0.50	0.00
22	37	Elution	0.00	0.00
37	38	Elution + inject	0.00	0.00
38	40	Elution	0.00	0.00

### Polymersomes:

Start time (min)	End time (min)	Mode	Crossflow start (mL min <sup>-1</sup> )	Crossflow end (mL min <sup>-1</sup> )
0	1	Elution	3.00	3.00
1	2	Focus	-	
2	3	Focus + inject	-	
3	4	Focus	-	
4	6	Elution	3.00	1.17
6	8	Elution	1.17	0.49
8	10	Elution	0.49	0.24
10	13	Elution	0.24	0.10
13	30	Elution	0.10	0.10
30	31	Elution	0.00	0.00
31	32	Elution + inject	0.00	0.00
32	37	Elution	0.00	0.00

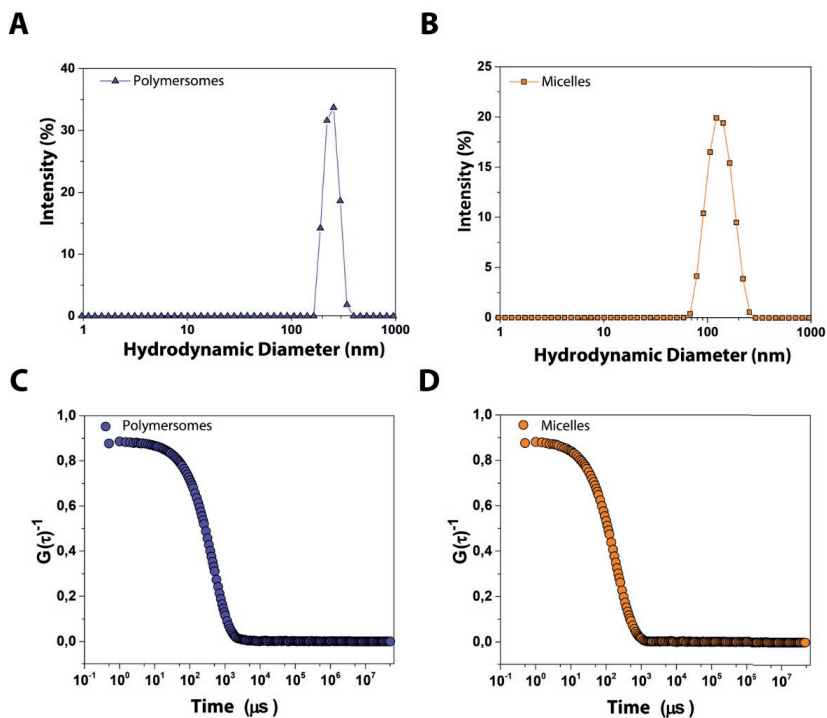


**Figure S4:** DLS intensity profile: **A)** cross-linked polymersomes and **B)** cross-linked micelles showing the hydrodynamic diameters  $D_H$ . **C)** and **D)** are the correlograms of cross-linked polymersomes and micelles, respectively. For the polymersomes:  $D_H$  at 25 °C is 345.2 nm and the polydispersity index  $PDI \sim 0.2$ . For the micelles, the  $D_H$  at 25 °C is 126.8 nm, and the  $PDI \sim 0.056$ .

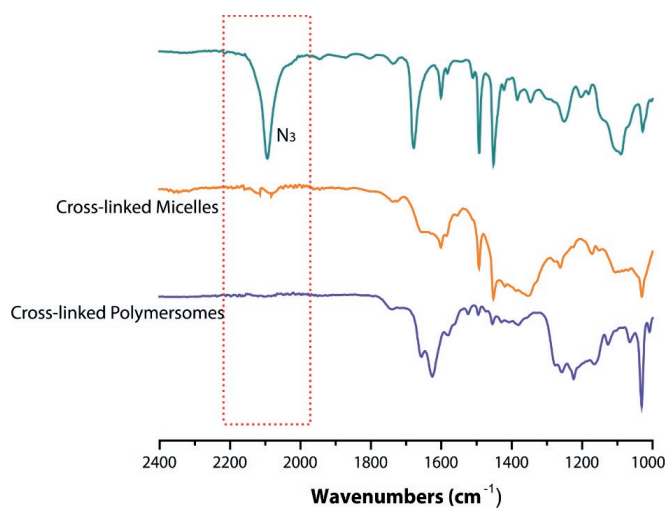




**Figure S5:** FTIR showing the disappearance of the  $N_3$  ( $2043\text{ cm}^{-1}$ ) band as a result of the CuAAC cross-linking reaction. Micelles before CuAAC (green curve). Cross-linked micelles (orange curve) and cross-linked polymersomes (purple curve) after the CuAAC reaction.

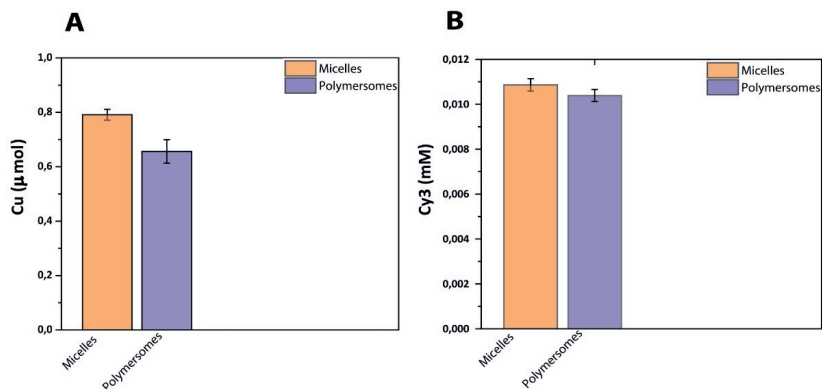


**Figure S6: A)** Amount of Cu ( $\mu\text{mol}$ ) in the micelles and polymersomes after cross-linking determined with ICP-MS. The amount of Cu ( $\mu\text{mol}$ ) is referred to  $100\ \mu\text{L}$  of sample ( $10\ \text{mg mL}^{-1}$ ) and is given as the average of 6 measurements. **B)** Concentration of Cy3 loaded in the samples determined by the absorbance, given as the average of 6 measurements. The results prove that both samples are able to load a similar amount of Cy3, regardless of their morphology.

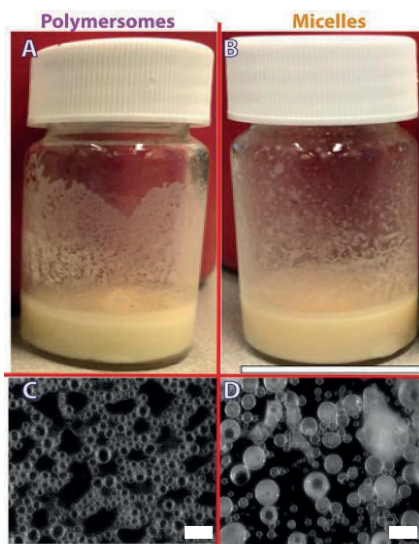


**Figure S7:** Appearance of Pickering emulsions prepared with equal volumes ( $2\ \text{mL}$ ) of an aqueous phase containing either: polymersomes or micelles and an organic phase consisting of **A)** styrene ( $100\ \mu\text{L}$ ,  $0.872\ \text{mmol}$ ) and EDA ( $25\ \mu\text{L}$ ,  $0.2\ \text{mmol}$ ) with polymersomes or **B)** styrene ( $100\ \mu\text{L}$ ,  $0.872\ \text{mmol}$ ) in toluene with micelles. In **B)** EDA ( $25\ \mu\text{L}$ ,  $0.2\ \text{mmol}$ ) was added after preparation of the emulsion. Images taken 30 min after preparation. Scale bar equal to  $2.5$

cm . **C**) and **D**) are optical microscope images of emulsions stabilised with **C**) polymersomes and **D**) micelles. Scale bar equal to 50  $\mu\text{m}$

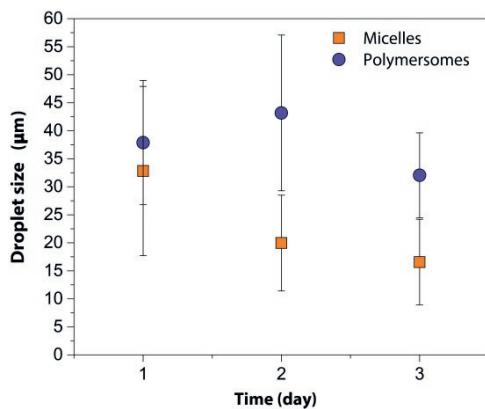


**Figure S8:** Average droplet diameter of the emulsions presented in Figure S7 at three different time points.

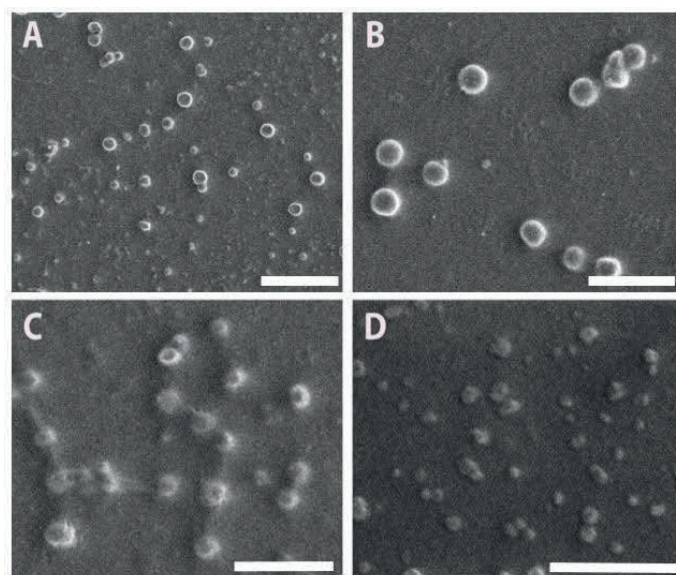


**Figure S9:** SEM images of the recovered (**A,B**) polymersomes and (**C,D**) micelles after reaction in Pickering emulsions at different magnifications. Scale bars equal to 10  $\mu\text{m}$ , 4  $\mu\text{m}$ , 4  $\mu\text{m}$  and 500 nm in (A), (B), (C) and (D), respectively.

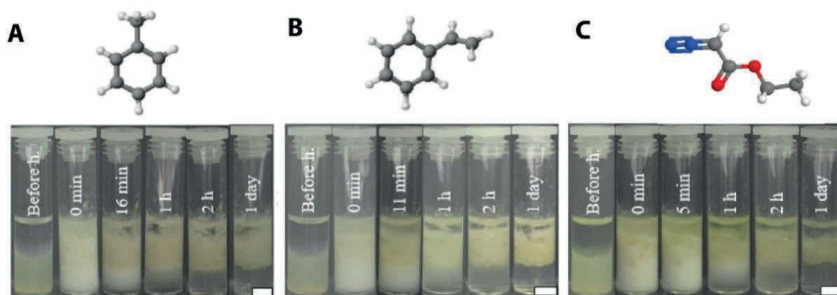
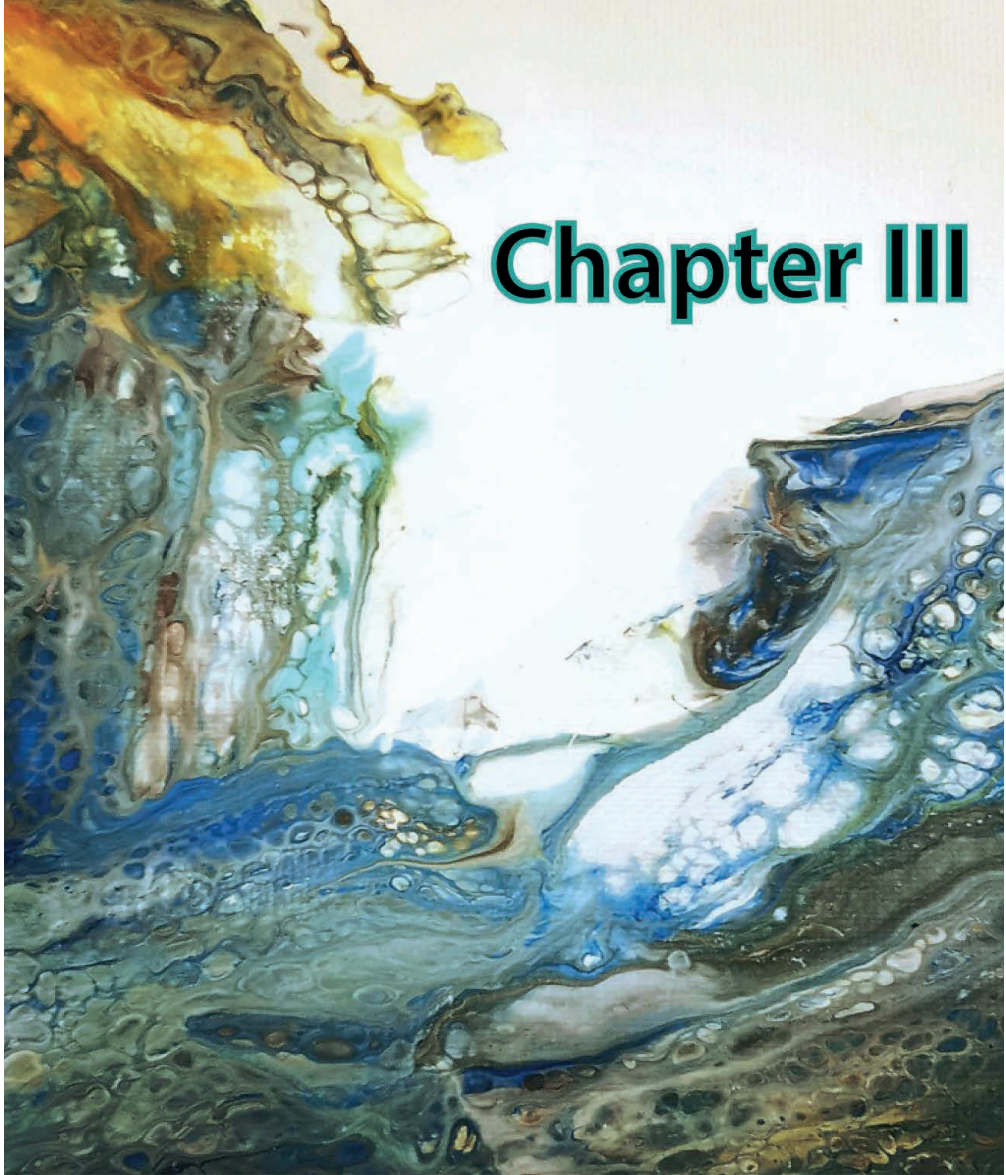


**Figure S10:** Visual of the control emulsions prepared by ultrasonication ( $t = 1$  min,  $A = 40$ , pulse = 2 s) at different times prepared between (A) water and toluene, (B) water and (toluene + styrene) and (C) water and (toluene + ethyldiazoacetate). The fraction of oil in the emulsion ( $\phi^o$ ) is 0.5 in all cases. The volumes of each compound used in each emulsion are given in Table S2. Scale bars equal to 0.45 cm. Clear phases were obtained 1 day after preparation in all cases indicating that neither of the reagents can stabilise the emulsion.

**Table S2.** Volumes of the different compounds used to prepare the control emulsion.

Compound	Volume/ $\mu\text{L}$		
	(A)	(B)	(C)
Milli-Q water	500	500	500
Toluene	500	494.72	421.81
Styrene	0	5.28	0
Ethyl diazoacetate	0	0	78.19



Dr. Victor Bloemendal, Paul van der Ven, Dr. Andrey Goryachev and Dr. Chenyue Zhang are kindly acknowledged for their contribution to this chapter.

# Designed ONE-FLOW system for the synthesis of Rufinamide

## Abstract

In this chapter, a one-flow, one-solvent procedure for the two-step synthesis of Rufinamide and an amide analogue is presented. The strategy introduced followed a combined computational and experimental approach. Using COSMO-RS<sup>1</sup> simulations a functional solvent was selected; the choice of solvent was based on its capacity to allow the reaction to take place in one phase at elevated temperatures, while upon cooling down it enabled the separation of the final product from the reaction mixture. Having found this optimal solvent, its appropriateness was investigated experimentally. The synthetic route encompassed an azidation of the starting benzyl chloride, followed by a Cu-catalyzed azide-alkyne cycloaddition (CuAAC) reaction to afford the desired products. To perform the azidation reaction and CuAAC effectively in a microfluidic system, both the azidation reagent and the Cu catalyst were immobilized, respectively on a packed bed and in the hydrophobic membrane of polymer vesicles, as this allowed a higher reaction efficiency and facile recovery of the metal catalyst thanks to compartmentalization. The packed-bed azidation reagent could furthermore be regenerated and reused several times without undesired cross-reactivity with the metal catalyst. Based on previously established systems, already discussed in Chapter II, a Cu-based catalyst immobilized in the hydrophobic membrane of polymersomes was employed for the CuAAC reaction. The innovative ONE-FLOW approach, in which computer-aided solvent selection is combined with reagent/catalyst compartmentalization in a continuous flow set up, is thought to have great benefits for the pharmaceutical industry in their quest for scalable, efficient, and safer synthetic processes with minimal waste generation.

## 3.1. Introduction

The process design for the synthesis of pharmaceuticals has attracted much attention over the years. One of the most intriguing developments has been the continuous end-to-end processing of medicines from raw material in one run, which even involved the connection with compounding/formulating equipment to deliver ready-to-use pills.<sup>2</sup> Chemists have in the past two decades expanded the concept of continuous microflow reactors, initially employed for a plethora of single chemical reactions, to a much broader choice of chemistries involving multi-step reactions in continuous-flow<sup>3</sup>, which has been coined flow chemistry.<sup>4-5</sup> Still, this process chain commonly needs to incorporate work-up steps in between the flow reactors, due to compatibility issues, which leads to a high number of reactor and separator units and complicated controller tasks, i.e. high system complexity.<sup>6,7</sup> This sequential arrangement of a series of flow equipment is also referred to as “vertical” hierarchy.<sup>8</sup>

To simplify the complicated and expensive production process, an alternative approach might be to employ an integrated reactor-separator unit that can cope with these issues.<sup>9,10</sup> The inspiration for this process design can be found in nature, specifically in living cells.<sup>11,12</sup> Each cell carries out a range of different processes within the same

environment and without the requirement of intermittent separation steps.<sup>11,13,14</sup> One of the reasons this is possible is because our cells are intrinsically compartmentalized (with their membranes and organelles). To distinguish this from the traditional flow process, this approach is coined 'horizontal' hierarchy<sup>8,15,16</sup>. By translating this concept to synthetic processes, reactors/separators can work simultaneously, thereby reducing the time-complexity of a process; the key element of this novel approach is thus compartmentalization.<sup>13,17,18</sup>

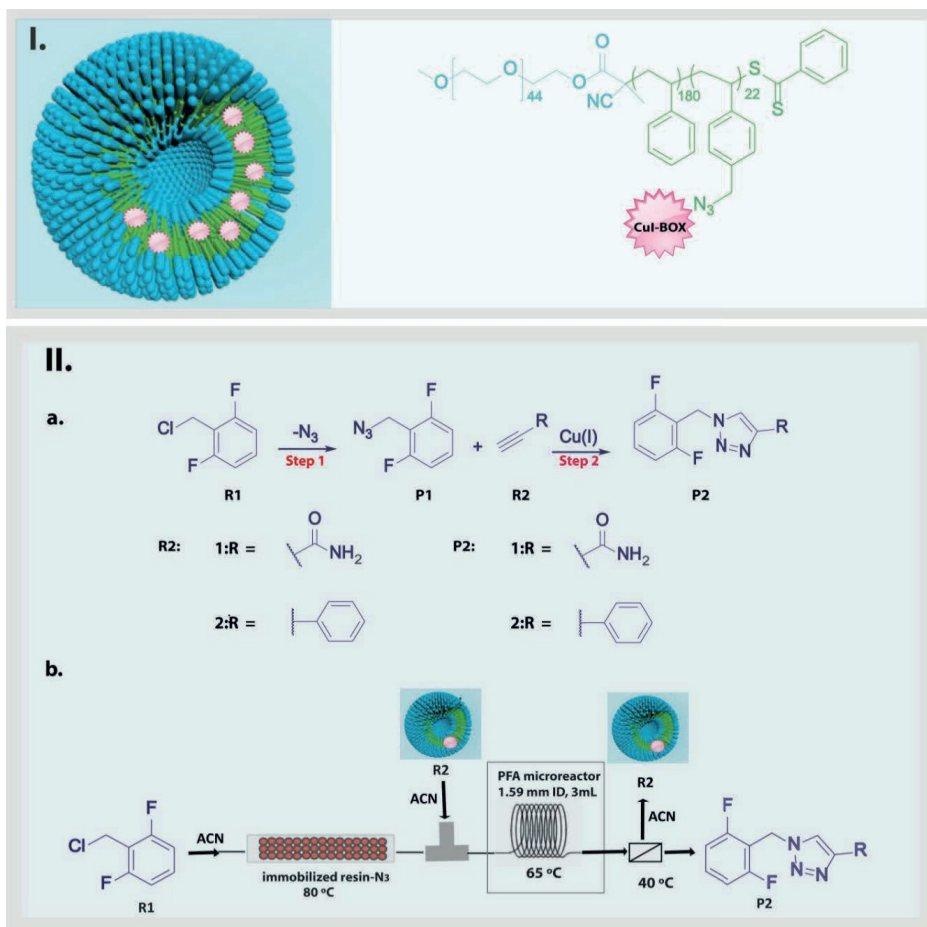


**Figure 1- I.** Schematic representation of a cross-linked polymersome; the bis-oxazoline ligand complexed with Cu(I) (Cu(I)-BOX, pink) is attached to the azide groups in the hydrophobic bi-layer (green), which is composed of block copolymer PEG<sub>44</sub>-*b*-P(S<sub>180</sub>-VBA<sub>22</sub>); - **II. a.)** Reaction scheme for the 2-step Rufinamide synthesis. **b.)** Integration of the two-step synthesis in a one-flow process for the preparation of Rufinamide and a triazole analogue. The resin used is an Amberlite® IRA400 functionalized with -N<sub>3</sub>. The residence time for the optimized process was 1h at 0.1 mL min<sup>-1</sup>

Compartmentalization can be achieved in different ways. First of all, particulate systems can be used to physically separate different catalysts involved in the process and to facilitate catalyst and product separation after the reaction has been completed. Especially catalysts immobilized in nanosized compartments combine the benefits of homogeneous catalysis, i.e. high accessibility, with ease of separation from the product flow. Secondly, functional solvents<sup>19,20</sup> can be employed. The solvent plays in this case a dual role, in the sense that it provides a homogeneous solution for the reaction to take place, whereas the final product is separated from the reaction mixture, for example via a temperature trigger. This 'Green Spaciant Solvent Factory' will fluidically open and close interim reaction compartments to facilitate orthogonality during the reaction, recycling of catalysts and reactants, purification of products and to ensure activity and stability of the catalysts. Combining these compartmentalization strategies allows the development of flow cascade processing, which ideally needs just one reactor passage ('ONE-FLOW').

As a case study, in this chapter the synthesis of Rufinamide (**1**) and its analogue 1-(2,6-difluorobenzyl)-4-phenyl-1*H*-1,2,3-triazole (**2**) (Figure 1-II.a.) were chosen<sup>9,21,22</sup>. The current production of Rufinamide and its amide analogue requires multiple steps, with high-energy consumption and extended operation times. Meanwhile, sustainability issues such as reagent and catalyst recovery are in most published papers still not addressed.<sup>9</sup> In our design we have proposed a system, which is meant to simplify the whole cascade of reactors and separators traditionally used, to a one-flow operation leading directly to the purified solid product. This is achieved by the selection of a functional solvent, screened by COSMO-RS<sup>1,20,23</sup>, which enables a selective separation of the product simply by temperature variation, and a designed catalytic nanoreactor based on cross-linked polymer vesicles (Figure 1-II.b.), which facilitates catalyst recycling.<sup>24-25</sup> The latter will be the main focus of this chapter.

## 3.2. Results and discussion

### 3.2.1. Optimization of reaction conditions

The synthesis of Rufinamide and analogue **2** consists of two parts. First, the benzyl chloride is azidated, followed by a Huisgen cycloaddition reaction catalyzed by Cu(I) (CuAAC).<sup>10</sup> For the first part of the reaction, the synthesis of 2,6-difluorobenzyl azide in a continuous flow process, an azide-functional resin (resin-N<sub>3</sub>) was prepared using an ion exchange process in batch for 6 hours<sup>26</sup> (as described in the experimental section), resulting in an azide loading capacity of 3.9 mmol g<sup>-1</sup>. Then, a packed-bed was made of the resin-N<sub>3</sub> in a flow device, and the synthesis of 2,6-difluorobenzyl azide from 2,6-difluorobenzyl chloride (**R1**) was executed. When the temperature was 80 °C, the resin-N<sub>3</sub> reactor reached quantitative conversion at flow rates of 0.1 ml min<sup>-1</sup> starting with 1 mol L<sup>-1</sup> of 2,6-difluorobenzyl chloride. Using the same initial feed of **R1** and decreasing the temperature to 65 °C, conversions of 87% were obtained. When the flow rate was increased to 0.15 ml min<sup>-1</sup> at 80 °C, the conversion still reached 97% .

The resin could be recovered easily and reused up to at least 3 times with similar conversions (Figure 2b). Therefore, 0.1 ml min<sup>-1</sup> and 80 °C were defined as optimal conditions for the azidation step.

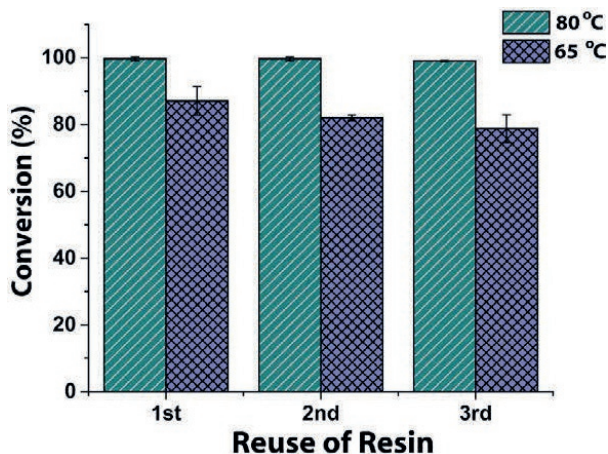


**Figure 2-** Azidation of benzyl chloride with resin-N<sub>3</sub> at different temperatures and different runs, with 0.1 ml min<sup>-1</sup> flow rate. The plot reports the conversion obtained when the N<sub>3</sub>-Resin was reused three times, the total volume of benzyl chloride passed through the resin bed at the optimized conditions was 18 mL (6mL per each use). This resulted in a total production of 2,6-difluorobenzyl azide of 0.0179 mol at 80°C (average conversion 99.5 ±0.4%) and 0.0148 mol at 65°C (average conversion 82.6 ±3.1%).

For the second reaction, Cu(I)-bis(oxazoline)<sup>27</sup> (Cu(I)-BOX) loaded cross-linked polymersomes (Cu(I)-PLs) were employed as a nanosized reactor and separator. The objective of introducing polymersomes in the microflow process was to integrate the two-step synthetic procedure into one step, and to protect the Cu(I)-BOX catalyst positioned in the bilayer membrane from undesired interactions with the resin-N<sub>3</sub>. Functionalized polymersomes were successfully applied previously at room temperature in a batch reactor,<sup>24</sup> but were never exploited before in a CuAAC reaction toward the synthesis of pharmaceuticals, using elevated temperatures and pure organic solvent. For the polymersome preparation, first the polymer building block was constructed using reversible addition fragmentation chain transfer (RAFT) polymerization using a poly(ethylene glycol) macroinitiator and styrene and vinyl benzyl chloride as the monomers for the hydrophobic part. Subsequently, the chlorides were replaced by azides via a nucleophilic substitution reaction. The PEG<sub>44</sub>-*b*-(PS<sub>180</sub>-VBA<sub>22</sub>) polymer was assembled using the solvent switch method as previously reported in this thesis (Chapter II), which led to the formation of well-defined polymersomes. Using the azide anchor, the bisoxazoline ligand with two alkyne moieties was incorporated via CuAAC to stabilize the polymer membrane via a cross-linking reaction – as already discussed for the nanoreactors in Chapter II – and to provide a ligand for the loading with Cu(I). A high Cu(I)-BOX catalyst loading (5 mol%) in the polymersomes was achieved by incubating the polymersome solution twice with Cu(I)-BOX. The excess of the unbound catalyst was removed using dialysis (4 days in total). The final Cu content in the loaded polymersomes (Cu(I)-PLs) was 0.035 mol



L<sup>-1</sup> (Figure S3). The polymersome morphology, copper distribution, and oxidation state were determined under reaction conditions (Figure S6).

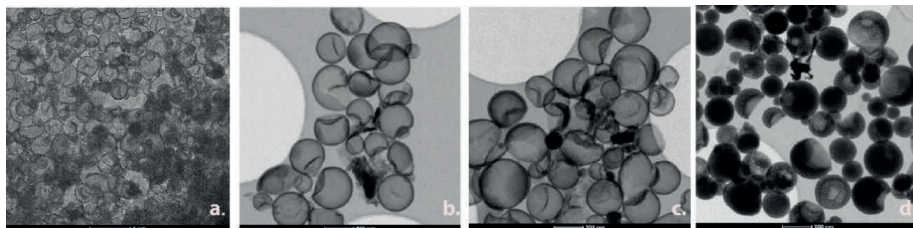


**Figure 3-** TEM images showing the CuI-BOX loading optimization. **a.)** A fresh solution of polymersomes (diluted to 1 mg mL<sup>-1</sup>) before cross-linking. Scale bar is 1 μm **b.)** and **c.)** cross-linked polymersomes (first loading of CuI-BOX). The darker spots on the membrane are attributed to the presence of the loaded catalytic species. The scale bar is 500nm. **d.)** cross-linked polymersomes (second loading with CuI-BOX). The dark contrast of the polymersome membrane is a result of the increased catalyst loading. The scale bar is 500nm.

The functional solvent was selected to be ACN. Based on COSMO-RS simulation, this solvent proved to be optimal with regard to a change in solubility of the product when lowering the temperature (Table S1). In order to set the optimal conditions in terms of temperature and stability with the solvent, the polymersomes were dispersed in ACN and the size and polydispersity were measured with DLS overnight using a flow cell. Temperature stability was determined by analyzing the polymersomes before cross-linking by varying the temperature between 20-70 °C either in water or in ACN (Figure 4A-4B). For the samples after cross-linking and loading with Cu(I) a temperature range between 20-90 °C was used in pure ACN (Figure 4C and 4D-S7). From this analysis 60-65 °C was found to be the optimal temperature as the cross-linked Cu(I)-PLs kept their integrity.

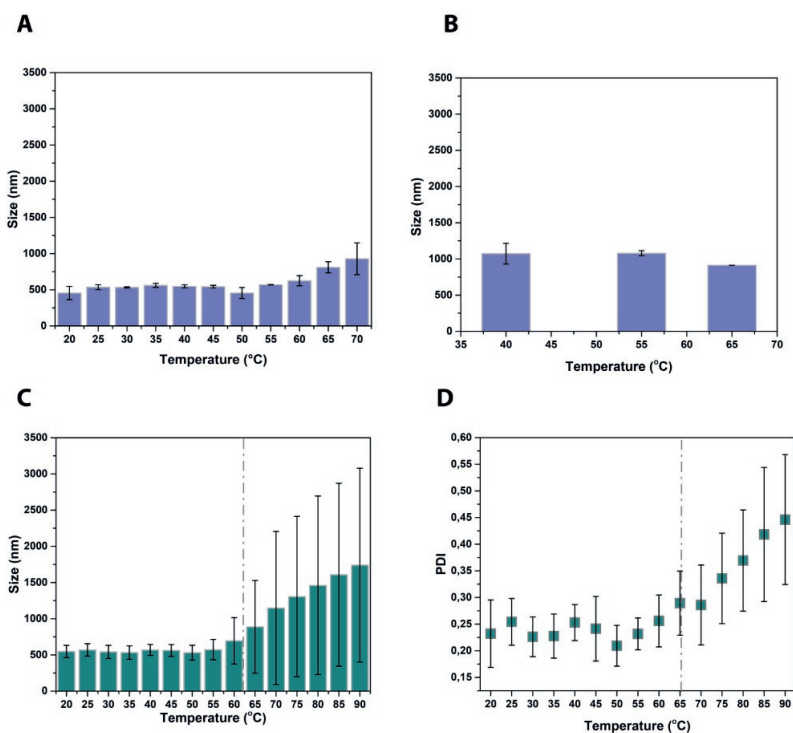


**Figure 4- A)** Size change with temperature for un-crosslinked polymersomes in water; above 55 °C the size increased with approximately 300 nm from the initial value. **B)** Un-crosslinked polymersomes in 100% ACN showed severe destabilization of the vesicles with evident deformation already at 40°C where the size of the polymersomes was doubled. **C) and D)** display respectively the size dependency with temperature increase and the PDI for crosslinked Cu(I)-PLs in ACN.

Next, the polymersomes were employed for the CuAAC reaction. First, this reaction was executed in batch at 80°C to examine the effect of type of catalyst, solvent, and reaction time on conversion. The Cu(I)- PLs were compared with Cu(I) powder and the homogeneous Cu(I)-BOX (Table 1).

**Table 1-** Optimization of the batch reaction conditions at 80°C with [R2] = 2 mol L<sup>-1</sup>.

Entry	Solvent	Catalyst	R	t [min]	Yield [%]
1	ACN	CuI powder	Phenyl	120	89
2	ACN	Cu(I)-BOX	Phenyl	120	89
3	1:1= ACN: H <sub>2</sub> O	Cu(I)-PLs	Phenyl	120	-
4	ACN	Cu(I)-PLs	Phenyl	120	86
5	DMSO	Cu(I)-PLs	Phenyl	120	90
6	ACN	Cu(I)-PLs	Phenyl	60	86
7	ACN	Cu(I)-PLs	Phenyl	30	72
8	ACN	Cu(I) powder	Amide	30	95
9	ACN	Cu(I)-PLs	Amide	30	93
10	ACN	Cu(I)-PLs	Amide	15	93
11	ACN	Cu(I)-PLs	Amide	5	82

From the results, it is evident that the polymersomes performed at least equally well as the Cu powder or the homogeneous BOX catalyst. Furthermore, as expected, the reaction toward Rufinamide (employing propiolamide) was considerably faster than the reaction with phenylacetylene. It is worth mentioning that the experiment performed using water as a co-solvent was not successful. This could be possibly caused by the increased polarity that makes the bilayer membrane of the polymersomes less accessible to reagents. After the reaction was completed, the reaction mixture was cooled down to r.t. (in 10 mins), and gratifyingly, for all reactions that were performed in pure ACN, the product crystallized out and could be conveniently collected from the bottom of the vials. This demonstrates a good agreement with the COSMO-RS prediction. Furthermore, in the case of the reaction with phenylacetylene, the polymersomes were effectively retrieved in the ACN layer, which contained mostly residual reactants and approximately 8 % of product **2**. In the case of Rufinamide, due to the faster reaction time and lower solubility compared to **2**, only 15 mins reaction were needed for full conversion and product precipitation already occurred after 2 mins of cooling. The fast crystallization led to some entrapment of polymersomes in the product. This could be further purified by washing out the polymersomes with a second aliquot of ACN. The isolated Rufinamide yield was 93%, with 4 % of product retained in the organic layer.

### 3.2.2. Integration of reaction steps into a ONE-FLOW process

To integrate both reaction steps in a ONE-FLOW setup, first, the polymersomes and reagents were passed over the packed-bed of resin- $N_3$ , to synthesize **2**. The conditions that were used were a reaction temperature of  $65^\circ\text{C}$  (to prevent polymersome deformation), and a flow rate of  $0.1\text{ ml min}^{-1}$ . A total of  $7\text{ mmol}$  2,6-difluorobenzyl chloride ( $1\text{ mol L}^{-1}$ ), phenylacetylene ( $2\text{ mol L}^{-1}$ ) and  $5\text{ mol}\%$  Cu(I)-PLs were passed through the resin- $N_3$  reactor which was loaded with  $14\text{ mmol}$   $N_3$ . This process only led to the isolation of the intermediate 2,6-difluorobenzyl azide ( $60\%$  conversion); the absence of precipitation upon cooling to room temperature indicated that the formation of product **2** was less effective. The triazole product was still dissolved in the reaction mixture and the crystalline product could be isolated after solvent evaporation (Figure 6). Most probably, the polymersomes were adsorbed in the first fraction of the resin and therefore not capable to effectively interact with the benzyl azide for the CuAAC reaction.

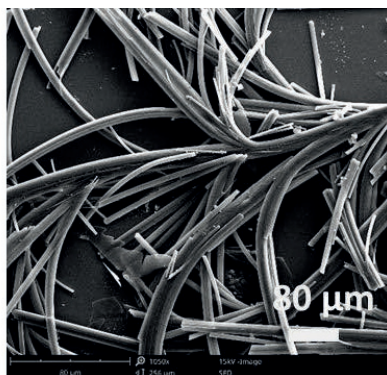


**Figure 6.** SEM analysis of the crystallized product after formation of **2** using phenylacetylene as R2. The crystalline product is obtained after evaporation of ACN from the reaction mixture.

To prevent adsorption of the polymersomes on the resin, a mixture of dispersed polymersomes and alkyne R2 was introduced into the one-flow system after the azidation of R1 ( $1\text{ mol L}^{-1}$ ). The product was collected in a heated vessel at  $40^\circ\text{C}$  to prevent the crystallization in the reactor, which would lead to clogging. Several experiments were performed to find the optimal conditions for both synthetic steps (Table 3). When  $1\text{ mol L}^{-1}$  of benzyl chloride were passed through the micro-reactor and  $0.2\text{ mL min}^{-1}$  was selected as flow rate with a residence time of 14 min, this yielded  $89\%$  of desired triazole product **2** (entry 2, table 3). For the synthesis of Rufinamide, the concentrations of the starting compounds had to be lowered by a factor of three ( $0.66\text{ mol L}^{-1}$ ) to achieve a homogeneous phase during the flow reaction (entry 5, table 3). Using a flow rate of  $3.2\text{ ml min}^{-1}$  and a residence time of approximately 1 min, gratifyingly, Rufinamide was obtained in  $87\%$  yield. This demonstrates that the combined functional solvent

approach and catalyst compartmentalization strategy work very well in effectively performing a cascade reaction in flow, without intermediate purification steps.

**Table 3-**Rufinamide yields for the one-flow process with optimized conditions at 65°C.

Entry	R	R2 Feed [mol L <sup>-1</sup> ]	Flow Rate [mL min <sup>-1</sup> ]	Yield [%]
1	Phenyl	2	0.1	87
2	Phenyl	2	0.2	89
3	Phenyl	2	0.4	83
4	Amide	0.66	1.6	90
5	Amide	0.66	3.2	87
6	Amide	0.66	6.4	81

### 3.3. Conclusion

We have successfully introduced an integrated reactor-separator concept combining nano-compartmentalized catalysts with a functional solvent system. The synthesis of Rufinamide was chosen as the model reaction and the conceptual approach of a “designed micro-nano one-flow system” was verified via the selected functional solvent acetonitrile and the application of Cu(I)-loaded polymersomes. This chapter shows that the combination of a functional solvent and the use in a continuous setup of catalytic polymeric nanoreactors can lead to an improvement in the process (e.g. by reducing the number of steps of a synthetic procedure) and can enable a rapid separation of the product, while a full conversion is still ensured. The final aim is to intensify multiple-step cascade reactions and separations by fully integrating them in an automatic one-flow process. This will increase the attractiveness of flow chemistry as a synthetic modality for scalable and cost-efficient pharmaceutical processes.

### 3.4. Experimental Section

#### 3.4.1. Materials and Methods

All chemicals were used as received unless otherwise stated. For the block copolymer synthesis, poly(ethylene glycol) 4-cyano-4-(phenylcarbonothioylthio)pentanoate ( $\sim M_n$  2000 g mol<sup>-1</sup>) was used as RAFT macro-initiator and

purchased from Sigma Aldrich.  $\text{NaN}_3$  obtained from Sigma Aldrich was used for both the polymer functionalization and for the preparation of the resin. Ultra pure MilliQ water obtained from a Labconco Water Pro PS purification system (18.2 M $\Omega$ ) was used for the polymersome self-assembly and dialysis. Dialysis Membranes MWCO 3000 g mol<sup>-1</sup> Spectra/Por® were used to remove the excess of organic solvent, or copper catalyst after cross-linking. For the cross-linking,  $\text{CuSO}_4 \cdot 5\text{H}_2\text{O}$ , sodium ascorbate and bathophenanthroline, sulfonated sodium salt were obtained from Sigma Aldrich. Amberlite® IRA400 chloride form (mesh 16–50) was used for the azide resin preparation and purchased from Sigma Aldrich. Amicon Ultra-0.5 mL Centrifugal Filter Unit 3 kDa, Ultrafree-MC centrifugal filters 0.1  $\mu\text{m}$  were purchased from Millipore.

**Proton nuclear magnetic resonance spectroscopy (<sup>1</sup>H-NMR):** <sup>1</sup>H-NMR spectra were recorded on a Varian Inova 400 spectrometer with  $\text{CDCl}_3$  as a solvent and TMS as internal standard.

**Gel permeation chromatography (GPC):** GPC was used to determine the molecular weights of the block copolymer. A Shimadzu Prominence GPC system equipped with a PL gel 5  $\mu\text{m}$  mixed D column (Polymer Laboratories) and differential refractive index and UV (254 nm) detectors was used. THF was used as an eluent with a flow rate of 1 mL min<sup>-1</sup>.

**Transmission Electron Microscopy (TEM):** TEM images were recorded on a FEI Tecnai 20 (type Sphera) at 200 kV. 5  $\mu\text{L}$  of sample was dropped onto a carbon-coated copper grid (200 mesh, EM science). Samples were dried at ambient conditions overnight.

**Scanning Electron Microscopy (SEM):** SEM images were obtained with a Quanta 3D FEG (FEI, The Netherlands) with a field emission electron gun at 10kV-15kV. All samples were diluted ten times with ultrapure MilliQ water. 5  $\mu\text{L}$  of the diluted solution was drop cast on a silicon wafer, which was first washed in 70% EtOH and dried for 24h. The samples were then gold sputter coated for 30 seconds at 60 mA in an EMITECH 575K coater.

**Dynamic Light Scattering (DLS):** DLS measurements were performed on a Malvern instrument Zetasizer (model Nano ZSP) equipped with a flow cell. Zetasizer software was used to process and analyse the data. The results are given as average of 6 repetitions on 6 samples measured overnight.

**X-Ray Photoelectron Spectroscopy (XPS):** XPS spectra were acquired on a Thermo Scientific K-Alpha spectrometer using an Al K $\alpha$  ( $h\nu = 1486.6$  eV) monochromatic small-spot X-ray source. Charging effects were corrected by using the adventitious carbon C1s (sp<sup>3</sup>) peak as reference for all samples at a binding energy (BE) of 284.8 eV. Fitting of the spectra (BE, FWHM, peak shape, asymmetry, number of species) was performed with CasaXPS® software, version 2.3.16. Samples were drop cast onto a silicon wafer in a glow box before measurements.

**Inductively Coupled Plasma Mass-Spectroscopy (ICP-MS):** ICP-MS measurements were performed on a Thermo Fisher Scientific Xseries I quadrupole machine using 10.0 mL tubes containing 0.49 mg L<sup>-1</sup>  $\text{InCl}_3$  solutions as internal standard. 100  $\mu\text{L}$  of polymersomes (10 mg mL<sup>-1</sup>) were used in each measurement.

### 3.5. Experimental procedures

#### 3.5.1. Synthesis of PEG<sub>44</sub>-*b*-P(S<sub>180</sub>-*co*-4-VBA<sub>22</sub>) via RAFT polymerization

In a flame dried Schlenk flask equipped with a magnetic stirrer, poly(ethylene glycol) 4-cyano-4-(phenylcarbonothioylthio) pentanoate ( $\sim M_n$  2000 g mol<sup>-1</sup>) (137 mg, 0.06 mmol, 1.0 eq) was added with AIBN (2 mg, 0.012 mmol, 0.2 eq), styrene (1.8 g, 17.3 mmol, 288eq) and 4-vinyl benzyl chloride (4-VBC, 326 mg, 1.92 mmol, 32 eq). After the addition of the reactants, the flask was capped with a septum and two needles were inserted to allow for degassing (ca. 30mins). The reaction was initiated by immersing the reaction mixture in an oil bath at 80 °C under stirring for 28h, conversion was monitored by <sup>1</sup>H-NMR spectroscopy. The reaction was quenched by adding 3 mL of DCM and the product was purified in cold methanol. The final product was dried *in vacuo* overnight, yielding 350 mg of polymer ( $M_n$  = 24.02 kg mol<sup>-1</sup>,  $\bar{D}$  = 1.04)

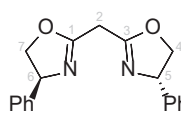
The final product was allowed to react with an excess of NaN<sub>3</sub> (666 mg, 10.2 mmol, 488 equiv) in 2.5 mL of DMF at room temperature for 3 days. At the end of the substitution reaction, the mixture was diluted with DCM and precipitated in cold methanol. The final product was analyzed by <sup>1</sup>H-NMR spectroscopy and GPC ( $M_n$  = 24.2 kg mol<sup>-1</sup>,  $\bar{D}$  = 1.1) .

#### 3.5.2. Preparation of PEG<sub>44</sub>-*b*-P(S<sub>180</sub>-*co*-4-VBA<sub>22</sub>) polymersomes

Polymersomes were prepared via a solvent switch method. A 15 mL vial was equipped with a magnetic stirrer and 20 mg of polymer were dissolved in 2 mL of THF before capping the vial with a rubber septum. After 30 minutes under vigorous stirring (700 rpm) 2 mL of MilliQ water were added by a syringe pump (1 mL h<sup>-1</sup>).<sup>25</sup>

#### 3.5.3. Synthesis of bisoxazoline ligands

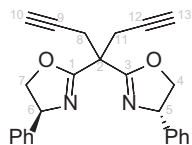
##### 2,2'-methylenebis[(4*S*)-4-phenyl-2-oxazoline]



Diethyl malonimidate dihydrochloride (346 mg, 1.50 mmol) and (*S*)-phenyl glycinol (412 mg, 3.00 mmol) were dissolved in CHCl<sub>3</sub> (15 mL) and stirred for 16 h at rt. The reaction was diluted with sat. aq. NaHCO<sub>3</sub> (10 mL), and extracted with DCM (3 × 10 mL). The organic layers were collected and concentrated *in vacuo* to afford the product as a yellow solidified oil (454 mg, 99%). TLC (EtOAc/*n*-heptane, 1:1, v/v): R<sub>f</sub> = 0.21 <sup>1</sup>H NMR (500 MHz, CDCl<sub>3</sub>) δ 7.23 – 7.11 (m, 10H, 10 × CH phenyl), 5.11 (dd, J = 9.9, 7.8 Hz, 2H, H-5, H-6), 4.53 (dd, J = 10.2, 8.4 Hz, 2H, H-4a, H-7a), 4.02 (t, J = 8.2 Hz, 2H, H-4b, H-7b), 3.44 (s, 2H, H-2). <sup>13</sup>C NMR (126 MHz, CDCl<sub>3</sub>) δ 163.06 (C-1, C-3),

142.09 (2 × C<sub>quart</sub>-Ph), 128.72 (4 × C-Ph), 127.61 (2 × C-Ph), 126.67 (4 × C-Ph), 75.33 (C-4, C-7), 69.72(C-5, C-6), 28.40 (C-2). Data correspond to literature<sup>25</sup>

#### (4*S*,4'*S*)-2,2'-(Hepta-1,6-diyne-4,4-diyl)bis(4-phenyl-4,5-dihydrooxazole) (BOX)



A solution of 2,2'-methylenebis[(4*S*)-4-phenyl-2-oxazoline] (2.03 g, 6.62 mmol) in dry THF (66 mL) was cooled to -60 °C and stirred vigorously. *n*-Butyllithium (14.6 mmol, 9.10 mL of 1.6 M solution in hexanes) was added dropwise over 15 min using a dropping funnel. After addition, the mixture was stirred for 1 h at -60 °C after which propargyl bromide (2.17 g, 14.6 mmol, 80 wt% solution in toluene) was added dropwise using a dropping funnel. The reaction mixture was subsequently stirred for 4 h at -10 °C. After the reaction was quenched with sat aq. NH<sub>4</sub>Cl (50 mL), the product was extracted with Et<sub>2</sub>O (3 × 20 mL). The organic layers were combined, dried using MgSO<sub>4</sub> and concentrated *in vacuo*. Column chromatography (EtOAc/*n*-heptane, 0→30%, v/v) afforded compound **BOX** as a yellow solidified oil (1.89 g, 75%) **TLC** (EtOAc/*n*-heptane, 1:1, v/v): R<sub>f</sub> = 0.56. **<sup>1</sup>H NMR** (400 MHz, CDCl<sub>3</sub>) δ 7.44 – 7.25 (m, 10H, 10 × CH phenyl), 5.30 (dd, J = 10.2, 8.1 Hz, 2H, H-5, H-6), 4.74 (dd, J = 10.2, 8.4 Hz, 2H, H-4a, H-7a), 4.20 (t, J = 8.3 Hz, 2H, H-4b, H-7b), 3.30 (dd, J = 5.6, 2.7 Hz, 4H, 2 × H-7, 2 × H-10), 2.13 (t, J = 2.6 Hz, 2H, H-9, H-12). **<sup>13</sup>C NMR** (101 MHz, CDCl<sub>3</sub>) δ 166.06 (C-1, C-3), 141.78 (2 × C<sub>quart</sub>-Ph), 128.65 (4 × C-Ph), 127.72 (2 × C-Ph), 126.92 (4 × C-Ph), 79.23 (C-2), 75.87 (C-4, C-7), 71.60 (C-10, C-13), 69.88 (C-5, C-6), 45.15 (C-9, C-12), 23.75 (C-8, C-11). Data correspond to literature<sup>25</sup>

#### 3.5.4. [(4*S*,4'*S*)-2,2'-(hepta-1,6-diyne-4,4-diyl)bis(4-phenyl-4,5-dihydrooxazole)]-copper(I) iodine (CuI-BOX)

**BOX** (100.0 mg, 0.26 mmol, 1.0 equiv) was added to a solution of CuI (51 mg, 0.26 mmol, 1.0 equiv) in anhydrous methanol (1.5 mL). After stirring for 24 h, the resulting product was separated by filtration, washed with methanol and dried under vacuum overnight to afford Cu(I)-BOX (135 mg, 89.9%) as an oil<sup>25</sup>.

#### 3.5.5. CuI-BOX cross-linking via CuAAC click chemistry (CuI-PLs)

A solution of Cu(I)-BOX catalyst (100 μL of a 12 mg mL<sup>-1</sup> solution in THF) was added to 2 mL of a 10 mg mL<sup>-1</sup> polymersome solution. The cross-linking reaction was initiated by subsequently adding CuSO<sub>4</sub>·5H<sub>2</sub>O (2.7 mg, 0.011 mmol), bathophenanthroline, sulfonated sodium salt (5.6 mg, 0.011 mmol) and sodium ascorbate (4.3 mg, 0.022 mmol) dissolved in MilliQ (200 μL) to the vial. The final solution was then stirred (400 rpm) for three days at room temperature. To remove the excess of un-crosslinked catalyst, the solution of cross-linked polymersomes was



dialyzed against 1L MilliQ for 3 days (dialysis membrane MW 3000 g mol<sup>-1</sup>). The MilliQ was refreshed after 1h, and after 1 day. After dialysis the final concentration was adjusted to 10 mg mL<sup>-1</sup> by spin filtration (10kDa filters, 15 mins at 10000 rpm). Procedure was adapted from<sup>28</sup>.

### 3.5.6. Cul-BOX loading optimization (2<sup>nd</sup> loading Cul-PLs)

To a Cul-BOX cross-linked polymersome solution (10 mg mL<sup>-1</sup>) prepared as indicated in 3.5.5. a second aliquot of Cul-BOX catalyst (100  $\mu$ L of a 20 mg mL<sup>-1</sup> solution in THF) was added, the resulting solution was left stirring for 24h. In order to remove the excess of THF and Cul-BOX the final sample was dialysed against water for 24h and the concentration was adjusted to 10 mg mL<sup>-1</sup> by spin filtration.

### 3.5.7. Resin preparation

The azide supported amberlite resin was prepared via ion exchange using 10% NaN<sub>3</sub> aqueous solution following a previously reported methodology<sup>26</sup>. 2 grams of Amberlite <sup>®</sup> IRA400, chloride form (mesh 16–50) were stirred for 6 h in an aqueous solution of 10% NaN<sub>3</sub> (100 mL). After 6h, the solid was washed and filtered several times with water; it was then stirred for an additional 5 min and finally decanted. The washing procedure was repeated several times until no azide was detected in the supernatant liquid.

### 3.5.8. Flow experiments

The flow experiments were carried out in the designed setup shown in the main text (Figure 1,IIb). The concentrations in all the experiments correspond to 1 mol L<sup>-1</sup> for **R1** and 2 mol L<sup>-1</sup> for **R2** unless clearly specified in the main text. R1 was introduced in the flow reactor *via* a syringe pump and passed over the fixed bed reactor containing the azide-resin (at 80 °C). The outlet of the reactor was connected to a T-junction which allowed for the mixing of the azidation product with **R2** and catalytic polymersomes needed for the second step. The combined flows were introduced into the microreactor where the second reaction took place (65 °C). The outflow of the microreactor was collected in a separation vessel (40°C), in which **P2** was allowed to crystallize. Polymersomes were separated from the reaction mixture by using spin filtration.

## 3.6. COSMO-RS

A list of solvents from the COSMO-RS database (ver. C30\_1801, COSMOlogic) was selected and generated in an output excel file; this selection included in total 11957 species. The desired candidates were selected from the generated file using solubility as the selection parameter<sup>29</sup>. The desired solubility  $\log_{10}(x_j)$  ( $\log S$ ) was calculated from the difference between the chemical potentials of the solute in the solvent  $\mu_j^{solvent}$  and in the pure solute  $\mu_j^{pure}$ .  $\Delta G_{j, fus}$  is defined as the Gibbs free energy of fusion.  $\Delta G_{j, fus}$  is zero for liquid solutes

and has to be given or estimated for solid compounds (eq. S1)<sup>29</sup>. The obtained solubilities showed the following relation:

$$\log_{10}(x_j) = \log_{10}\left[\exp\left(\frac{\mu_j^{\text{pure}} - \mu_j^{\text{solvent}} - \Delta G_{j,\text{fus}}}{RT}\right)\right] \quad (\text{S1})$$

Other chemical and physical properties and the environmental/economic effect of solvents were considered to narrow the selection, also taking into account the inertness and availability of the solvent. Finally, acetonitrile (#27 Table S1) was recognized as the top solvent and its suitability was validated with solubility tests.

## References

- 1 A. Klamt, F. Eckert and W. Arlt, *Annu. Rev. Chem. Biomol. Eng.*, 2010, **1**, 101–122.
- 2 B. Gutmann, D. Cantillo and C. O. Kappe, *Angew. Chem. Int. Ed.*, 2015, **54**, 6688–6728.
- 3 J. C. Pastre, D. L. Browne and S. V. Ley, *Chem. Soc. Rev.*, 2013, **42**, 8849–8869.
- 4 S. V. Ley, *Chem. Rec.*, 2012, **12**, 378–390.
- 5 M. B. Plutschack, B. Pieber, K. Gilmore and P. H. Seeberger, *Chem. Rev.*, 2017, **117**, 11796–11893.
- 6 A. Adamo, R. L. Beingessner, M. Behnam, J. Chen, T. F. Jamison, K. F. Jensen, J. C. M. Monbaliu, A. S. Myerson, E. M. Revalor, D. R. Snead, T. Stelzer, N. Weeranoppanant, S. Y. Wong and P. Zhang, *Science (80-. )*, 2016, **352**, 61–67.
- 7 S. Mascia, P. L. Heider, H. Zhang, R. Lakerveld, B. Benyahia, P. I. Barton, R. D. Braatz, C. L. Cooney, J. M. B. Evans, T. F. Jamison, K. F. Jensen, A. S. Myerson and B. L. Trout, *Angew. Chem. Int. Ed.*, 2013, **52**, 12359–12363.
- 8 D. F. Rivas, E. Castro-Hernández, A. L. Villanueva Perales and W. van der Meer, *Chem. Eng. Process. Process Intensif.*, 2018, **123**, 221–232.
- 9 S. Borukhova, T. Noël, B. Metten, E. De Vos and V. Hessel, *Green Chem.*, 2016, **18**, 4947–4953.
- 10 S. B. Semenovna, *Flow Reactor Networks for integrated synthesis of active pharmaceutical ingredients*, 2016.
- 11 C. M. Agapakis, P. M. Boyle and P. A. Silver, *Nat. Chem. Biol.*, 2012, **8**, 527–535.
- 12 C. G. Palivan, R. Goers, A. Najer, X. Zhang, A. Car and W. Meier, *Chem. Soc. Rev.*, 2016, **45**, 377–411.
- 13 H. Lee, W. C. DeLoache and J. E. Dueber, *Metab. Eng.*, 2012, **14**, 242–251.
- 14 M. B. Quin, K. K. Wallin, G. Zhang and C. Schmidt-Dannert, *Org. Biomol. Chem.*, 2017, **15**, 4260–4271.
- 15 R. E. Lawrence and R. Zoncu, *Nat. Cell Biol.*, 2019, **21**, 133–142.
- 16 R. W. Klemm and P. Carvalho, *Mol. Biol. Cell*, 2020, **31**, 401–402.
- 17 A. Lu and R. K. O'Reilly, *Curr. Opin. Biotechnol.*, 2013, **24**, 639–645.
- 18 M. T. De Martino, L. K. E. A. Abdelmohsen, F. P. J. T. Rutjes and J. C. M. Van Hest, *Beilstein J. Org. Chem.*, 2018.

- 19 C. Zhang, Z. Song, C. Jin, J. Nijhuis, T. Zhou, T. Noël, H. Gröger, K. Sundmacher, J. van Hest and V. Hessel, *Chem. Eng. J.*, 2020, **385**, 123399.
- 20 O. O. Wahab, L. O. Olasunkanmi, K. K. Govender and P. P. Govender, *Theor. Chem. Acc.*, 2019, **138**, 80.
- 21 S. Chatterjee, M. Guidi, P. H. Seeberger and K. Gilmore, *Nature*, 2020, **579**, 379–384.
- 22 D. Ott, S. Borukhova and V. Hessel, in *Green Chemistry*, Royal Society of Chemistry, 2016, vol. 18, pp. 1096–1116.
- 23 A. Klamt, J. Schwöbel, U. Huniar, L. Koch, S. Terzi and T. Gaudin, *Phys. Chem. Chem. Phys.*, 2019, **21**, 9225–9238.
- 24 M. C. M. Van Oers, L. K. E. A. Abdelmohsen, F. P. J. T. Rutjes and J. C. M. Van Hest, *Chem. Commun.*, 2014, **50**, 4040–4043.
- 25 M. T. De Martino, F. Tonin, N. A. Yewdall, M. Abdelghani, D. S. Williams, U. Hanefeld, F. P. J. T. Rutjes, L. K. E. A. Abdelmohsen and J. C. M. Van Hest, *Chem. Sci.*, 2020, **11**, 2765–2769.
- 26 M. Keshavarz, N. Iravani, A. Ghaedi, A. Z. Ahmady, M. Vafaei-Nezhad and S. Karimi, *Springerplus*, 2013, **2**, 1–8.
- 27 A. K. Ghosh, P. Mathivanan and J. Cappiello, *Tetrahedron Asymmetry*, 1998, **9**, 1–45.
- 28 M. C. M. M. van Oers, L. K. E. A. E. A. Abdelmohsen, F. P. J. T. J. T. Rutjes and J. C. M. M. Van Hest, *Chem. Commun.*, 2014, **50**, 4040–4043.
- 29 F. Eckert, A. Klamt, COSMOtherm User's Manual, version C2. 1, Release 01.05; COSMOlogic GmbH & Co, KG: Leverkusen, Germany (2005).

### 3.7. Supporting Figures and Tables

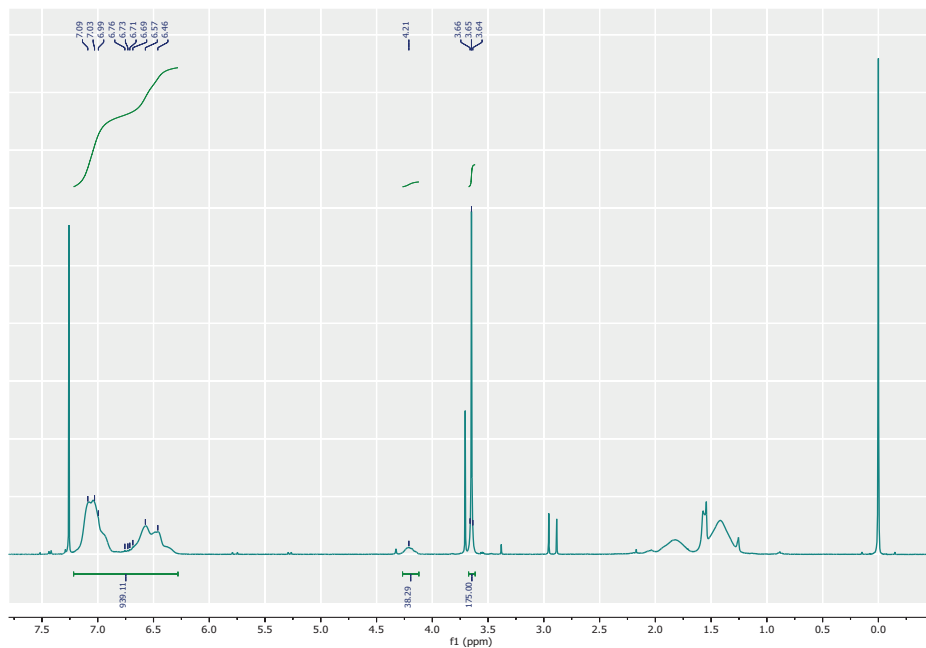


Figure S1- <sup>1</sup>H-NMR spectrum of PEG<sub>44</sub>-b-P(S<sub>180</sub>-co-4-VBA<sub>22</sub>) 400 MHz, CDCl<sub>3</sub>

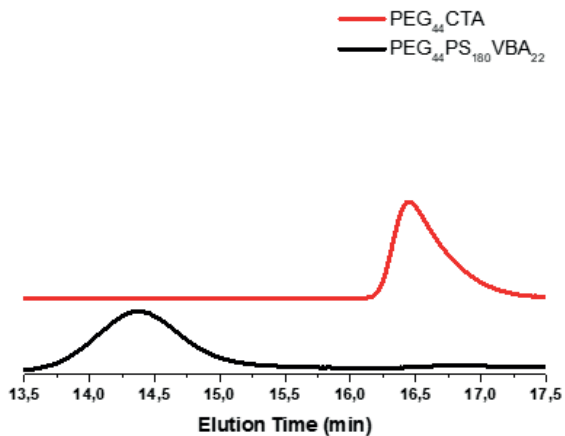
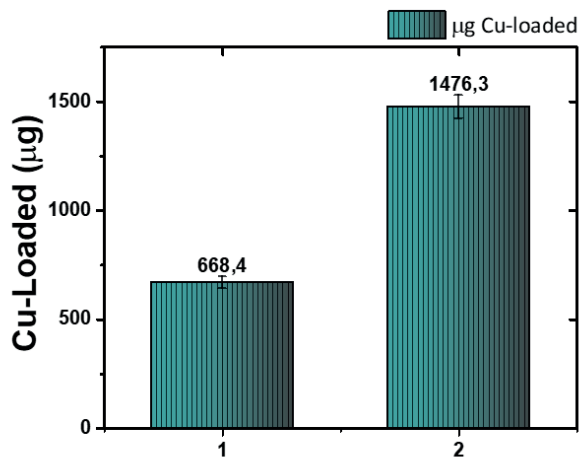
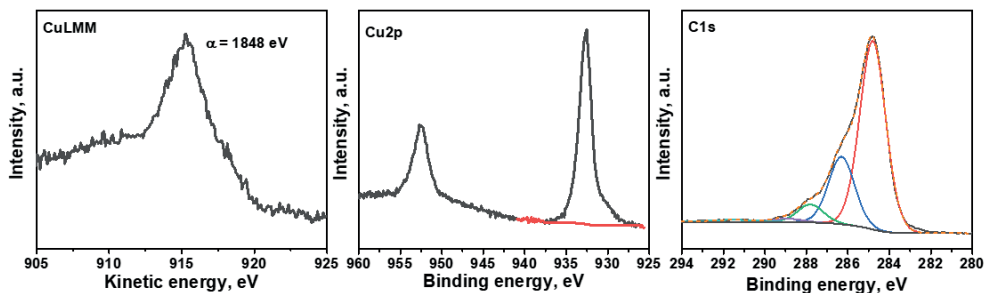


Figure S2-GPC traces of the polymer and of the macroinitiator (PEG<sub>44</sub>CTA).



**Figure S3-** The optimization of the loading steps was achieved monitoring the amount of copper loaded with ICP-MS in 100  $\mu\text{L}$  of the polymersomes ( $10 \text{ mg mL}^{-1}$ ) after dialysis. The bar plot reports the measured Cu ( $\mu\text{g}$ ) after each loading step and after purification.



**Figure S4:** XPS spectroscopy on the free CuI-BOX catalyst, showing the presence of only Cu(I) as oxidation state. Cu(I) undergoes easily oxidation to Cu(II), however the formation of the complex stabilized the oxidation state, which was maintained during the cross-linking as well.

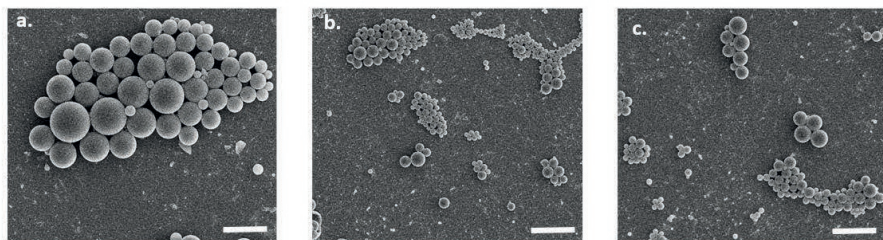


**Figure S5-** SEM images of polymersomes before cross-linking. Scale bars correspond to: 500 nm (a), 4  $\mu\text{m}$  (b), 2  $\mu\text{m}$  (c).

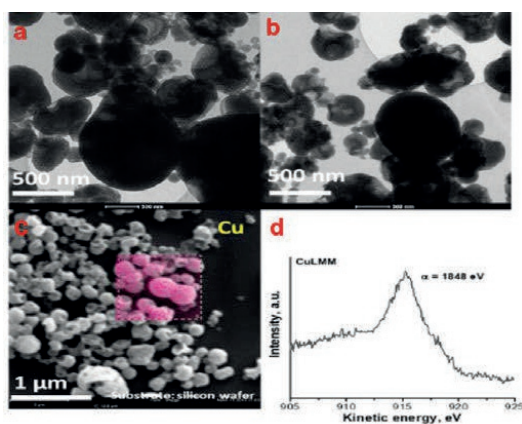


**Figure S6-** a) TEM Crosslinked Cu(I) polymersomes in water. b) TEM Crosslinked Cu(I) polymersomes after 2 hrs in ACN at 65°C. The scale bar is 500nm. c) SEM Phenom EDX elemental analysis for Cu identification, proving the presence of Cu (pink) in the polymersome membrane. The scale bar is 1  $\mu\text{m}$  d) XPS analysis of Cu (I) on the cross-linked polymersomes proving the oxidation state of the copper is maintained to (I)

#### COSMO-RS

**Table S1.** Substrate solubility in top 37 solvents

No.	Solvent Name	$\log_{10}(x_{r2\_25})$	$\log_{10}(x_{r1\_25})$	$\log_{10}(x_{p2\_25})$	$\log_{10}(x_{p2\_65})$
1	glycidylaldehyde	-0.935	-0.473	-2.256	-1.463
2	1,3-dioxolan-2-one	-0.725	-0.963	-2.207	-1.432
3	beta-propiolactone	-0.759	-0.498	-2.178	-1.408
4	formaldehyde	-0.681	-0.159	-1.746	-0.991

---

5	propylenecarbonate	-0.777	-0.435	-2.214	-1.468
6	3h-furan-2-one	-0.901	-0.497	-2.167	-1.421
7	trans-butenedial	-0.755	-0.572	-2.125	-1.384
8	methyloxalate	-0.806	-0.167	-2.135	-1.405
9	chinone	-0.897	-0.359	-2.163	-1.433
10	5-methylene-2(5h)-furanone	-0.944	-0.448	-2.212	-1.485
11	cis-butenedial	-0.732	-0.672	-2.059	-1.335
12	furazolidone	-0.693	-0.999	-2.186	-1.463
13	ethyleneglycoldiformate	-0.741	-0.603	-2.065	-1.346
14	n-methylmaleimide	-0.869	-0.303	-2.183	-1.464
15	1,3,5,7-tetroxane	-0.586	-0.658	-2.211	-1.495
16	(4s)-solerone	-0.622	-0.383	-2.185	-1.472
17	(4r)-solerone	-0.610	-0.380	-2.176	-1.466
18	cyanoaceticacidmethylester	-0.949	-0.925	-2.200	-1.493
19	2,5-dihydro-2-methyl- thiophene-1,1-dioxide	-0.641	-0.395	-2.166	-1.460
20	divinylsulfone	-0.724	-0.574	-2.122	-1.420
21	propionitrile	-0.850	-0.071	-2.170	-1.470
22	4-oxo-2-pentenal	-0.679	-0.284	-2.105	-1.406
23	2,5-dihydrothiophenesulfone	-0.515	-0.656	-2.063	-1.367
24	2,5-dihydro-3- methylthiophene-1,1-dioxide	-0.595	-0.377	-2.123	-1.429

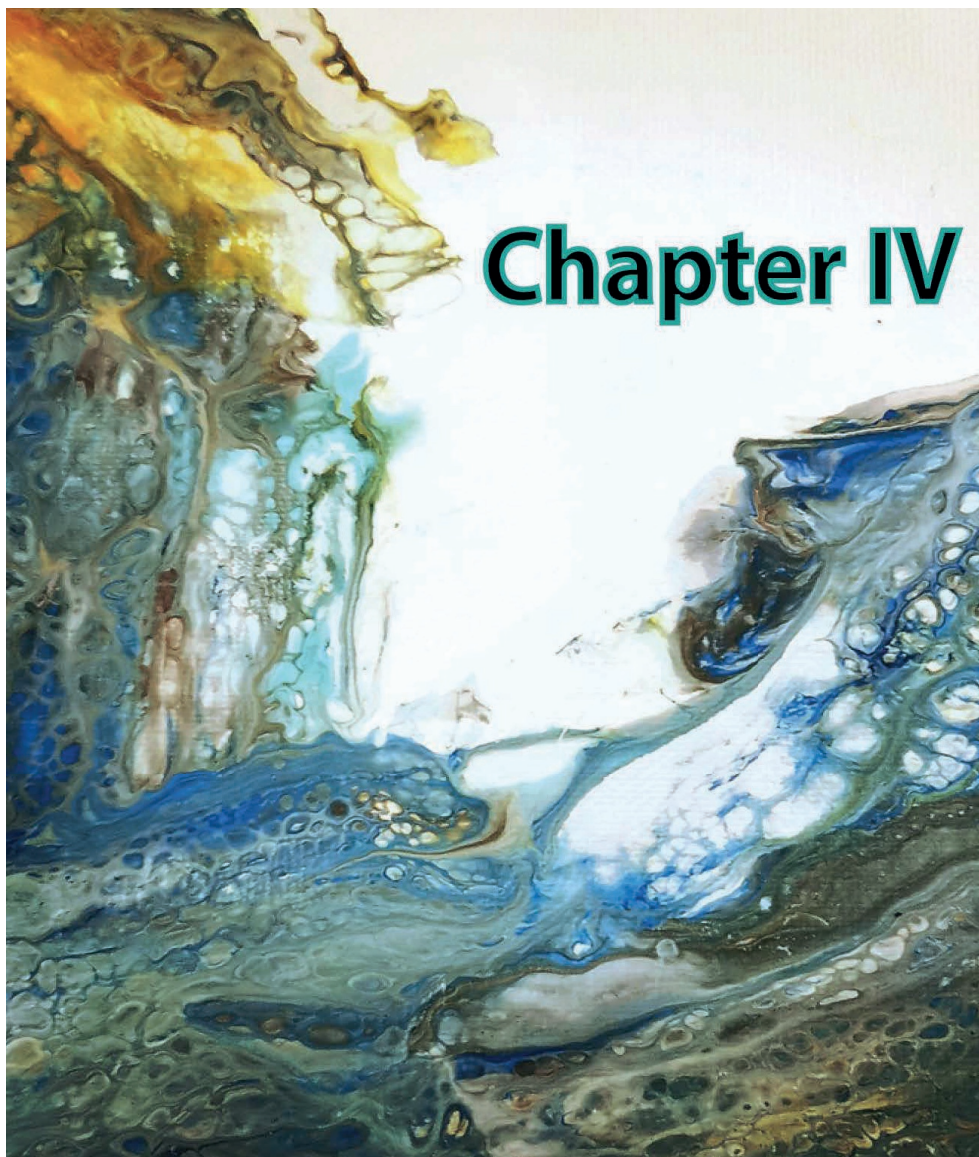
---

---

25	methylformate	-0.748	-0.148	-1.959	-1.266
26	2,2-dimethyl-1,3-dioxane-4,6-dione	-0.787	-0.629	-2.108	-1.415
27	acetonitrile	-0.635	-0.506	-1.974	-1.284
28	2-coco-furylfuran	-0.932	-0.492	-2.159	-1.473
29	3-(5-nitro-2-furyl)-2-propenal	-0.841	-0.483	-2.004	-1.322
30	dilactide(dl)	-0.903	-0.639	-2.069	-1.387
31	1,3-dimethylbarbituricacid	-0.619	-0.472	-2.052	-1.372
32	2-methylene-4-butanolide	-0.646	-0.141	-2.103	-1.427
33	1,3-cyclohexanedione	-0.561	-0.329	-2.104	-1.430
34	e,e-2,4-hexadienedial	-0.542	-0.441	-2.038	-1.366
35	glutaraldehyde	-0.542	-0.215	-2.096	-1.426
36	trans-3-hexene-2,5-dione	-0.652	-0.141	-2.144	-1.475
37	4-nitropyridine-1-oxide	-0.779	-0.668	-1.876	-1.209
38	ethanol	-0.851	-0.793	-2.150	-1.489

---





This Chapter is published as “*Compartmentalized cross-linked enzymatic nano-aggregates (c-CLEnA) for efficient in-flow biocatalysis*” *Chem. Sci.*, 2020,11, 2765-2769.

J. Lopes, Dr. Fabio Tonin, dr. Amy Yawdall and dr. Mona Abdelghani are kindly acknowledge for their contribution in this chapter.

# Compartmentalized Cross-linked Enzymatic nano-Aggregates (*c-CLEnA*) for Efficient In-flow Biocatalysis

## Abstract

Nano-sized enzyme aggregates, which preserve their catalytic activity are of great interest for flow processes, as these catalytic species show minimal diffusional issues, and are still sizeable enough to be effectively separated from the formed product. The realization of such catalysts is however far from trivial. The stable formation of micro- to millimeter-sized enzyme aggregates is feasible via the formation of cross-linked enzyme aggregates (CLEAs); however, such a process leads to a rather broad size distribution, which is not always compatible with microflow conditions. In this chapter, we present the design of a compartmentalized templated CLEA (*c-CLEnA*), inside the nano-cavity of bowl-shaped polymer vesicles, coined stomatocytes. Due to the enzyme preorganization and concentration in the cavity, cross-linking could be performed with substantially lower amounts of cross-linking agents, which was highly beneficial for the residual enzyme activity. Our methodology is generally applicable, as demonstrated by using two different cross-linkers (glutaraldehyde and genipin). Moreover, *c-CLEnA* nanoreactors were designed with *Candida antarctica* Lipase B (CalB) and Porcine Liver Esterase (PLE), as well as a mixture of glucose oxidase (GOx) and horseradish peroxidase (HRP). Interestingly, when genipin was used as cross-linker, all enzymes preserved their initial activity. Furthermore, as proof of principle, we demonstrated in this chapter the successful implementation of different *c-CLEnAs* in a flow reactor in which the *c-CLEnA* nanoreactors retained their full catalytic function even after ten runs. These *c-CLEnA* nanoreactors represent a significant step forward in the area of in-flow biocatalysis.

## 4.1. Introduction

In recent years microreactor technology for continuous flow catalysis has developed into an attractive alternative for traditional batch processes, because of the higher level of control over mass and heat transfer.<sup>1-5</sup> Reactions in-flow are furthermore scalable and offer broader windows of operation and automated optimization protocols.<sup>6,7</sup> In case catalytic steps are involved, heterogeneous catalysts are preferred from a processing point of view, as they enable easy separation from the product flow and allow catalyst recycling.<sup>8</sup> Catalyst immobilization however can also lead to some disadvantages, such as diffusional limitations and problems associated with catalyst leaching.<sup>9,10</sup> The current implementation of enzymes in in-flow reactions relies on their immobilization, which mostly involves binding and/or physical adsorption to porous or solid supports (e.g. resin or silica) or encapsulation in an inert carrier, affording a biocatalyst with acceptable performance in flow.<sup>11,12</sup> Indeed, immobilization is advantageous in terms of reusability and stability and is a well-established route for the commercial application of enzyme-based catalysis.<sup>10</sup> However, these traditional types of immobilization often affect enzyme performance, provide limited physical protection and leaching remains an important issue which limits the recyclability.<sup>13</sup> Leaching can be limited via the

formation of cross-linked enzyme aggregates (CLEAs).<sup>14</sup> CLEAs provide enhanced stability, with the ability to be recaptured, recycled and reused after filtration or centrifugation processes.<sup>12</sup> CLEAs have been studied over the past decade as a green and facile route towards industrial catalysis.<sup>10</sup> However, due to their broad distribution in size, such CLEAs are less well-defined regarding enzyme display and are therefore less effectively introduced in microflow systems. In an ideal situation, catalytic systems can operate freely in solution without diffusional barriers, and can still be effectively separated and recovered from the product flow. This can for example be achieved by applying nanoreactors, nanoparticles functionalized with catalytic species that function as homogeneous catalysts in a continuous flow system.<sup>15,16</sup> In our group we have much experience with employing copolymeric vesicles or polymersomes, as enzyme carriers.<sup>17–20</sup> Over the past years we have developed two different strategies; we have constructed semi-permeable vesicles in which the enzymes were encapsulated in the lumen,<sup>21</sup> and we have created bowl-shaped polymersomes, also known as stomatocytes, in which the enzymes were engulfed in the bowl, or stomach of the particles.<sup>22</sup> In both cases the robust polymer membrane provided protection against mechanical forces and enabled physical separation from undesired interactions with other catalytic species. In the case of stomatocytes, diffusional barriers are hardly present, as the stomach is in direct contact with the reaction medium. However, the physical encapsulation of enzymes inside the stomatocytes' cavity still poses a challenge; the encapsulated enzymes are prone to leaching and the nanoreactors are subsequently deactivated upon extended usage.

In this chapter, we present the formation of nanoreactors that combine the unique structural elements of stomatocytes with the functional aspects of CLEAs, displaying the potential of such robust catalytic systems, for the first time, in a flow reactor. Our strategy to achieving this is based on the utility of the stomach of poly(ethylene glycol)-polystyrene (PEG-*b*-PS) stomatocytes for in situ formation of compartmentalized cross-linked enzyme nano-aggregates (*c*-CLEnA) (Figure 1). Remarkably, the amount of cross-linkers needed was much less compared to the macroscopic CLEA process, which resulted in a much better preservation of catalytic activity. We first demonstrated the feasibility of the *c*-CLEnA process using the lipase *Candida antarctica* Lipase B (CalB). Indeed, upon formation of the CalB *c*-CLEnA nanoreactors the PEG-PS stomatocytes retained their structural integrity and demonstrated enzymatic activity similar to the free enzyme. To demonstrate the generality of this approach, we repeated the process to generate *c*-CLEnAs with different enzymes, including porcine liver esterase (PLE) and an enzymatic cascade involving glucose oxidase (GOx) and horse radish peroxidase (HRP). Importantly, reactions using the *c*-CLEnA nanoreactors were successfully implemented in a flow reactor where there was no apparent loss of activity, even after ten cycles.

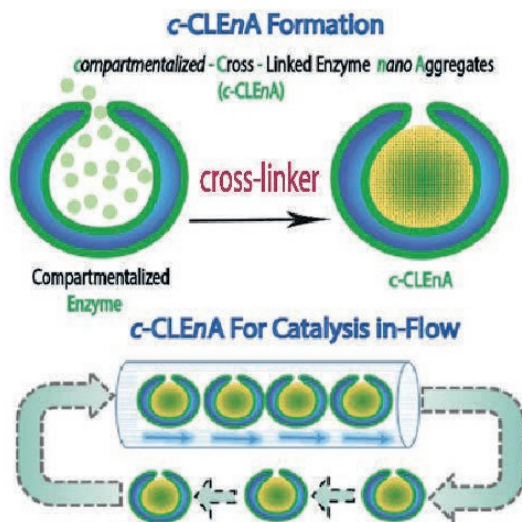


**Figure 1: (Top)** Formation of *compartmentalized-Cross-Linked Enzyme nano-Aggregates (c-CLEnAs)* via cross-linker addition (either glutaraldehyde or genipin). **(Bottom)** *c-CLEnA* application and reuse for in-flow catalysis

## 4.2. Results and Discussion

In this chapter, we present a robust platform for the compartmentalization of enzymes in bowl-shaped stomatocyte nanoparticles.<sup>18,22</sup> Such stomatocytes were formed through osmotic-induced shape transformation of spherical polymer vesicles (polymersomes) that were comprised of poly(ethylene glycol)-block-poly(styrene) (PEG-PS) copolymers. Stomatocytes are able to encapsulate one, or more enzymatic species within their inner compartment, with relatively high encapsulation efficiency ranging from 8 to 35%, depending on the initial feed and the enzyme properties. The high local concentration of catalyst and the easy accessibility of the substrate toward the cavity, makes stomatocytes an interesting tool in catalytic aqueous processes. In our present strategy, we utilized PEG-PS stomatocytes to entrap proteins, which were subsequently turned into cross-linked enzyme nano-aggregates (CLEnA) under the action of glutaraldehyde (Figure 2A) or genipin.

In the first instance, glutaraldehyde was used to validate our ability to cross-link enzymes inside the cavity of the stomatocytes. To this end, formation of *c-CLEnA* was initiated by encapsulation of the 34 kDa lipase CalB within PEG-PS stomatocytes under relatively mild conditions, whereby CalB ( $12 \text{ mg mL}^{-1}$ ) was added to open neck stomatocytes ( $0.5 \text{ mL}$ ,  $10 \text{ mg mL}^{-1}$ ), and the enzyme was encapsulated in the stomatocytes' cavity by narrowing the neck via a shape change process induced by a small aliquot of organic solvent and subsequent washing with salt solution (Figures 2-3,S1).<sup>18,22</sup> Afterwards, stomatocytes were dispersed in phosphate-buffered saline (PBS), and glutaraldehyde ( $0.1 \text{ mL}$ ,  $150 \text{ mM}$ ) was slowly added. Employing this CLEA-based enzyme cross-linking strategy, in which lysine residues are chemically bonded, templated formation of CLEnA was performed in the stomach of the

PEG-PS stomatocytes. The resulting *c*-CLEnAs maintained their unique morphological characteristics (Figure 2B, 3) with increasing internal density (due to CLEnA formation). This was also confirmed via analysis of the shape factor,  $\rho$  (the ratio between radius of gyration,  $R_g$ , and hydrodynamic radius,  $R_h$ ), where the  $\rho$  value of stomatocytes compartmentalizing CalB CLEnA was ca. 0.73 (Figure S2), indicative of the formation of a solid sphere.<sup>22,23</sup> In order to characterize the nature of the CLEnA formed during this process, stomatocytes were unloaded via adding an excess of organic solvent, which dissolved the polymer shell so that the templated CalB particles could be characterized. Dynamic Light Scattering (Figure S3) analyses showed formation of CLEnA particles of ca. 45 nm. This size was larger than the neck size of the PEG-PS stomatocytes (ca. 5 nm, Figure 2, Figure S7A), ensuring better entrapment than the free CalB enzymes. Furthermore, from SDS-PAGE gel analysis it was evident that no monomeric enzyme existed (Figure S4), as only a high molecular weight species was observed, which showed that the cross-linking process proceeded with high efficiency. When CalB was free in solution, similar conditions of cross-linking led to formation of CLEAs, however, with less control over the size of the structures and a broad size distribution ranging from 10 to 100  $\mu$ m, as confirmed by scanning electron microscopy (Figure S5).

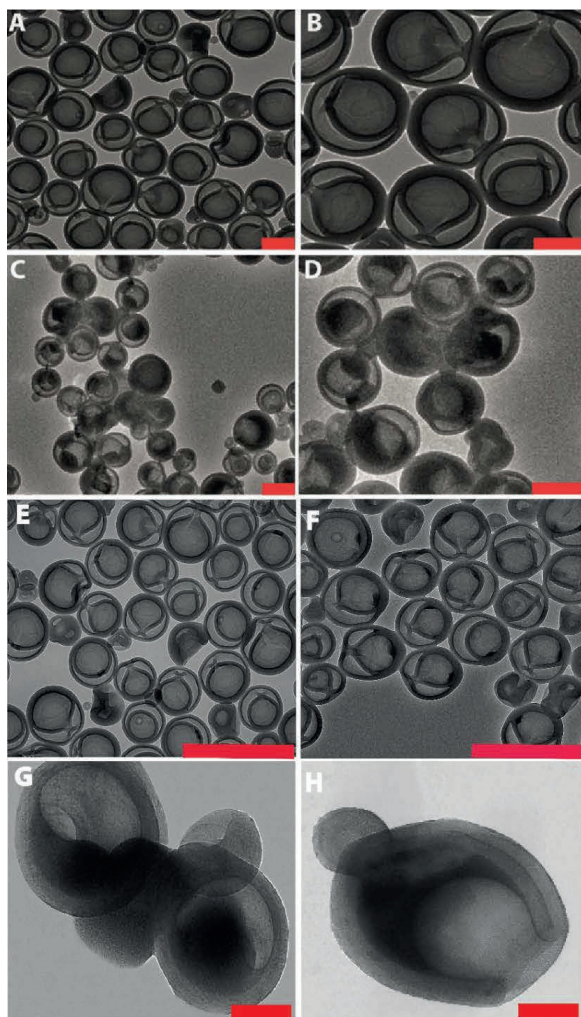


**Figure 2:** Transmission electron microscopy (TEM) images of **A and B**) CalB loaded stomatocytes with narrow neck. **C and D**) Stomatocytes compartmentalizing cross-linked CalB; CalB *c-CLEnA* formed with glutaraldehyde. Scale bars correspond to 200 nm. **E**) PLE- loaded stomatocytes after neck closure, **F**) GOx/HRP- loaded stomatocytes after neck closure. Scale bar corresponds 1 $\mu$ m. **G**) Stomatocytes compartmentalizing cross-linked PLE; PLE *c-CLEnA* formed with genipin . **H**) GOx/HRP *c-CLEnA* formed with genipin. Scale bar corresponds to 100nm.

To demonstrate the ability of the formed *c-CLEnA* to function as catalytic system we measured the activity of the CalB-mediated hydrolysis of *p*-nitrophenyl acetate (*p*NPA). The activity of *c-CLEnA* was superior to that of the free enzyme or the encapsulated CalB into stomatocytes prior to cross-linking (Figure S6). Although this seems remarkable, as activity is normally diminished due to cross-linking with glutaraldehyde, CalB is a known exception to

this rule.<sup>24,25</sup> In order to confirm the generality of our methodology, we set out to cross-link a different enzyme, PLE, employing the same conditions as for CalB (0.1 mL of 150 mM of glutaraldehyde, supporting information 2.3 and 2.4). However, these initial conditions had a strong negative impact on PLE activity (Figure 4A). Through careful tuning of the amount of glutaraldehyde employed, we were able to induce the formation of PLE *c*-CLEnAs under milder conditions by using 50 mM of glutaraldehyde instead of 150 mM. These milder conditions of cross-linking led to a higher  $V_{MAX}$  (Figure 4B and 5A). It is worth to mention that 50 mM glutaraldehyde was not enough to cross-link PLE present in a free enzyme solution when the same ratio enzyme/glutaraldehyde was used and even the addition of 75mM and 100 mM of glutaraldehyde led only to partial cross-linking of the free enzyme (Figure S7). This highlights the advantageous effect of enzyme compartmentalization as it increases the enzyme local concentration and facilitates the cross-linking process. Since genipin is known to be a milder cross-linker and is widely used in applications in medicine and food technology,<sup>26–28</sup> we set out to cross-link PLE using genipin instead of glutaraldehyde - aiming at preserving its activity. Gratifyingly, when genipin was used (30-50 mM), the activity of PLE *c*-CLEnA was maintained as no significant decrease of enzyme activity was observed (Figure 4C-4D).

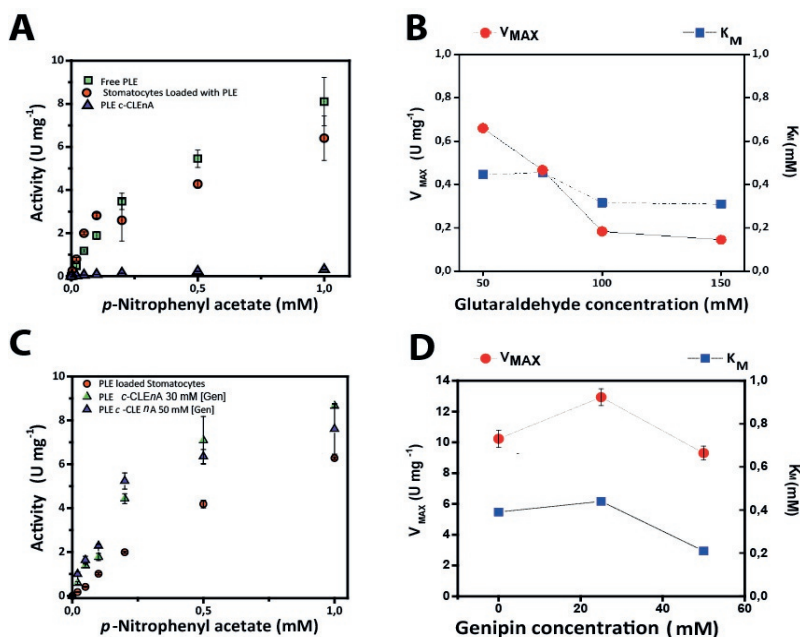


**Figure 4- A)** Comparison between specific activity (U mg<sup>-1</sup>) of free PLE, PLE loaded stomatocytes (with un-cross-linked PLE), and PLE *c*-CLEnA using glutaraldehyde. The absorbance of the product is measured at 405 nm at different concentrations of substrate. **B)** PLE *c*-CLEnAs prepared at different glutaraldehyde concentration show a clear decrease of  $V_{MAX}$  with increasing concentration of glutaraldehyde. **C)** Comparison between specific activity (U mg<sup>-1</sup>) of PLE loaded stomatocytes (with un-cross-linked PLE), and PLE *c*-CLEnA prepared with genipin at different concentrations. **D)** PLE *c*-CLEnAs prepared at different genipin concentrations show  $V_{MAX}$  is not affected by the cross-linker addition.

The shape of the stomatocyte nanoreactor was not affected by genipin (Figure S8). Furthermore, to demonstrate that this method is not restricted to single enzyme systems we generated a dual enzyme *c*-CLEnA where glucose oxidase (GOx) and horseradish peroxidase (HRP) were co-encapsulated in stomatocytes prior to cross-linking. The presence of both enzymes within the stomatocyte was confirmed by SDS-PAGE (Figure S9). Again, cross-linking inside the stomatocytes proved to be a more efficient process than cross-linking of a free enzyme solution at the same concentration. The activity of the dual-functional *c*-CLEnA was confirmed with the peroxidation of Amplex Red, and compared with the activity of stomatocytes loaded with un-crosslinked GOx/HRP and with the free enzymes (Figure 6). Similarly to the case of PLE, the activity was dependent on the concentration of cross-linker; when using 30mM of glutaraldehyde the native activity was preserved (Figure 5B and 6A). Again, when genipin was used as cross-linker the native activity of GOx/HRP was not affected (Figure 6B).

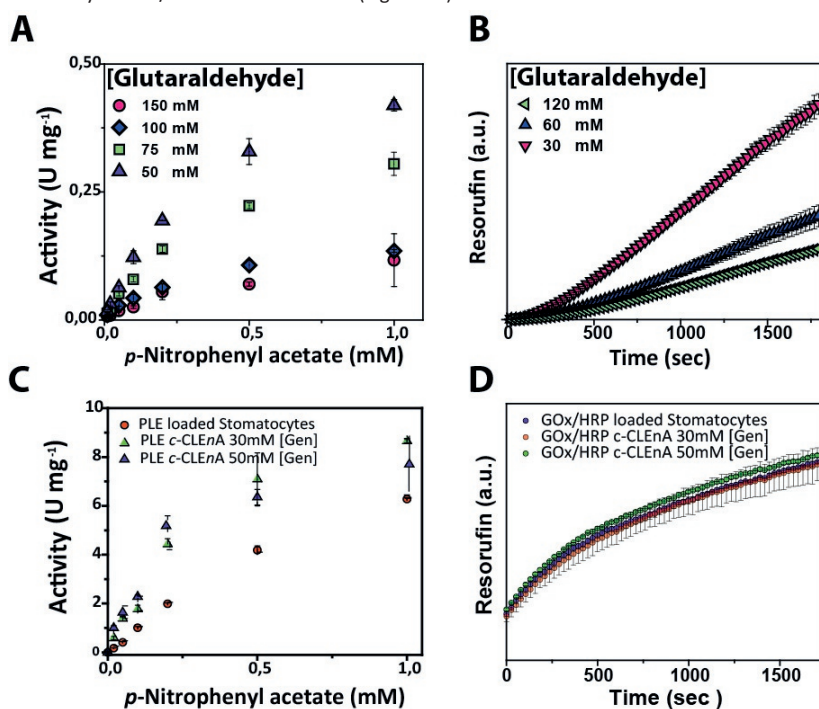


**Figure 5:** **A)** Activity of PLE *c*-CLEnA formed at different concentrations of glutaraldehyde. An increase in activity is observed when glutaraldehyde concentrations are decreased. The absorbance of the product is measured at 405 nm at different concentrations of *p*-NPA. **B)** Activity of GOx/HRP *c*-CLEnA formed at different concentrations of glutaraldehyde. Resorufin formation is measured at a (D)-glucose concentration of 20mM. **C)** Activity of PLE *c*-CLEnA formed at different concentrations of genipin. The absorbance of the product is measured at 405 nm at different concentrations of *p*-NPA. An increase in activity is observed when genipin is added. **D)** Activity of GOx/HRP *c*-CLEnA formed at different concentrations of genipin. Resorufin formation is measured at a (D)-glucose concentration of 20mM.



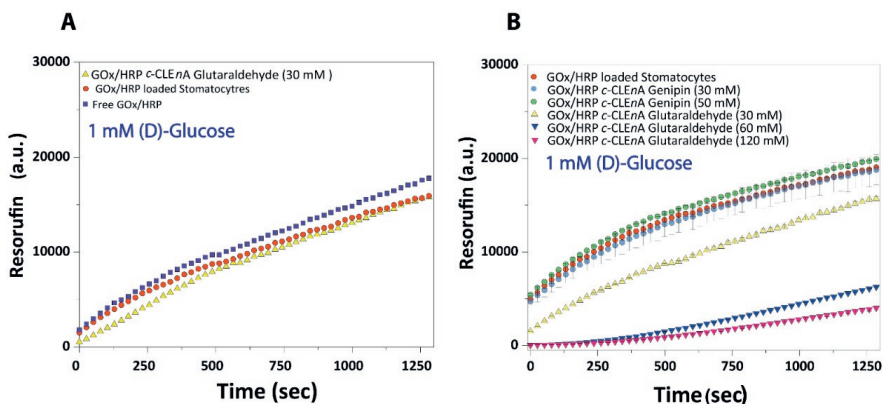


**Figure 6- A)** Resorufin formation at 1 mM of (D)-Glucose when free GOx/HRP activity is compared with GOx/HRP loaded stomatocytes (13% loaded and diluted 10 times) and GOx/HRP *c-CLEnA* formed with 30 mM of glutaraldehyde (13% loaded and diluted 10 times). **B)** Resorufin formation at 1 mM of (D)-Glucose comparing GOx/HRP loaded stomatocytes with GOx/HRP *c-CLEnA* formed with 30-60-120 mM of glutaraldehyde and GOx/HRP *c-CLEnA* formed with 30-50 mM of genipin. Average results of triplicates with samples at the same loading efficacy.

Finally, the performance of CalB *c-CLEnA* was evaluated in a flow setup. We first set out to optimize the enzyme loading for maximum efficiency in flow. Three different enzyme feeds were added to different stomatocyte batches prior to the encapsulation process. When  $12 \text{ mg mL}^{-1}$  of CalB was initially added, an encapsulation efficiency of 14 % of the initial feed was reached, whilst 33 % and 8 % were achieved when  $16 \text{ mg mL}^{-1}$  and  $6 \text{ mg mL}^{-1}$  were added, proving that a good control over the loading efficiency could be achieved by simply varying the initial enzyme concentration. We next set out to test the capacity of stomatocytes in flow. CalB loaded stomatocytes and CalB *c-CLEnA* (with 33 %, 14 % and 8 % encapsulation efficiency) were immobilized into a flow reactor (Figure 7, S10), equipped with an internal membrane to retain the polymeric vesicles. Catalytic tests were performed after which the stomatocytes or the *c-CLEnA* were recollected from the membrane outlet, and washed by spin filtration before the next catalytic cycle (described in 4.5.11.). When the different non-cross-linked CalB loaded stomatocytes were fed in the flow reactor, after the first catalytic run ( $\sim 13 \text{ min}$ ,  $0.3 \text{ mL min}^{-1}$ ), a clear loss in activity was observed (Figure S10). This loss in activity was most severe with the 8% loaded stomatocytes, which only retained approximately 60% of the initial catalytic efficiency, after the second run. A clear loss in activity was observed in all non-crosslinked stomatocyte samples over the course of 5 runs of the flow experiments (Figure 8A and S10). It was evident that the loss of activity was related to significant leaching of the enzyme during the reaction. Due to the small size of the protein, the entrapped enzyme was partially flushed away from the stomatocytes' cavity due to the washing and reloading process. In contrast, when in the same process *c-CLEnA* was employed, no loss in activity, over the course of five runs, was observed (Figure 8A). Even when CalB *c-CLEnA* were reused in-flow for ten reaction runs in flow, still no leaching or loss in activity was detected (Figure 8B), confirming their potential for continuous flow

applications. Moreover, after ten runs in flow (flow rate  $0.6 \text{ ml min}^{-1}$ ) there was no apparent change in particle morphology, with fully intact stomatocytes being observed by scanning electron microscopy (SEM) (Figure S11). Due to the strong negative effect of glutaraldehyde on the PLE enzyme, PLE *c-CLEnA* was formed using genipin for all studies in-flow (Figure 8C and 8D). Similar to CalB *c-CLEnA*, PLE *c-CLEnA* was recycled for ten runs in flow, after which *ca.* 20 % decrease in activity was observed. In comparison to PLE loaded stomatocytes, the decrease in activity of PLE *c-CLEnA* was however much less severe. The loss of activity can be attributed to the highly sensitive nature of PLE, making it prone to denaturation. Another plausible reason is that the mild cross-linking effect of genipin might lead to the presence of a small fraction of non-cross-linked PLE. After several cycles, such non cross-linked PLE would be able to escape the stomatocyte, leading to this decrease in activity. That notwithstanding, this experiment is a direct proof of the applicability of our approach toward more sensitive enzymes – a promising platform for enzymatic catalysis in flow.

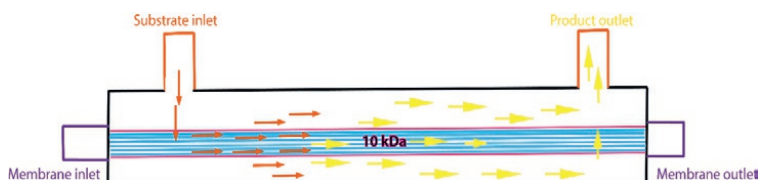


**Figure 7-** Schematic representation of the flow reactor system. The orange arrows indicate the diffusion of the substrate throughout the permeable membrane, and its conversion into the product *p*-nitrophenol (yellow arrows) that can be collected at the product outlet.

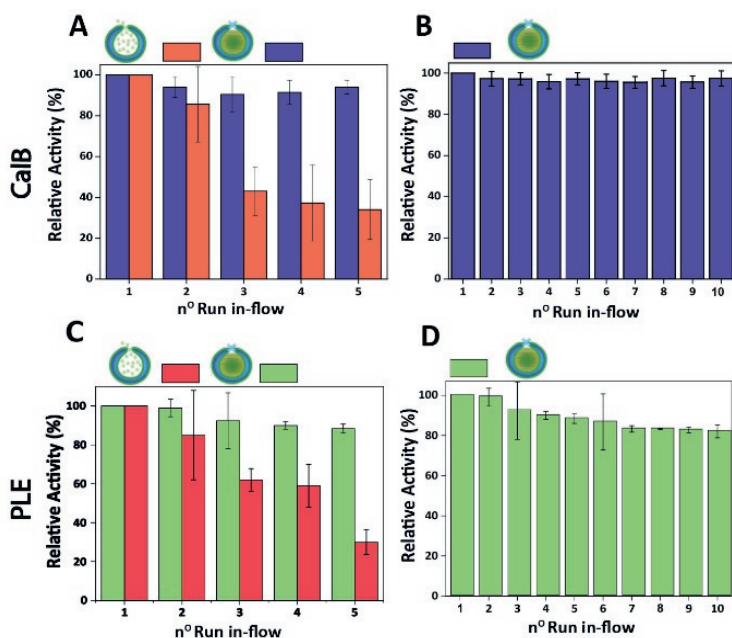


**Figure 8:** **A)** Comparison between the relative activity of CalB loaded stomatocytes (with non-cross-linked CalB) and CalB *c-CLEnA* (both with 33% encapsulation efficiency) during five runs in-flow. **B)** Relative activity of CalB *c-CLEnA* (with 33% encapsulation efficiency) during ten runs in-flow. **C)** Comparison between the relative activity of PLE loaded stomatocytes (with non-cross-linked PLE) and PLE *c-CLEnA* (both with 21% encapsulation efficiency) during five runs in-flow. **D)** Relative activity of PLE *c-CLEnA* (with 21% encapsulation efficiency) during ten runs in-flow.

### 4.3. Conclusions

In summary, we have shown a novel and robust methodology to construct nano-sized cross-linked enzyme aggregates (*c-CLEnA*) via their templated formation in the cavity of bowl-shaped polymeric compartments, or stomatocytes. The preorganization of enzymes in the stomatocyte cavity resulted in a high local concentration, which therefore required a substantially smaller amount of cross-linking agent to obtain stable cross-linked systems. These milder conditions enabled a better preservation of enzyme activity, proving the general advantages of our method for applications in biocatalysis. Our cross-linking methodology worked equally well for single enzymes and enzyme mixtures. The robustness of the *c-CLEnA* systems was tested in a micro-reactor flow set-up, in which the *c-CLEnA* could be reused for ten times without losing any activity, in clear contrast to the controls. This conceptually new approach allows the mild cross-linking of enzymes into well-defined nano-sized particles, which can find their application in flow chemistry and other processes in which catalytic nano-aggregates are beneficial.

## 4.4. Experimental Section

### 4.4.1. Materials and Methods

All chemicals and enzymes were purchased from Sigma-Aldrich and used as received, unless otherwise stated. For the synthesis of the block copolymer, CuBr was activated using acetic acid for 3 h and dried in vacuum. Ultra-pure MilliQ water (Labconco Water Pro PS purification system) was used for the self-assembly of polymersomes and dialysis. The dialysis membranes (MWCO 12-14 kDa Spectra/Por®), Amicon Ultra- 0.5 mL centrifugal filter Unit 3 kDa (Millipore), and Ultrafree-MC centrifugal filters (with 0.1 and 0.22  $\mu\text{m}$  pore size) (Millipore) were used to remove the excess of enzyme after encapsulation, and to wash the nanoreactors after the flow experiments. The proteins used for the experiments included *Candida antarctica* Lipase B recombinant from *Aspergillus Oryzae* (CalB, E.C. 3.1.1.3.) as lyophilized powder with  $\sim 9 \text{ U mg}^{-1}$  activity, esterase from porcine liver (PLE, E.C. 3.1.1.1.) as lyophilized powder with  $\geq 15 \text{ U mg}^{-1}$  activity, glucose oxidase from *Aspergillus Niger* Type II (GOx, E.C. 1.1.3.4) as lyophilized powder with  $228.25 \text{ U mg}^{-1}$  activity, and peroxidase from horseradish Type I (HRP, E.C. 1.11.1.7) with  $50\text{-}150 \text{ U mg}^{-1}$  activity. The glutaraldehyde solution (25% w/w in  $\text{H}_2\text{O}$ ) was purchased from Sigma Aldrich and solutions at different concentrations were prepared for the c-CLEnA formation. Genipin ( $\geq 98\%$  (HPLC) in powder) was also purchased from Sigma Aldrich and solutions at different concentrations were prepared in MilliQ water.

**Proton nuclear magnetic resonance ( $^1\text{H}$  NMR):**  $^1\text{H}$  NMR spectra were recorded on a Varian Inova 400 spectrometer with  $\text{CDCl}_3$  as a solvent and TMS as internal standard.  $^1\text{H}$  NMR spectra were used to determine the molecular weight of the synthesized copolymers.

**Gel permeation chromatography (GPC):** The dispersity ( $\mathcal{D}$ ) of the copolymers was determined using a Shimadzu Prominence GPC system equipped with a PL gel 5  $\mu\text{m}$  mixed D column (Polymer Laboratories) and differential refractive index and UV (254 nm) detectors. THF was used as an eluent at a flow rate of  $1 \text{ mL min}^{-1}$ .

**Size Exclusion Chromatography (SEC):** For an efficient separation of the stomatocytes from the unencapsulated enzymes, a Shimadzu Prominence SEC system equipped with a Superose™ 6 column and a UV detector (220 nm) was used. The separation was performed using filtered PBS buffer at  $0.8 \text{ mL min}^{-1}$ .

**Transmission electron microscopy (TEM):** TEM images were recorded using a FEI Tecnai 20 (type Sphera) at 200 kV.  $5 \mu\text{L}$  sample was dropped on top of a carbon-coated copper grid (200 mesh, EM science), and the samples were left to dry at room temperature overnight.

**Scanning electron microscopy (SEM):** SEM images were obtained using a Quanta 3D FEG (FEI, The Netherlands) with a field emission electron gun at 10 kV-15 kV. All samples were diluted ten times with MilliQ, and  $5 \mu\text{L}$  diluted solution was placed on a silicon wafer, which was previously washed in 70% EtOH and dried at RT overnight. Prior to measurement, all samples that were drop cast on the silicon wafer were coated with gold via sputtering for 30 s at 60 mA using an EMITECH 575K coater.

**Asymmetric flow field flow fractionation – light scattering (AF4-LS):** The AF4-LS experiments were performed on a Wyatt Eclipse AF4 instrument connected to a Shimadzu LC-20A Prominence system with Shimadzu CTO20A injector. The AF4 was further connected to the following detectors: a Shimadzu SPD20A UV detector, a Wyatt DAWN HELEOS II light scattering detectors (MALS) installed at different angles (12.9°, 20.6°, 29.6°, 37.4°, 44.8°, 53.0°, 61.1°, 70.1°, 80.1°, 90.0°, 99.9°, 109.9°, 120.1°, 130.5°, 149.1°, and 157.8°) using laser operating at 664.5 nm, a Wyatt Optilab Rex refractive index detector and a Quels detector installed at angle of 140.1°. The detectors were normalized using bovine serum albumin protein. The AF4 channel was pre-washed with a running solution of PBS, which was also used for the separation. The processing and analysis of the LS data, and hydrodynamic radii calculations, were performed using the Astra 7.1.2 software. All AF4 separations were performed on an AF4 short channel equipped with regenerated cellulose (RC) 10 kDa membrane (Millipore) and spacer of 350 µm. The method for the AF4 fractionation is described in Table S1.

**Dynamic light scattering (DLS):** DLS measurements were performed on a Malvern instrument Zetasizer (model Nano ZSP). Zetasizer software was used to process and analyse the data. The results are given as an average of six runs.

**Fluorescence measurements:** The fluorescence measurements were performed using 96-black well Flat Bottom microplates (Greiner Bio-One) and a Tecan Spark 10M Multidetector microplate reader equipped with a 530 nm excitation filter and a 590 nm emission filter, bandwidth 20 nm, integration time 40 µs.

**Hydrolysis assays:** All assays were performed in 96-transparent well Flat Bottom microplates (Greiner Bio-One) on a Synergy2, Biotek, Winooski, US Multidetector plater reader. Reader was set at a fixed wavelength (405 nm).

**In-flow setup:** A tubular reactor with a filter module: ID (mm) 0.5, pore size 10 kDa of poly(ether sulfone) (mPES Effective Length (cm) 20.0, Total Length (cm) 23.0, surface area 28.0 cm<sup>2</sup> was purchased from Spectrum Lab<sup>®</sup>. The inlet was equipped with a peek ferrule (VWR<sup>®</sup>) to facilitate the syringe attachment to the tubular module.

**High Performance Liquid Chromatography (HPLC):** The product collected at the reactor outlet was analyzed with a Shimadzu LC-20AD Prominence system, which was equipped with an RP Alltima C18 5u (150mm x 3.2mm) column and a UV detector. The column was pre-equilibrated with a solution of 0.1 % formic acid (v/v) in water and 60% acetonitrile (ACN) (v/v) was used as eluent at a flow rate of 0.5 mL min<sup>-1</sup>.

**Bradford assay:** The Bradford method was used to quantify the enzyme loading. Pierce<sup>™</sup> Coomassie Plus (Bradford) assay kit was used as described in the protocol of the assay.

**Sodium dodecyl sulfate polyacrylamide gel electrophoresis (SDS-PAGE):** The samples of interest were mixed with 4X non-reducing loading buffer and were loaded on 4-20% Mini-PROTEAN<sup>®</sup> TGX<sup>™</sup> Precast Gels (Biorad) according to the manufacturer's instructions. The gel was stained for proteins using Pierce<sup>™</sup> Silver Stain Kit (Thermo Fischer) for the CalB samples, and Coomassie Blue (BioRad) in all the other cases.

## 4.5. Experimental procedures

### 4.5.1. Synthesis of poly(ethylene glycol)<sub>44</sub>-polystyrene<sub>140</sub> (PEG<sub>44</sub>-*b*-PS<sub>140</sub>) block copolymer

PEG-*b*-PS was synthesized using atom-transfer controlled radical polymerization (ATRP), according to previously reported literature procedures.<sup>2</sup> For the macro initiator synthesis, poly(ethylene glycol) methyl ether (5.0 g, 2.5 mmol), was twice dried by co-evaporation with toluene. In a flame-dried Schlenk tube, the poly(ethylene glycol) methyl ether was then dissolved in dry THF (2.0 mL) and triethylamine (1.04 mL, 7.5 mmol) was added to the solution. The Schlenk tube was placed on an ice bath, followed by the dropwise addition of  $\alpha$ -bromoisobutyryl bromide (616.0  $\mu$ L, 5.0 mmol) while stirring. The solution was then stirred for a further 24 h, while slowly warming to room temperature, to form a white solid due to the precipitation of the amine salt in the colorless solution. The amine salt was filtered off and the solution was concentrated in vacuum. The precipitation of macro-initiator poly(ethylene glycol)<sub>44</sub> methyl ether 2-bromoisobutyrate was induced by ice-cold diethyl ether.

For the PEG<sub>44</sub>-*b*-PS<sub>140</sub> synthesis, copper bromide (CuBr) (45.0 mg, 0.32 mmol) was first added to a flame dried Schlenk tube equipped with a stirring bar under argon atmosphere. The Schlenk tube was sealed with a septum, and evacuated for 15 min, after which argon was filled back into the flask. PMDETA (66.0  $\mu$ L, 0.32 mmol) was dissolved in 0.5 mL toluene and added to the CuBr powder. The mixture was left stirring for 15 min with argon for oxygen removal. Polyethylene glycol macroinitiator (215 mg, 0.10 mmol), dissolved in 1 mL toluene, was added into the Schlenk tube. The solution was degassed for 15 min while cooling in an ice bath. Distilled styrene (5.0 ml, 43.6 mmol) was added to the reaction mixture. The mixture was then degassed and the Schlenk tube was inserted into a preheated 70 °C oil bath, overnight. At the end of the reaction, dichloromethane (CH<sub>2</sub>Cl<sub>2</sub>) (75 mL) was added to the polymer solution and the mixture was filtered over an alumina column to remove the CuBr. The final solution was then concentrated and the polymer was precipitated in cold methanol, filtered and dried overnight in vacuum. The amphiphilic polymer obtained, PEG<sub>44</sub>-*b*-PS<sub>140</sub> had a number average molecular weight ( $M_n$ ) of 16.8 kg mol<sup>-1</sup> and  $\bar{D}$  = 1.06.

### 4.5.2. General procedure for polymersome preparation

The polymersomes were self-assembled using a slightly modified variation of a previously reported solvent switch method. In short, 20.0 mg synthesized PEG<sub>44</sub>-*b*-PS<sub>140</sub> polymer was dissolved in a 1.0 mL mixture of THF: dioxane (4:1 v/v), to which 1.0 mL MilliQ was added via a syringe pump with a flow rate of 1.0 mL h<sup>-1</sup>, resulting in the formation of a cloudy solution. The assembly was performed inside a 5.0 mL vial which contained a magnetic stirring bar and which was capped with a septum. The cloudy solution was then dialyzed against MilliQ water for 24 h, with the MilliQ frequently refreshed.

Stomatocyte nanoreactors were prepared using the previously reported solvent addition methodology.<sup>22</sup> 300  $\mu$ L THF:dioxane solution (4:1 v/v) was added via syringe pump at a rate of 300  $\mu$ L h<sup>-1</sup> to 500  $\mu$ L of the previously prepared polymersome solution (10.0 mg mL<sup>-1</sup>), while continuously stirring. The organic mixture was removed from the polymeric solution using spin filtration (20 mins, 13523 rcf) which was repeated two times using Amicon 3 kDa

filters). The polymersomes were re-suspended to their initial concentration by adding MilliQ water. At the end of this process, opened neck stomatocytes (Figures 3, S1) were formed which were used for enzyme entrapment. Next, 1 mL of a 12 mg mL<sup>-1</sup> CalB solution in 50 mM sodium phosphate buffer, pH 7.5, was added to the stomatocytes and mixed vigorously at 7000 rpm for 30 mins. To narrow the neck of the stomatocytes (Figures 3, S1), 150  $\mu$ L THF:dioxane (4 : 1 v/v) at 150  $\mu$ L h<sup>-1</sup> flow rate was added to the solution. To remove the THF, samples were purified using spin filtration (15 mins, 13523 rcf) two times with Amicon 3 kDa filters. To remove non-encapsulated enzymes, stomatocytes were purified from the solution mixture using size exclusion chromatography (SEC). After SEC, the stomatocytes were concentrated again to a final volume of 500  $\mu$ L (10 mg mL<sup>-1</sup>).

For the preparation of CalB and PLE samples, the initial concentration of each enzyme was varied between 3.0 and 16.0 mg mL<sup>-1</sup>. In the case of the GOx/HRP loaded stomatocytes, the molar ratio between GOx:HRP was kept at 1:4 (mol/mol), with [GOx] = 4.05 mg mL<sup>-1</sup> and [HRP] = 4.77 mg mL<sup>-1</sup> and with an encapsulation efficiency of 13%.

#### **4.5.3. General procedure for the formation of compartmentalized cross-linked enzyme nano aggregates (c-CLEnA) with Glutaraldehyde**

Having ensured complete removal of free enzyme from the previously prepared stomatocyte nanoreactors, glutaraldehyde (100  $\mu$ L, at different concentrations varying between 30 mM and 150 mM) was slowly added, at a rate of 100  $\mu$ L h<sup>-1</sup>, to a 500  $\mu$ L solution of enzyme loaded stomatocytes (10 mg mL<sup>-1</sup>) while stirring. In case of either CalB or PLE, the cross-linking reaction was quenched with 1mL of sodium phosphate buffer (1M, pH = 7.5) solution, and in the case of GOx/HRP, the reaction was quenched with 1mL of PBS (pH = 7.4). To remove the excess of buffer and glutaraldehyde, all resulting c-CLEnAs were concentrated via spin filtration. In the case of CalB and PLE, the c-CLEnAs were re-dispersed in sodium phosphate buffer (50 mM, pH = 7.5). In the case of GOx/HRP, the c-CLEnA was re-dispersed in PBS (pH = 7.4). In all cases, no change of the stomatocytes' morphology was observed after glutaraldehyde addition (Figure S1 and S11).

#### **4.5.4. General procedure for the formation of cross-linked enzyme aggregates (CLEA) with Glutaraldehyde**

To a 1mL solution of CalB (3 mg mL<sup>-1</sup>, in sodium phosphate buffer pH 7.5), 100  $\mu$ L of glutaraldehyde (150 mM) was slowly added, at a rate of 100  $\mu$ L h<sup>-1</sup> while stirring. The reaction mixture was incubated for 8 h. To remove the excess of buffer and glutaraldehyde, all resulting CLEAs were concentrated via spin filtration (0.1  $\mu$ m), and imaged using SEM (Figure S5)<sup>29</sup>.

#### **4.5.5. General procedure for the formation of compartmentalized cross-linked enzyme nano aggregates (c-CLEnA) with genipin**

1 mL of genipin solution (concentration 30mM to 50 mM ) was added to 500  $\mu$ L of stomatocyte sample (10 mg mL<sup>-1</sup> ) in an Eppendorf tube. The solutions were kept for 24h at RT under gentle stirring.<sup>22</sup> For the PLE c-CLEnA formation, stomatocyte samples were mixed with 1mL of an 8 mg mL<sup>-1</sup> solution of PLE which resulted in 17% of encapsulation.

For the GOx/HRP *c-CLEnA*, the molar ratio between GOx:HRP was kept at 1:4 (mol/mol), with [GOx] = 4.05 mg mL<sup>-1</sup> and [HRP] = 4.77 mg mL<sup>-1</sup> (total volume 1mL) and the encapsulation efficiency was 13%.

After 24h genipin was removed from the solution, by using 10 kDa filters in a centrifuge at 12000 rpm for 15 min. The occurrence of *nano*-aggregates was also confirmed by the dark colour of the solution. Finally the *c-CLEnA* were recollected from the filter and their volume adjusted to 100 µL.

#### 4.5.6. General procedure for the formation of cross-linked enzyme aggregates (CLEA) with genipin

To a 1mL solution of PLE (3 mg mL<sup>-1</sup>, in sodium phosphate buffer pH 7.5), 1 mL of genipin (50 mM) was added while gently stirring the solution at RT. The reaction mixture was incubated for 24h. The solution became dark after CLEA formation. To remove the excess of buffer and genipin, all resulting CLEAs were concentrated via spin filtration (0.1 µm), and imaged using SEM (Figure S13).

#### 4.5.7. Quantification of enzyme loading

The Bradford assay was used to quantify the amount of enzyme loaded in the stomatocytes and in the *c-CLEnAs*. All the samples were treated with CH<sub>2</sub>Cl<sub>2</sub> to completely remove the polymeric membrane, which would alter the absorbance measured in the test. 150 µL of enzyme loaded stomatocytes were mixed with 500 µL of CH<sub>2</sub>Cl<sub>2</sub> for 30 mins. The final solution was then spin filtered with a centrifugal filter Unit 3 kDa (Millipore) to remove the organic solvent. The fraction collected was adjusted with buffer to the final volume of 150 µL. The measurements were performed in triplicate using 50 µL. For protein quantification, the Coomassie Plus (Bradford) assay kit was used (Pierce™) according to the manufacturer's instructions. In each cuvette both 1.5 mL of Coomassie reagent and 50 µL of sample were added. Before measuring the absorbance at 595 nm, all samples and the standard solutions were incubated for 5 mins at room temperature and the spectrophotometer was calibrated with a cuvette containing a blank solution.

Using the protein concentrations that were measured, the encapsulation efficiency (E.E. %) was determined by considering the protein concentration in the initial feed solution.

$$E.E.(%) = \frac{\text{Protein concentration measured with the Bradford assay (mg mL}^{-1}\text{)}}{\text{Lowest value of protein concentration used in the feed (mg mL}^{-1}\text{)}} \times 100$$

The encapsulation efficiency is given as average of triplicate measurements per each sample (Table S2). These encapsulation efficiencies were measured before the *c-CLEnA* formation.



#### 4.5.8. SDS-PAGE analysis

The effectiveness of enzyme cross-linking for CalB was analyzed using SDS-PAGE. Different sample volumes of the free and cross-linked enzymes were mixed with 4X non-reducing loading buffer and were loaded, along with the marker for protein molecular weight standards (Precision Plus Protein™ All Blue, Biorad) on 4-20% Mini-PROTEAN® TGX™ precast gels (Promega). As per manufacturer's instructions, the electrophoresis was carried out at constant voltage (110V) for 2h and the gel was stained using Pierce™ Silver Stain Kit, ThermoFisher; in the case of CalB, after gel fixation, the gel was sensitized for 1 min and stained for just 5-10 mins. The gel was developed for 1 min and the reaction was stopped with 10 % acetic acid. For the PLE and GOx/HRP reactions, the gel was stained with Bio-Safe™ Coomassie Stain, Biorad, for 1-4 hr and destained with MilliQ overnight. The gel was visualized by the white light box. For all the experiments the concentration of enzyme and the loaded volume were the same in each lane.

#### 4.5.9. CalB and PLE activity assays

All activity assays were conducted in triplicate. The activity of both CalB and PLE was assessed using an assay which monitors the hydrolysis reaction of *p*-nitrophenyl acetate to the *p*-nitrophenol product. The product formation over time was monitored at 405 nm.

The reaction was performed in a slightly basic environment, using a filtered sodium phosphate buffer (50mM, pH 7.5) at 25 °C. In all experiments, a master mix solution of 2 mM *p*-NPA in DMSO was used. The activity of free CalB, CalB loaded stomatocytes and CalB *c*-CLEnA was measured (Figure 3A). The same buffer and substrate conditions were applied when the activity of free PLE, PLE loaded stomatocytes and PLE *c*-CLEnA was assessed (Figure 3B). The reactions were carried out at different concentrations of substrate (ranging from 0 to 2 mM) and the activity was obtained by using equations 1 and 2:

(Equation 1.)

$$\frac{U}{\text{mL}} = \frac{\left( \frac{\Delta\text{Abs}}{\text{min}} \right) \times V_{\text{tot}} \times \text{Dilution}}{(\epsilon \times V_{\text{enzyme}})}$$

Where

$$\frac{\Delta\text{Abs}}{\text{min}} = \frac{\Delta\text{Abs (reaction)}}{\text{min}} - \frac{\Delta\text{Abs (background)}}{\text{min}}$$

$V_{\text{tot}}$  = is the total volume in the well,

Dilution = is the dilution factor used in the enzyme solutions;

$\epsilon = 18.5 \text{ mM}^{-1} \text{ cm}^{-1}$  is the extinction coefficient of *p*-NP at 405 nm.

$V_{\text{enzyme}}$  = volume of *c*-CLEnAs, enzyme loaded stomatocytes or free enzymes used.

(Equation 2.)

$$\frac{U}{\text{mg}} = \frac{\frac{U}{\text{mL}}}{\frac{\text{mg}}{\text{mL}} (\text{enzyme})}$$

The absorption (Abs (background)) is given by the absorbance of the negative control (the free enzymes, the enzyme loaded stomatocytes and the *c-CLEnA*s absorbance without substrate) together with the absorbance due to self-hydrolysis of substrate (*p*-NPA in buffer without enzyme).

#### 4.5.10. GOx/HRP activity assays

The activity of the GOx/HRP *c-CLEnA* was studied using the cascade reaction between HRP and GOx, where (D)-glucose and 10-acetyl-3,7-dihydroxyphenoxazine (Amplex® red) are substrates that are converted to the products, gluconolactone and resorufin. The reaction was monitored using resorufin fluorescence ( $\lambda_{\text{ex}} = 530 \text{ nm}$ ,  $\lambda_{\text{em}} = 590 \text{ nm}$ ) on the Spark® 10M microplate reader (TECAN). The samples tested included the free enzymes, GOx/HRP loaded stomatocytes and the combined *c-CLEnA* samples prepared using different glutaraldehyde concentrations (30, 60, and 120 mM) and genipin concentration (30, 50 mM). 20  $\mu\text{L}$  sample was mixed with 130  $\mu\text{L}$  reaction master mix containing Amplex red (250  $\mu\text{M}$ ), and (D)-glucose (final concentrations of either 1 mM, (Figure 15 and 6) or 20 mM for the *c-CLEnA* prepared at different amounts of glutaraldehyde (Figure 3C) at 25 °C in PBS, pH 7.4. The fluorescence values were background subtracted. Each assay was conducted twice. The error is the standard deviation from three different assays on samples at the same loading. The samples were always diluted 10 times unless stated otherwise. The final results are given as the fluorescent signal of resorufin corrected for the background.

#### 4.5.11. Flow experiments

Spectrum Lab® tubular filters were used as tubular reactors for the in-flow experiments. The flow setup (Figure 7) was equipped with two perpendicular inlets and two outlets, membrane and substrate inlets and membrane and product outlet. Membrane inlet and outlet were respectively used to introduce CalB-loaded stomatocytes (cross-linked or not cross-linked) on a 10 kDa membrane of poly(ether sulfone) (mPES and recollect them after the reaction. The inlet was connected to a syringe pump. Substrate inlet and product outlet were used to feed *p*-nitrophenyl acetate into the flow reactor and to collect the product, respectively. The tangential configuration of this flow setup did not only facilitate the recollection of the polymeric vesicles at the end of each flow run, but also ensured a good contact between the stomatocytes and the substrates.

In separate experiments: 0.5 mL of CalB loaded stomatocyte solution and 0.5 mL CalB *c-CLEnA* solutions were introduced in the 10 kDa membrane of the reactor *via* a syringe pump (at 0.1 mL min<sup>-1</sup>), ensuring homogeneous distribution throughout the whole length of the reactor's membrane. The porosity of the membrane (10 kDa) ensured the capture of the stomatocytes and prevented their loss. In the case of the first set of experiments in which five catalytic in-flow runs were performed, a 3 mM *p*-NPA stock solution in a mixture of 50 mM sodium phosphate buffer, pH 7.5, and 5% DMSO (v/v) was prepared, and fed to the tubular reactor using the lateral inlet via a syringe pump at 0.3 mL min<sup>-1</sup>. In the case of the ten runs experiments this flow rate was increased to 0.6 mL min<sup>-1</sup>. In both

cases, the product was collected at the end of the reaction (after ~13 mins), from the product outlet before performing further HPLC measurements. The flow reactor was washed by flushing the membrane with MilliQ water before the next catalytic experiment.

The CalB loaded stomatocytes and CalB *c-CLEnA* were unloaded from the membrane and recollected at the membrane outlet by manual injection of 1 mL of MilliQ. After washing with sodium phosphate buffer (50mM, pH = 7.5) three times using spin filtration (0.22  $\mu\text{m}$  Ultrafree<sup>®</sup>-CL filters) the recovered particles were re-dispersed in the same buffer and the final volume was adjusted again to 0.5 mL and used in the next run. Both CalB loaded stomatocytes and CalB *c-CLEnA* retained their structural integrity after all catalytic cycles (Figure S10). The same procedure was applied for PLE *c-CLEnA* formed using genipin (Figure 4).

## References

- 1 A. Adamo, R. L. Beingessner, M. Behnam, J. Chen, T. F. Jamison, K. F. Jensen, J. C. M. Monbaliu, A. S. Myerson, E. M. Revalor, D. R. Snead, T. Stelzer, N. Weeranoppanant, S. Y. Wong and P. Zhang, *Science* (80-), 2016, **352**, 61–67.
- 2 M. B. Plutschack, B. Pieber, K. Gilmore and P. H. Seeberger, *Chem. Rev.*, 2017, **117**, 11796–11893.
- 3 S. V. Ley, *Chem. Rec.*, 2012, **12**, 378–390.
- 4 Q. Deng, N.N. Tran, M. Razi Asrami, L. Schober, H. Gröger and V. Hessel, *Ind. Eng. Chem. Res.*, 2020, **59**(48), 21001–21011.
- 5 K. Jähnisch, V. Hessel, H. Löwe, and M. Baerns, *Angw. Chem. Int. Ed.*, 2004, **43**, 4, 406–446
- 6 M. U. Kopp, A. J. De Mello and A. Manz, *Science*, 1998, **280**, 1046–1048.
- 7 J. C. Pastre, D. L. Browne and S. V. Ley, *Chem. Soc. Rev.*, 2013, **42**, 8849–8869.
- 8 J. Britton, S. Majumdar and G. A. Weiss, *Chem. Soc. Rev.*, 2018, **47**, 5891–5918.
- 9 S.-H. Jun, J. Lee, B. C. Kim, J. E. Lee, J. Joo, H. Park, J. H. Lee, S.-M. Lee, D. Lee, S. Kim, Y.-M. Koo, C. H. Shin, S. W. Kim, T. Hyeon and J. Kim, *Chem. Mater.*, 2012, **24**, 924–929.
- 10 R. A. Sheldon and S. van Pelt, *Chem. Soc. Rev.*, 2013, **42**, 6223–6235.
- 11 I. Denčić, S. De Vaan, T. Noël, J. Meuldijk, M. De Croon and V. Hessel, *Ind. Eng. Chem. Res.*, 2013, **52**, 10951–10960.
- 12 R. A. Sheldon, *Appl. Microbiol. Biotechnol.*, 2011, **92**, 467–477.
- 13 K. Ariga, Q. Ji, T. Mori, M. Naito, Y. Yamauchi, H. Abe and J. P. Hill, *Chem. Soc. Rev.*, 2013, **42**, 6322.
- 14 I. Matijošyte, I. W. C. E. Arends, S. de Vries and R. A. Sheldon, *J. Mol. Catal. B Enzym.*, 2010, **62**, 142–148.
- 15 S. H. Petrosko, R. Johnson, H. White and C. A. Mirkin, *J. Am. Chem. Soc.*, 2016, **138**, 7443–7445.
- 16 H.-P. M. De Hoog, I. W. C. E. Arends, A. E. Rowan, J. J. L. M. Cornelissen and R. J. M. Nolte, *Nanoscale*, 2010, **2**, 709.
- 17 R. J. R. W. Peters, M. Marguet, S. Marais, M. W. Fraaije, J. C. M. van Hest and S. Lecommandoux, *Angew.*

- Chem. Int. Ed.*, 2014, **53**, 146–150.
- 18 M. Nijemeisland, L. K. E. A. Abdelmohsen, W. T. S. Huck, D. A. Wilson and J. C. M. Van Hest, *ACS Cent. Sci.*, 2016, **2**, 843–849.
- 19 M. T. De Martino, L. K. E. A. Abdelmohsen, F. P. J. T. Rutjes and J. C. M. van Hest, *Beilstein J. Org. Chem.*, 2018, **14**, 716–733.
- 20 S. F. M. Van Dongen, M. Nallani, J. J. L. M. Cornelissen, R. J. M. Nolte and J. C. M. Van Hest, *Chem. - A Eur. J.*, 2009, **15**, 1107–1114.
- 21 L. M. P. E. Van Oppen, L. K. E. A. Abdelmohsen, S. E. Van Ernst-De Vries, P. L. W. Welzen, D. A. Wilson, J. A. M. Smeitink, W. J. H. Koopman, R. Brock, P. H. G. M. Willems, D. S. Williams and J. C. M. Van Hest, *ACS Cent. Sci.*, 2018, **4**, 917–928.
- 22 L. K. E. A. Abdelmohsen, M. Nijemeisland, G. M. Pawar, G.-J. A. Janssen, R. J. M. Nolte, J. C. M. van Hest and D. A. Wilson, *ACS Nano*, 2016, **10**, 2652–2660.
- 23 O. Stauch, R. Schubert, G. Savin and W. Burchard, *Biomacromolecules*, 2002, **3**, 565–578.
- 24 T. Zisis, P. L. Freddolino, P. Turunen, M. C. F. van Teeseling, A. E. Rowan and K. G. Blank, *Biochemistry*, 2015, **54**, 5969–5979.
- 25 B. Stauch, S. J. Fisher and M. Cianci, *J. Lipid Res.*, 2015, **56**, 2348–2358.
- 26 Y. Beldengrün, J. Aragon, S. F. Prazeres, G. Montalvo, J. Miras and J. Esquena, *Langmuir*, 2018, **34**, 9731–9743.
- 27 S. H. Chiou, T. C. Hung, R. Giridhar and W. T. Wu, *Prep. Biochem. Biotechnol.*, 2007, **37**, 265–275.
- 28 B. Hu, L. Zhang, R. Liang, F. Chen, L. He and X. Zeng, *J. Agric. Food Chem.*, 2015, **63**, 2033–2040.
- 29 S. Khanahmadi, F. Yusof, A. Amid, S. S. Mahmud and M. K. Mahat, *J. Biotechnol.*, 2015, **202**, 153–161.
- 30 Y. Liu, H. Zhou, L. Wang and S. Wang, *J. Chem. Technol. Biotechnol.*, 2016, **91**, 1359–1367.

#### 4.6. Supplementary Figures and Tables

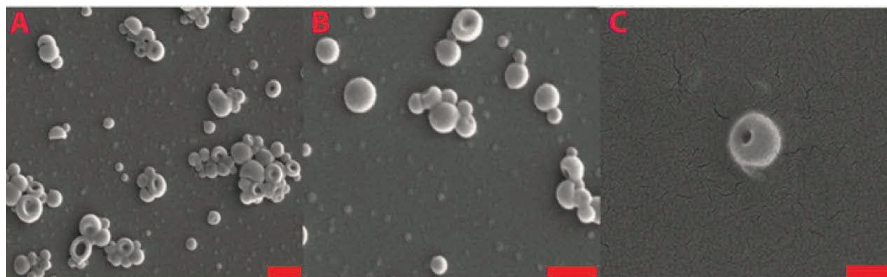


**Figure S1-** SEM images of A) open neck stomatocytes B) CalB stomatocytes after neck closure C), and subsequent cross-linking reaction of encapsulated CalB using 100 mM of glutaraldehyde. Scale bars correspond to 500 nm

Start (min)	End (min)	Mode	Crossflow start (mL min <sup>-1</sup> )	Crossflow end (mL min <sup>-1</sup> )
0	1	Elution	3.00	3.00
1	2	Focus	-	
2	3	Focus + inject	-	
3	4	Focus	-	
4	6	Elution	3.00	1.17
6	8	Elution	1.17	0.49
8	10	Elution	0.49	0.24
10	13	Elution	0.24	0.10
13	30	Elution	0.10	0.10
30	31	Elution	0.00	0.00
31	32	Elution + inject	0.00	0.00
32	37	Elution	0.00	0.00

**Table S1-** General method for the AF4 fractionations. The flow conditions applied were the following: 1.0 mL min<sup>-1</sup> detector flow, 1.00 mL min<sup>-1</sup> focus flow and 0.20 mL min<sup>-1</sup> injection flow.

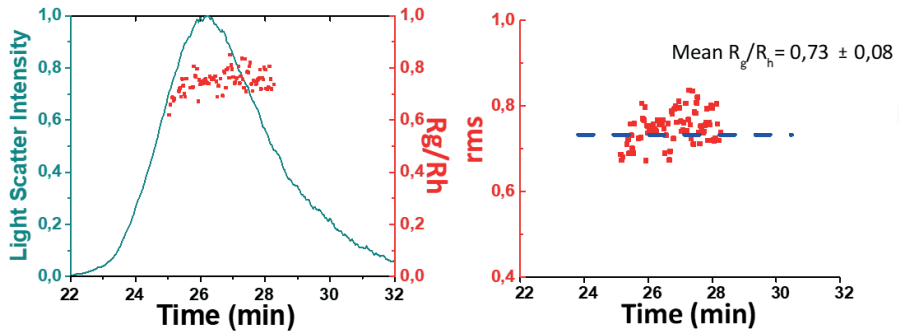


**Figure S2-** (Left) AF4 fractogram of CalB-loaded stomatocytes. (Right) The ratios between the radius of gyration ( $R_g$ ) and the hydrodynamic radius of ( $R_h$ ) of CalB-loaded stomatocytes. The blue dotted line represents the mean value of these ratios.

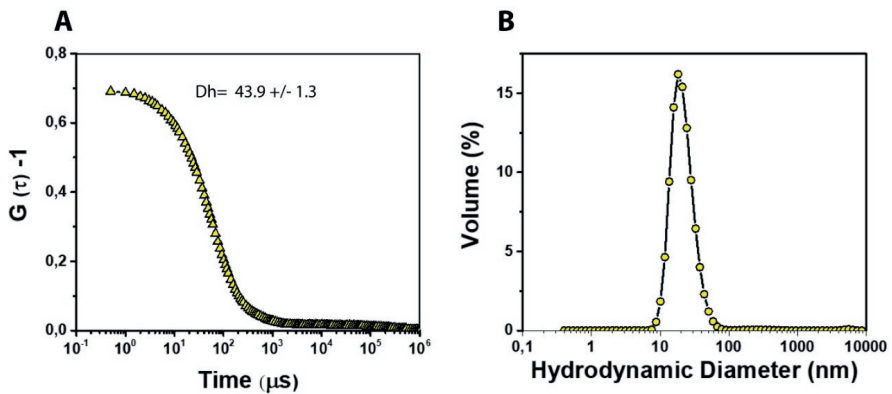


**Figure S3-** A) correlation function of the released CalB crosslinked enzyme aggregates from *c-CLEnA*; B) volume profile derived from A, showing a size distribution of  $\sim 43$  nm and a PDI of 0.5.

CalB concentration in the intital feed solution ( $\text{mg mL}^{-1}$ )	Encapsulation Efficiency (%)
3.0	$5.7 \pm 0.7$
6.0	$8.9 \pm 0.2$
12.0	$14.3 \pm 1.7$
8.0	$11.9 \pm 1.2$
14.0	$22.2 \pm 0.8$
16.0	$32.9 \pm 0.2$

PLE concentration in the initial feed solution (mg mL <sup>-1</sup> )	Encapsulation Efficiency (%)
3.0	4.9 ± 1.6
6.0	9.5 ± 1.1
8.0	11.5 ± 2.3
14.0	18.7 ± 1.5
16.0	21.0 ± 2.5

Table S2- Loading efficiency of the stomatocyte samples prepared with different enzymes.

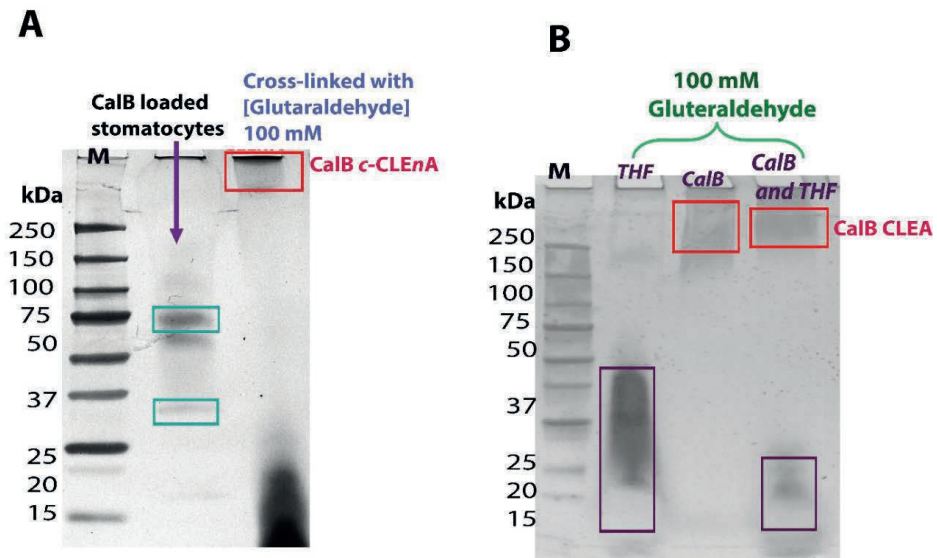


**Figure S4 – A)** SDS-PAGE gel analysis of CalB c-CLEnA formation upon cross-linking of CalB loaded stomatocytes with 100 mM of glutaraldehyde. The first lane contains Precision Plus Protein™ All Blue protein molecular weight markers (M); free CalB loaded stomatocytes are loaded in the second lane (arrow) and CalB c-CLEnA in the third lane. The expected molecular weight of CalB is 34 kDa, the dimeric form at ~70 kDa is also visible in the CalB loaded stomatocytes (green rectangles). The disappearance of these bands indicates c-CLEnA formation, which is also confirmed by the appearance of higher molecular weight species (red rectangle). **B)** SDS PAGE- Control of the low MW smear. Lane 1: Precision Plus Protein™ All Blue protein molecular weight markers (M); Lane 2: mixture of 100 mM glutaraldehyde and 150 µL of THF. Lane 3: mixture of CalB and glutaraldehyde (100 mM); lane 4: CalB c-CLEnA. The appearance of the smear at low MW only in the lanes 1 and 4 suggests that the smear is caused by presence of THF .

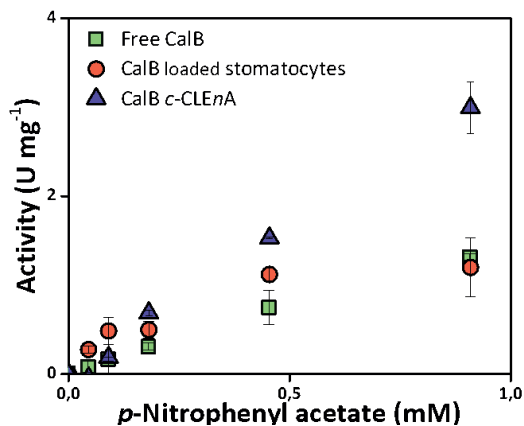


**Figure S5-** Comparison between specific activity ( $\text{U mg}^{-1}$ ) of free CalB, CalB loaded stomatocytes (with un-cross-linked CalB), and CalB c-CLEnA. The absorbance of the product is measured at 405 nm at different concentrations of substrate.

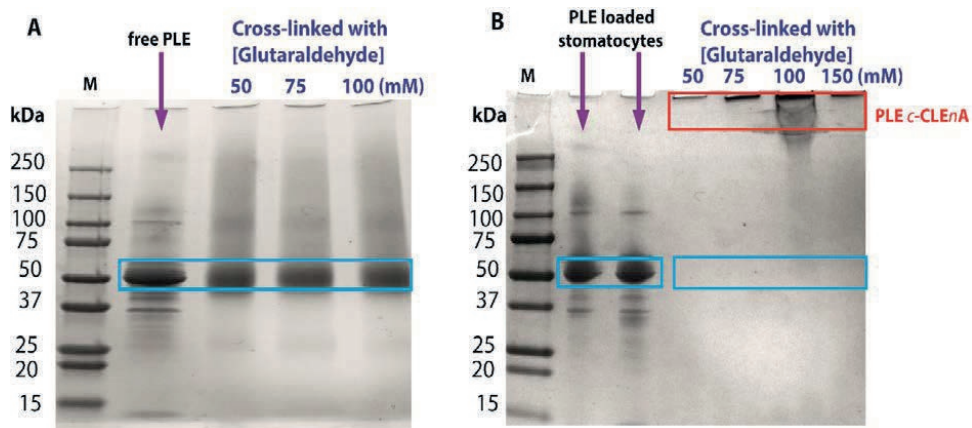


**Figure S6- A)** SDS-PAGE gel of PLE cross-linked with different glutaraldehyde concentrations in solution. From left to right: molecular weight ladder (M), the second lane (indicated with an arrow) un-cross-linked free PLE enzyme. Lane 3-5: different concentrations of glutaraldehyde used to cross-link the free PLE as depicted on top of each lane (50-75-100 mM). PLE has a molecular weight of  $\sim 60\text{kDa}$  (blue rectangle), the band was still observed after the addition of glutaraldehyde. **B)** SDS-PAGE gel of PLE-loaded stomatocytes cross-linked with different glutaraldehyde concentrations to form PLE c-CLEnA. From left to right: molecular weight ladder (M), lane 2 and 3 (indicated with arrows) PLE-loaded stomatocytes before cross-linking. Lane 4-7: different concentrations of glutaraldehyde used for PLE c-CLEnA formation, as depicted on top of each lane (50-75-100-150 mM). The disappearance of the band at 60 kDa is indicated with the blue rectangle and the appearance of higher molecular weight species is confirmed (red rectangle). All the samples in each lane are at the same concentrations.



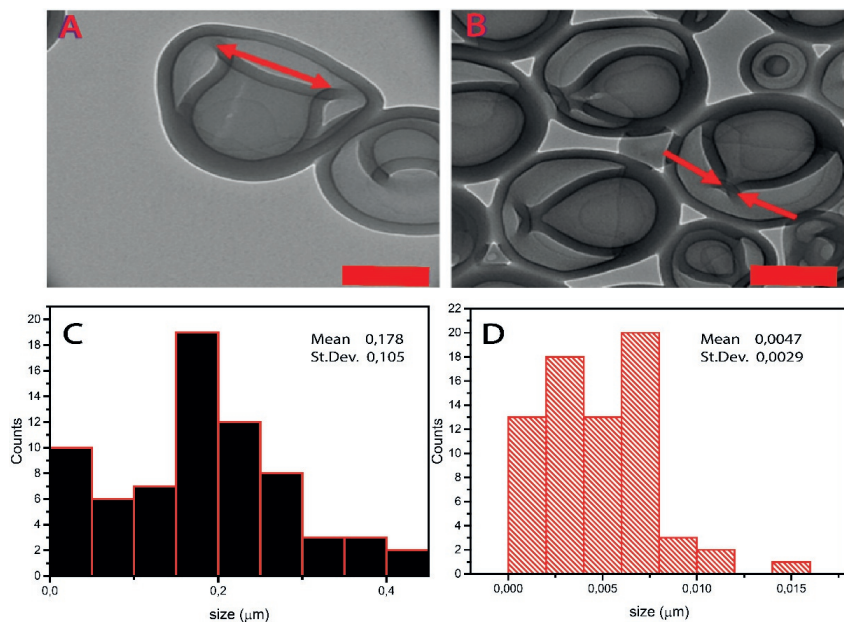


**Figure S7**-TEM images of **A)** Open neck stomatocytes **B)** CalB loaded stomatocytes after neck closure. **C)** and **D)** Mean size distribution of open and closed necks.

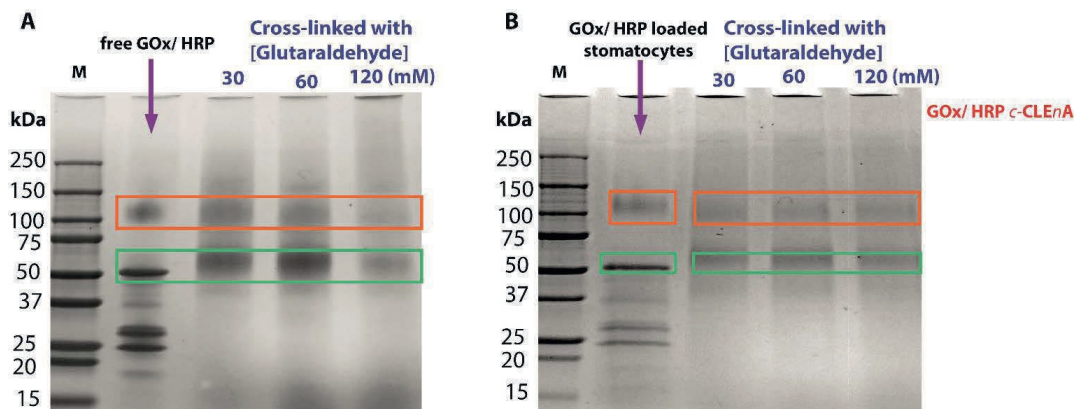


**Figure S8**- **A)** SDS-PAGE gel of free GOx/HRP cross-linked with different glutaraldehyde concentrations. From left to right: the molecular weight ladder (M), the second lane (indicated with an arrow) contains the free GOx/HRP enzymes. Lane 3-5: different concentrations of glutaraldehyde used to cross-link the free GOx/HRP as depicted on top of each lane (30-60-120 mM). The subunit enzyme molecular weights (44 kDa HRP, 160 kDa GOx) are indicated in the green and orange rectangles respectively; the bands are still observed after the addition of glutaraldehyde. **B)** SDS-PAGE gel of GOx/HRP loaded stomatocytes cross-linked with different

glutaraldehyde concentrations to form combined GOx/HRP *c*-CLEnA. From left to right: molecular weight ladder (M), the second lane (indicated with the arrow) contains the GOx/HRP loaded stomatocytes. Lane 3-5: different concentrations of glutaraldehyde used for the combined GOx/HRP *c*-CLEnA as depicted on top of each lane (30-60-120 mM). The cross-linking is confirmed by the gradual disappearance of the GOx and HRP monomer bands. All the samples in each lane are at the same concentrations.

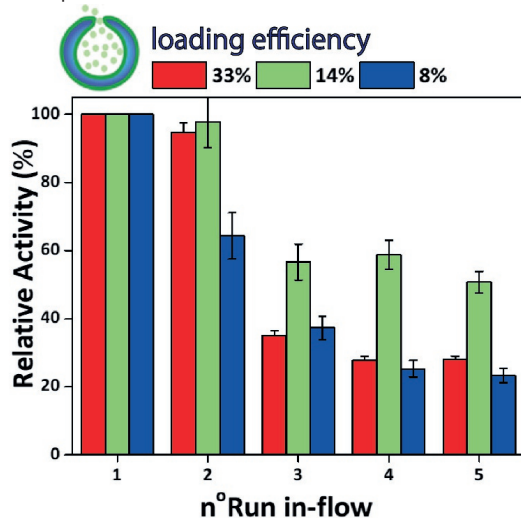


**Figure S9-** Relative activity of stomatocyte nanoreactors with different CalB loading during five runs in-flow (each run 13 min, 0.3 mL min<sup>-1</sup>).

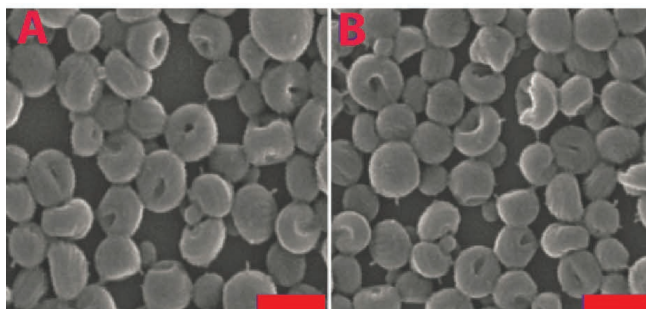


**Figure S10-** A) SEM images of CalB *c*-CLEnA after 10 runs in-flow. Scale bar corresponds to 500nm. B) SEM images of CalB *c*-CLEnA after 10 run in-flow . Scale bars correspond to 500nm.

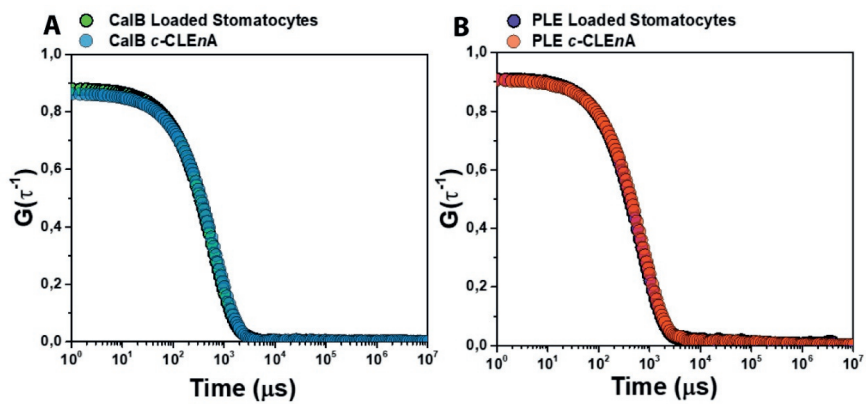
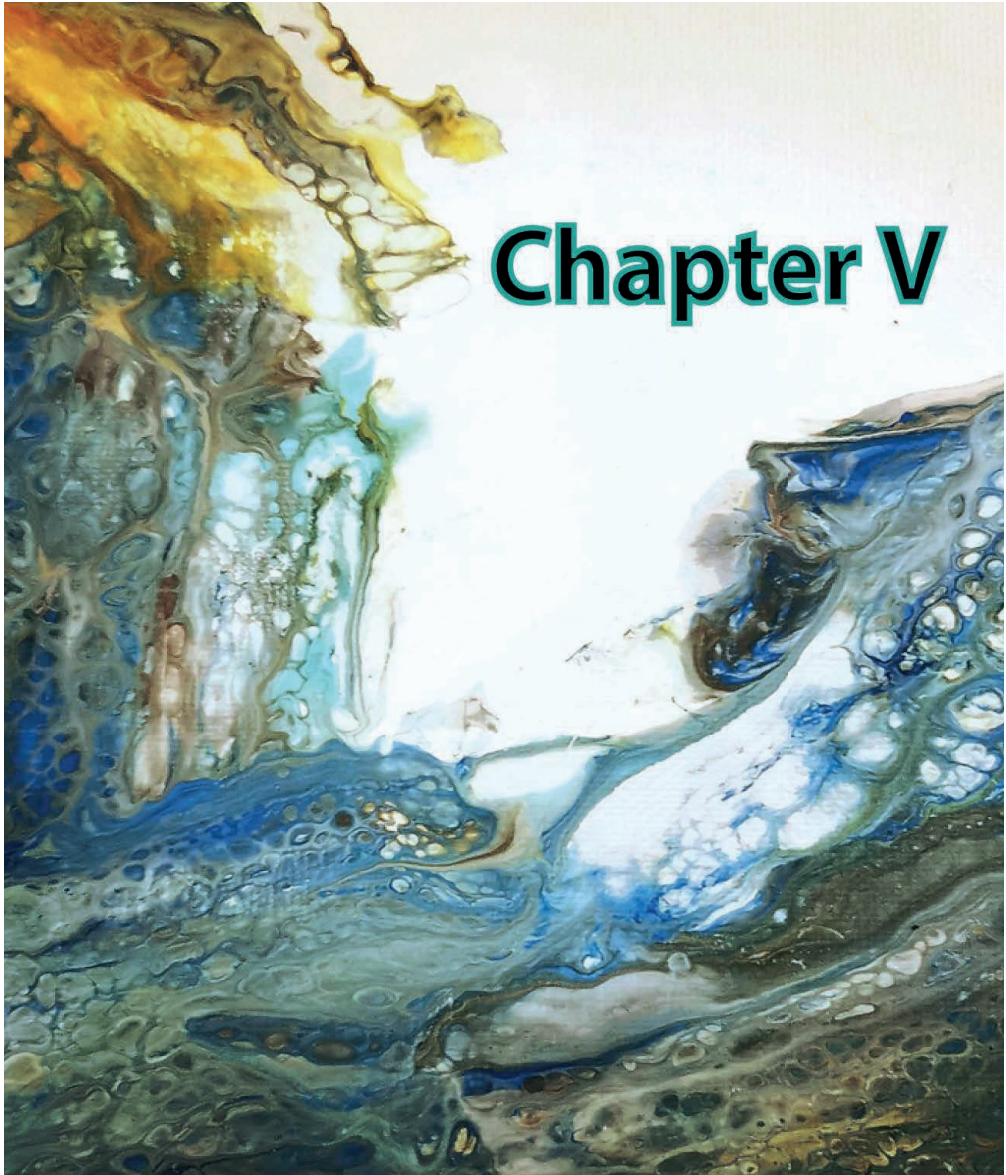


**Figure S11-** Correlation functions of **A)** CalB-loaded stomatocytes (green) and CalB c-CLEnA (blue); **B)** correlation function of PLE-loaded stomatocytes (purple) and PLE c-CLEnA (orange). No significant difference was observed after c-CLEnA formation.



Dr. Fabio Tonin and dr. Victor Bloemendal are kindly acknowledge for their contribution in this chapter.

## Extending the scope of *c*-CLEnAs: in-flow aldol condensation to Neu5Ac and one-pot multi-step synthesis of UDCA.

### Abstract

In this chapter the application of *compartmentalized*- cross-linked enzyme *nano* aggregate (*c*-CLEnA) nanoreactors is presented as an immobilization strategy for two bio-catalytic processes with relevance for the pharmaceutical industry: In the first example *N*-acetylneuraminidase (NAL) is internalized in NAL-*c*-CLEnAs and used in the in-flow aldol condensation of *N*-acetyl-D-mannosamine and sodium pyruvate to *N*-acetylneuraminic acid. In the second process the hydroxysteroid dehydrogenases (HSDH) 7 $\alpha$  and 7 $\beta$  HSDH are incorporated in *c*-CLEnAs and used in the two-step cascade batch synthesis of ursodeoxycholic acid (UDCA). The optimization of the *c*-CLEnA preparation and the application of NAL-*c*-CLEnAs in a flow process are described, demonstrating that this methodology is a versatile addition to the tool box of the process engineer.

### 5.1. Introduction

In the recent decade, there has been an ongoing search for effective implementation of enzymes in flow catalysis and multistep synthesis<sup>1-6</sup>. The use of enzymes in flow can be highly beneficial as it allows to combine the stereo and substrate selectivity of the biocatalysts with the excellent control in mass and heat transfer of the flow process<sup>7</sup>. In addition, flow applications with enzymes allow for improved kinetic control, as reactions can be steered away from equilibrium and higher conversions can be obtained, which is difficult to achieve in batch reactions. However, to make these biocatalytic processes economically feasible, often enzyme recycling is required, which necessitates enzymes to be immobilized and contained in the flow reactor. Although many immobilization strategies have been developed, they are often hampered by a loss of activity as a result of the conjugation or adsorption method employed and/or of the reduced accessibility of the catalytic sites<sup>1</sup>.

To address this issue, recently, nanoreactors have been developed which can accommodate different catalytic species and which, due to their size, on the one hand allow effective substrate access and on the other simplify workup operations<sup>8-11</sup>. In the previous chapter, we have described the development of compartmentalized- cross-linked enzyme *nano* aggregates (*c*-CLEnA) which were shown to be beneficial for preserving the native enzymatic activity, and in the case of combined-cross-linking of two enzymatic species, also resulted in enhanced activity<sup>12-14</sup>. Additionally, the stability towards leaching of the *c*-CLEnAs during flow operations was observed<sup>12</sup>. Until now, the concept of *c*-CLEnAs was demonstrated with robust model enzymes with little commercial relevance. In order to indicate the added value for the fine chemical and pharmaceutical industry, in this chapter we have investigated two

applications for *c*-CLE $n$ As as efficient bio-catalytic nanoreactors for an in-flow aldol condensation and for a one-pot biocatalytic two step reaction (Figure 1) toward useful pharmaceutical intermediates.

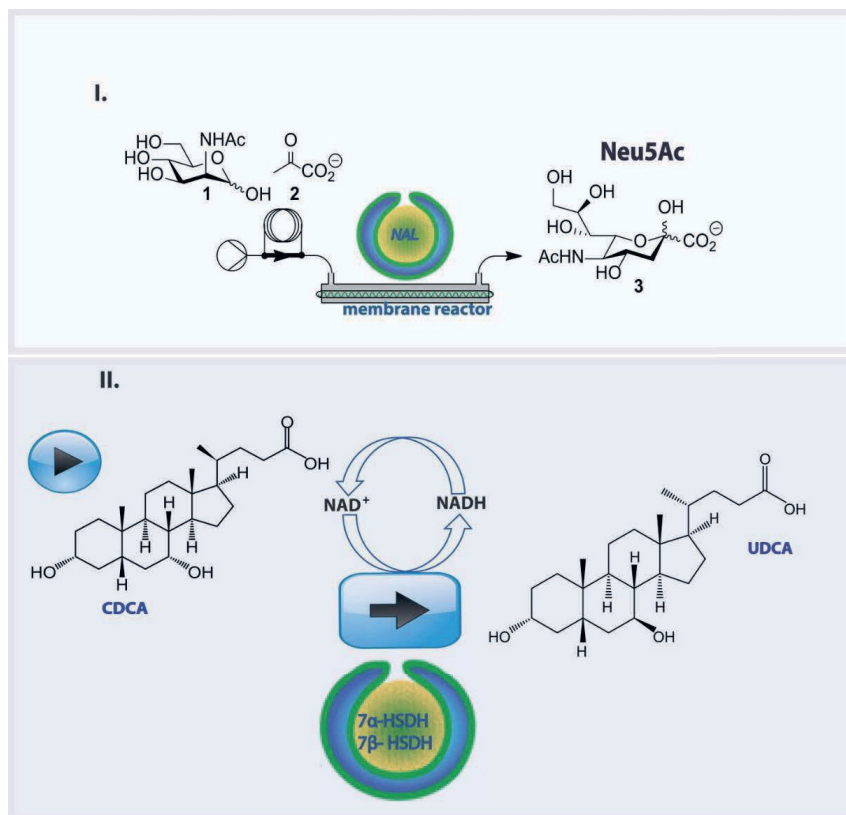


**Figure 1-** *Compartmentalized-cross-linked enzyme nano-aggregates c-CLE $n$ As for the execution of enzymatic transformations with pharmaceutical relevance I. NAL-c-CLE $n$ As for the in-flow synthesis of Neu5Ac; II. Combined 7 $\alpha$ /7 $\beta$ -HSDH c-CLE $n$ As for the one-pot cascade to UDCA.*

For the first example, we focused on *N*-acetylneuraminidase (NAL) which is a well-studied enzyme for the preparation of neuraminic acid derivatives (Neu5Ac) is<sup>15</sup>, and which excels in substrate variability and enzymatic stability (Figure 1. I.). Neu5Ac and its derivatives have a high relevance from a pharmacological point of view since they are involved in a range of physiological processes<sup>16</sup>. Derivatives of Neu5Ac have for example been used to inhibit the neuraminidases of influenza viruses A and B in a clinical setting and they are known to prevent avian influenza<sup>17,18</sup>. NAL has already been encapsulated in cross-linked enzyme aggregates (CLEA)<sup>19</sup> and crosslinked

inclusion bodies (CLIB)<sup>20,21</sup> which were both effective in retaining enzymatic activity but were challenging to prepare. In other studies, NAL has also been immobilized on Immobeads, but this process required considerable quantities of enzymes (ca. 60mg) to produce feasible amounts of Neu5Ac<sup>22</sup>. We hypothesized that using *c-CLEnAs* as a novel immobilization strategy for NAL would allow the effective implementation of this nanoreactor in a flow process with more economical use of the enzyme.

Secondly, the two enzymes  $7\alpha$  and  $7\beta$  hydroxysteroid dehydrogenase ( $7\alpha$ -HSDH and  $7\beta$ -HSDH) were encapsulated in stomatocyte nanoreactors to enable the cascade reaction for the synthesis of ursodeoxycholic acid (UDCA) (Figure 1. II.)<sup>23</sup>. The chemical transformation to UDCA, starting from chenodeoxycholic acid (CDCA), can be performed by  $7\alpha$ -HSDH and  $7\beta$ -HSDH that are respectively  $NAD^+$  and NADH dependent<sup>23</sup>. UDCA is an important secondary bile acid that is used as a pharmaceutical product in the clinic to improve liver function and solubilize cholesterol gallstones<sup>24,25</sup>. Traditionally, the non-enzymatic route for UDCA production involves many reaction steps, and besides the use of hazardous and toxic solvents, the final product is only recovered in a low yield ( $\sim 30\%$ )<sup>26</sup>. To make the synthesis more effective an enzymatic route has been developed, starting from cholic acid (CA), the cheapest bile acid available. The route entails a C12 dehydroxylation, followed by 7-OH epimerization. For the latter process  $7\alpha$ -HSDH and  $7\beta$ -HSDH work in a cascade fashion. The  $7\alpha$ -OH group of CDCA is oxidized by  $7\alpha$ -HSDH, with the concomitant reduction of  $NAD^+$  to NADH. The obtained compound (7-oxo-LCA) is subsequently reduced to the final product (UDCA) by  $7\beta$ -HSDH that utilizes the NADH produced in the first reaction. Notably, this epimerization reaction is carried out in redox-neutral manner, where the equilibrium between CDCA and UDCA is solely thermodynamically determined. Optimization of this enzymatic route can be achieved by an effective immobilization of these two complementary enzymes, allowing for an easy separation from the final product, without hampering their activity and without creating diffusional barriers for the substrates and cofactors. With this in mind, we developed the co-immobilization of  $7\alpha$ -HSDH and  $7\beta$ -HSDH in the same *c-CLEnA* nanoreactors, hypothesizing that the close proximity of the two species in the nanosized cavity of the stomatocytes would bring additional stability and high reactivity to this cascade.

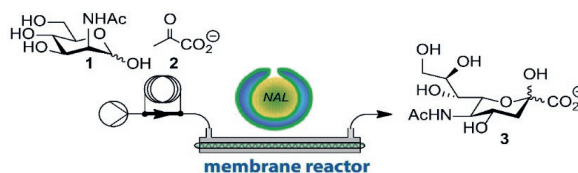
## 5.2. Results and Discussion

### 5.2.1 Development of *N*-acetylneuraminidase-based *c-CLEnAs* (NAL-*c-CLEnAs*)

In previous reports it was described that NAL is a selective but rather slow converting enzyme. As a result, to make the in-flow production of Neu5Ac feasible, the loading of NAL was an important design aspect to take into consideration<sup>15</sup>. Therefore, the preparation of NAL-*c-CLEnAs* needed some optimization from the previously described procedure<sup>12</sup>. In first instance it was attempted to create stomatocyte samples with a loading efficiency of  $\sim 30\%$  (loading efficiency calculated by Bradford assay, corresponding to  $3\text{mg mL}^{-1}$  of enzyme encapsulated starting from  $10\text{ mg mL}^{-1}$  NAL solution). The enzymes were subsequently cross-linked with either genipin (1% wt) or

glutaraldehyde (100mM-300mM).<sup>27</sup> However, these formulations showed severe problems. The formation of aggregates at the bottom of the solution was observed in the case of glutaraldehyde cross-linking, which was accompanied by a complete deactivation of the enzyme. As observed before, the fast reaction with glutaraldehyde resulted in the denaturation of the enzymes. Furthermore, the high enzyme loading led to cross-linking between particles, causing precipitation. When a solution (1% wt) of the milder cross-linking agent genipin was used for the NAL-c-CLEnA preparation this latter problem was resolved. However, also in this case enzyme activity was negligible. Surprisingly, this was not observed when using ca. 14% loaded samples (1.4 mg NAL loaded in 500  $\mu\text{L}$  of 10 mg  $\text{mL}^{-1}$  stomatocytes). Enzyme activity was preserved and no aggregation was observed. This NAL-c-CLEnA was subsequently used for the flow experiments.

Several solutions of 14% loaded NAL-c-CLEnAs were tested in the continuous aldol reaction of a stock solution of *N*-acetyl-D-mannosamine (**1**) and sodium pyruvate (**2**) using a membrane reactor (Figure 2, Table S1). For ensuring a NAL loading of at least 20 mg in the membrane reactor, 10mL samples (10 mg  $\text{mL}^{-1}$ ) were concentrated to 3 mL and the final solution was loaded in the membrane. The catalytic activity was investigated by varying flow rates, temperature, and also the type of membrane (Table S1). When 500 mM of (**1**) and 100 mM of (**2**) were fed at 35°C over a modified poly(ether sulfone) (mPES) membrane (10 kDa) at 20  $\mu\text{L min}^{-1}$  69% yield of Neu5Ac was observed. At higher temperatures (50°C) and for the rest of the same conditions, the activity was decreased to 50%. Increasing the flow rate resulted in a lower conversion, as expected. However, for the highest flow rate tested (100  $\mu\text{Lmin}^{-1}$ ) the conversion was still 35%.



Flow ( $\mu\text{Lmin}^{-1}$ )	$t_R$ (min)	T ( $^{\circ}\text{C}$ )	Conversion (%)
100	15	35	35
75	20	35	41
50	30	35	47
40	37.5	35	52
30	50	35	60
20	75	35	69
20	75	50	50
50	30	60	48
50	30	70	22



**Figure 2-** Schematic setup and conversions to *N*-acetylneuraminic acid **3** with NAL-*c*-CLEnA- Conditions: A stock solution of *N*-acetyl-D-mannosamine (**1**) and sodium pyruvate (**2**) (respectively 500 mM and 100 mM) in water (900  $\mu$ L) was injected in a sample loop (1 mL) and pumped (at different flow rates) over the microporous hollow fibre reactor (mPES 10 kDa, 1.5 mL) loaded with genipin cross-linked NAL-*c*-CLEnA (0.34 g mL<sup>-1</sup> of *c*-CLEnA, containing 18 mg of NAL) at various temperatures. The product flow was collected for at least  $2.0 \times t_R$ . The conversion was determined by <sup>1</sup>H NMR analysis of the crude reaction mixture.

The obtained conversions were comparable to previous results reported<sup>22</sup>, and could even potentially be improved by a further optimization. Still, the use of NAL-*c*-CLEnA already effectively decreased enzyme loading by a factor of  $\sim 3$ , thus increasing the turnover number of NAL. Furthermore, the stability of NAL-*c*-CLEnAs in flow was also object of our investigation (Figure 3).

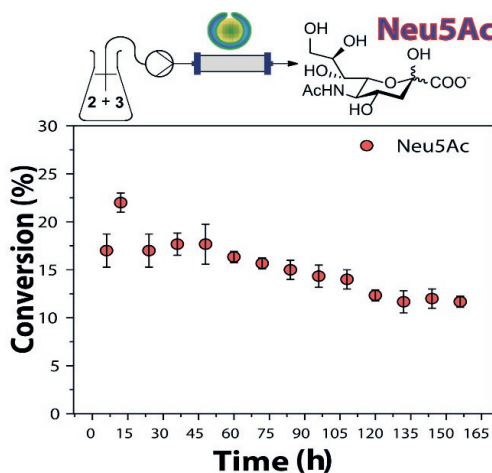


**Figure 3-** Stability test of NAL-*c*-CLEnA in a continuous flow setup. Conditions: ManNAc (**1**, 500 mM), sodium pyruvate (**2**, 100 mM), H<sub>2</sub>O, NAL-*c*-CLEnA (3 mL of 0.34 g mL<sup>-1</sup>, containing 18 mg of NAL). 25  $\mu$ Lmin<sup>-1</sup>, 35 °C. Conversions determined in triplo by <sup>1</sup>H NMR analysis of the crude reaction mixture (Figure S1).

For the stability experiments, the flow setup was based on a hollow fiber reactor with a membrane of mixed cellulose ether (ME) with 0.1  $\mu$ m pore size. This membrane would allow for the retention of the polymeric nanovesicles in the tubular reactor but not of the enzymes in case of leaching. The conditions were chosen to ensure a conversion below 50%, in order to have a more accurate insight on the change of conversion over time as a function of leaching. In this way, when NAL-*c*-CLEnAs were tested in the flow reactor for a week, Neu5Ac formation was still observed. The use of NAL immobilized-beads resulted in  $\sim 33\%$  of loss in activity in a previous report<sup>15</sup>; we proved that our NAL-*c*-CLEnAs demonstrated similar stability ( $\sim 31\%$  loss after the same period).

## 5.2.2 Development of 7 $\alpha$ -HSDH- and 7 $\beta$ -HSDH-*c*-CLEnAs for the synthesis of ursodeoxycholic acid (UDCA)

Another example of the employment of the *c*-CLE<sub>n</sub>A system in the synthesis of pharmaceutical compounds is in the enzymatic redox-neutral epimerization of CDCA. Recently, this reaction has been carried out by employing two enzymes (7 $\alpha$ -HSDH and 7 $\beta$ -HSDH)<sup>23</sup>.

The enzymes were produced and purified according to the literature<sup>23</sup>. Afterward, different nanoreactors were prepared by encapsulating the two enzymatic species either separately or together. Firstly, the two enzymes were encapsulated separately, leading to the construction of 7 $\alpha$ -HSDH-*c*-CLE<sub>n</sub>As and 7 $\beta$ -HSDH-*c*-CLE<sub>n</sub>As, both with a loading efficiency of 25% (2 mg of enzyme loaded in 500  $\mu$ L of 10 mg mL<sup>-1</sup> sample, determined by a Bradford assay)<sup>23</sup>. The optimal amount of genipin needed for the cross-linking of the enzymes was established by analyzing the residual specific activity of the enzymes after encapsulation and cross-linking. Similarly to the NAL-*c*-CLE<sub>n</sub>As, using glutaraldehyde as cross-linker deactivated significantly both enzymes. Still, none of the *c*-CLE<sub>n</sub>As showed the formation of clustering or sedimentation in contrast to the previous example with NAL. When a genipin solution at 1%wt was used to cross-link the samples the activity of both enzymes was conserved. In particular, 7 $\alpha$ -HSDSH-*c*-CLE<sub>n</sub>A showed a specific activity of 382.7 U mg<sup>-1</sup> (while for the free 7 $\alpha$ -HSDSH this is 432.8 U mg<sup>-1</sup>) and 7 $\beta$ -HSDH -*c*-CLE<sub>n</sub>A showed an activity of 6.0 U mg<sup>-1</sup> (2.38 U mg<sup>-1</sup> for the free 7 $\beta$ -HSDSH). Notably, batch-to-batch variations were observed using different amounts of genipin (1.6 wt% or 0.75wt%) (Table S2). The difference in the activity observed could be explained as an effect of the changed ratio between enzyme concentration and cross-linker concentration ([enzyme:genipin]). By increasing or decreasing this ratio, *e.g.* changing the enzyme loading or the genipin amount, the cross-linking process can result in inhomogeneous or inefficient formation of nano-aggregates with consequences on the final activity measured. When the amount of genipin was increased (1.6 wt% genipin) the formation of cross-linked nano-aggregates could be expected to occur faster but might have caused deformation on the enzyme structure that resulted in a partial deactivation in case of 7 $\alpha$ -HSDSH-*c*-CLE<sub>n</sub>A and in the total deactivation in the case of 7 $\beta$ -HSDSH. When less genipin was employed (0.75 wt% genipin) the cross-linking rate was slower, which could result in inefficient formation of nano-aggregates. In this case, again 7 $\beta$ -HSDSH results completely deactivated while 7 $\alpha$ -HSDSH-*c*-CLE<sub>n</sub>A maintained less than 5% of its native activity. When glutaraldehyde was used as a cross-linker, both the *c*-CLE<sub>n</sub>As were not active anymore, suggesting that using a faster bifunctional cross-linker might not be suitable for these particular enzymes. The use of 1wt% genipin reproducibly resulted in the optimal conditions for *c*-CLE<sub>n</sub>A formation, as 7 $\alpha$ -HSDSH-*c*-CLE<sub>n</sub>As displayed an activity still very close to the one shown by the free enzyme, and 7 $\beta$ -HSDH -*c*-CLE<sub>n</sub>As showed even an increase compared to the free enzyme in all the samples tested.

Next, the co-encapsulation of the two enzymes in a single nanoreactor was investigated. Ideally, co-encapsulation is advantageous since it reduces the diffusion limitations of the reagents and cofactors (CDCA/7-oxo-LCA and NAD<sup>+</sup>/NADH). The encapsulation and cross-linking processes were carried out using the same procedure as for the single enzyme encapsulation, therefore to 25% loaded 7 $\alpha$ /7 $\beta$ -HSDH stomatocyte samples (2mg of total enzyme mixture loaded in the sample), 1wt% genipin was added to afford 7 $\alpha$ /7 $\beta$ -HSDH *c*-CLE<sub>n</sub>As. A sample of co-encapsulated enzymes without cross-linking (7 $\alpha$ /7 $\beta$ -HSDH stomatocytes, 25% loading efficiency) was used as control

to evaluate the effect of the cross-linking step on the enzymatic activities. Notably, stomatocytes and *c*-CLEnA showed similar activities. This indicates that, despite the constraints formed by the cross-linker, the enzymes conserved their activity when a milder cross-linker as genipin is used.

To establish the applicability of the newly obtained nanoreactors for the epimerization of CDCA into UDCA, a series of bioconversions was performed (Figure 4).

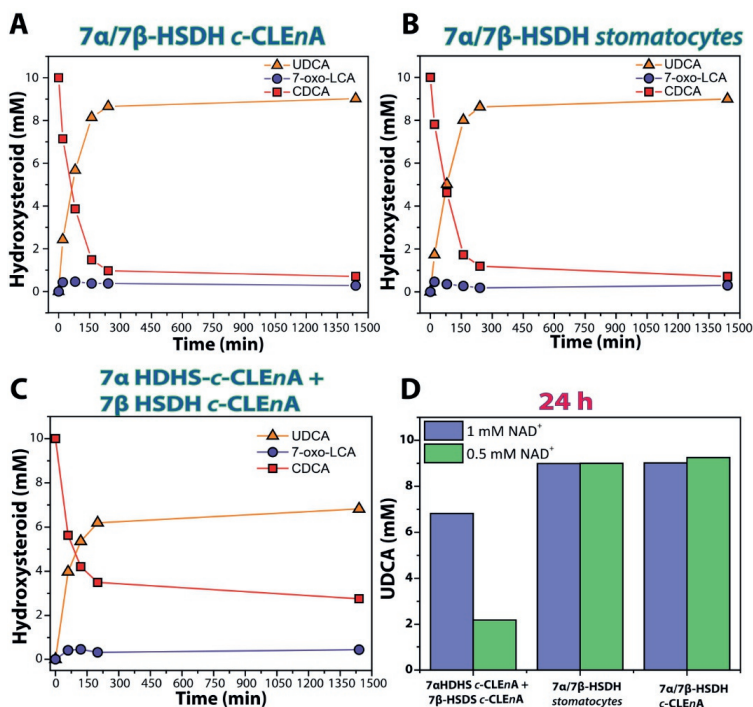


**Figure 4:** Bioconversion of 10 mM CDCA into UDCA with 1mM of NAD<sup>+</sup> by using **A)** co-encapsulated 7 $\alpha$ /7 $\beta$ -HSDH *c*-CLEnA **B)** co-encapsulated 7 $\alpha$ /7 $\beta$ -HSDH stomatocytes **C)** 7 $\alpha$  + 7 $\beta$ -HSDH in separate *c*-CLEnAs. **D)** bar plot reporting the amount of UDCA (mM) formed after 24h reaction with 0.5 mM and 1mM of NAD<sup>+</sup>. 7-oxo-LCA is the intermediate product 7-oxolithocholic acid. The amount of enzymes in A) and B) is 200  $\mu$ g (equivalent to 1.5 U and 0.9 U of 7 $\alpha$ - and 7 $\beta$ -HSDH activity, respectively) and in C) 1 U<sub>TOT</sub> of 7 $\alpha$  HSDH *c*-CLEnA (2.6  $\mu$ g) and 0.8 U<sub>TOT</sub> of 7 $\beta$ -HSDH *c*-CLEnA (133  $\mu$ g).

When the cascade reaction was performed using the co-encapsulated enzymes 7 $\alpha$  and 7 $\beta$ -HSDH in stomatocytes or in *c*-CLEnAs (Figure 4A-B) no significant differences between the two nanoreactors were observed. This again, proves that the optimized cross-linking with genipin did not influence the activity of the enzymes encapsulated. Using a catalyst loading of 200-300  $\mu$ g (equivalent to 1.5 U and 0.9 U of 7 $\alpha$ - and 7 $\beta$ -HSDH activity, respectively) and 1 mM of NAD<sup>+</sup>, 8.6 mM (conversion 86%) and 8.7 mM (conversion 87%) of UDCA were obtained after 200 min using 7 $\alpha$ /7 $\beta$ -HSDH stomatocytes and 7 $\alpha$ /7 $\beta$ -HSDH *c*-CLEnA, respectively. In comparison to literature in which the free enzymes

were used, the reaction with *c*-CLEnA showed comparable rates and conversion values<sup>28</sup>. In addition, when a catalyst loading of 20-30  $\mu\text{g}$  (equivalent to 0.15 U and 0.09 U of 7 $\alpha$ - and 7 $\beta$ -HSDH activity, respectively) was used, 9.0 mM of UDCA was obtained, (90% conversion) after 24 h using both kinds of preparations. Similar conversions were obtained when 0.5 mM  $\text{NAD}^+$  was used (Figure 4D).

On the other hand, when bioconversions were performed at similar conditions using separately encapsulated 7 $\alpha$  + 7 $\beta$ -HSDH *c*-CLEnAs (1  $U_{\text{TOT}}$  of 7 $\alpha$  HSDH *c*-CLEnA (2.6  $\mu\text{g}$ ) and 0.8  $U_{\text{TOT}}$  of 7 $\beta$ -HSDH *c*-CLEnA (133  $\mu\text{g}$ )) lower activities were observed (Figure 4C). When 1 mM of  $\text{NAD}^+$  was used, 6.2 mM (62% conversion) and 6.7 mM (67% conversion) of UDCA were obtained after 200 min and 24 h, respectively. Additionally, when 0.5 mM of  $\text{NAD}^+$  was used with separately encapsulated 7 $\alpha$  + 7 $\beta$ -HSDH *c*-CLEnAs, only 2.2 mM of UDCA (22% conversion) was obtained after 24 h (Figure 4D).

Our experiments suggest that having the enzymes encapsulated in two different compartments poses an additional barrier to the substrate/co-factor diffusion to activate the second step of the cascade, impacting the final conversion which is considerably lower compared to the free enzyme cascade. This is especially visible when the co-factor concentration is lowered, and the final conversion is 22%. However, this is not observed with the 7 $\alpha$ /7 $\beta$ -HSDH *c*-CLEnA and stomatocytes in which the bioconversions show good agreement with the cascade reaction performed with the 7 $\alpha$  and 7 $\beta$ -HSDH free enzymes. In these systems there is no diffusional constraint for the second enzymatic conversion. This demonstrates that the co-encapsulation in stomatocytes allows the cascade reaction to be performed without negative effects on conversion, but with the potential benefit of easy catalyst recovery

### 5.3. Conclusions

In summary, *c*-CLEnAs were implemented for the *N*-acetylneuraminic acid lyase mediated production of Neu5Ac in flow, and for the bioconversion of CDCA to UDCA via 7 $\alpha$ -HSDH and 7 $\beta$ -HSDH, combined in *c*-CLEnAs (7 $\alpha$ /7 $\beta$ -HSDH-*c*-CLEnAs). Both nanoreactor systems showed to be inactive when crosslinked using glutaraldehyde but gratifyingly retained enzymatic activity upon controlled crosslinking with genipin. For the *N*-acetylneuraminic acid lyase synthesis, the NAL-*c*-CLEnAs were loaded in a hollow fiber membrane flow reactor. After optimizing the reaction conditions by using a modified polyethersulfone reactor and low flow rates a conversion of 69% to Neu5Ac was achieved. Although this yield did not outrank previous results with the Immobead-NAL, it effectively decreased enzyme loading by a factor of three, thus increasing the turnover number of the neuraminic acid lyase. The stability of the NAL-*c*-CLEnAs was further demonstrated in a continuous experiment for 168 hours with a moderate loss in their activity. Regarding the cascade to UDCA, the activity of the two enzymes was preserved after cross-linking the two enzymes in the same stomatocytes with genipin, and no significant difference was observed between the uncrosslinked enzyme-loaded stomatocytes and the *c*-CLEnA. However, the combined *c*-CLEnA proved to be more active than when the two enzymes were compartmentalized in separated *c*-CLEnAs, especially at lower concentrations of the cofactor NADH.

## 5.4. Experimental Section

### 5.4.1. Materials and Methods

All chemicals and enzymes were purchased from Sigma-Aldrich and used as received unless otherwise stated. For the synthesis of the block copolymer, CuBr was activated using acetic acid for 3 h and dried in vacuum. Ultra-pure MilliQ water (Labconco Water Pro PS purification system) was used for the self-assembly of polymersomes and dialysis. The dialysis membranes (MWCO 12-14 kDa Spectra/Por®), Amicon Ultra-0.5 mL centrifugal filter Unit 3 kDa (Millipore), and Ultrafree-MC centrifugal filters (with 0.1 and 0.22  $\mu\text{m}$  pore size) (Millipore) were used to remove the excess of enzyme after encapsulation, and to wash the nanoreactors after the flow experiments. *N*-acetylneuraminidase - crystalline (EC 4.1.3.3) was supplied by Biosynth Carbosynth®, 7 $\alpha$ -HSDH and 7 $\beta$ -HSDH were recombinantly produced and purified in TU/Delft by Dr. F.Tonin. The glutaraldehyde solution (25% w/w in H<sub>2</sub>O) was purchased from Sigma Aldrich and solutions at different concentrations were prepared for the *c*-CLEnA formation. Genipin ( $\geq 98\%$  (HPLC) in powder) was also purchased from Sigma Aldrich and solutions at different concentrations were prepared in MilliQ water.

**Proton nuclear magnetic resonance (<sup>1</sup>H NMR):** <sup>1</sup>H NMR spectra were recorded on a Varian Inova 400 spectrometer with CDCl<sub>3</sub> as a solvent and TMS as internal standard. <sup>1</sup>H NMR spectra were used to determine the molecular weight of the synthesized copolymers.

**Gel permeation chromatography (GPC):** The dispersity ( $\bar{M}_w/\bar{M}_n$ ) of the copolymers was determined using a Shimadzu Prominence GPC system equipped with a PL gel 5  $\mu\text{m}$  mixed D column (Polymer Laboratories) and differential refractive index and UV (254 nm) detectors. THF was used as an eluent at a flow rate of 1 mL min<sup>-1</sup>.

**Size Exclusion Chromatography (SEC):** For an efficient separation of the stomatocytes from the unencapsulated enzymes, a Shimadzu Prominence SEC system equipped with a Superose™ 6 column and a UV detector (220 nm) was used. The separation was performed using filtered PBS buffer at 0.8 mL min<sup>-1</sup>.

**Transmission electron microscopy (TEM):** TEM images were recorded using a FEI Tecnai 20 (type Sphera) at 200 kV. 5  $\mu\text{L}$  sample was dropped on top of a carbon-coated copper grid (200 mesh, EM science), and the desalted samples were left to dry at room temperature overnight.

**High Performance Liquid Chromatography (HPLC):** HPLC analyses were performed on a Shimadzu apparatus equipped with an LC20AT pump and an ELSD-LTII detector and fitted with an XTerra RP C18 column (length/internal diameter 150/4.6 mm, pore size 5  $\mu\text{m}$ ) under the following conditions: eluent H<sub>2</sub>O/CH<sub>3</sub>CN/TFA (65/35/1), flux 1.0 mL min<sup>-1</sup>.

**NAL- *c*-CLEnA Activity in Flow:** Multiple NAL-*c*-CLEnAs (10mg mL<sup>-1</sup>) containing ca 1.4 mg of NAL were mixed together to reach a final amount of ca 20 mg NAL. The final solution was adjusted to 3mL via spin filtration (0.1  $\mu\text{m}$ ,

3000rpm) for 10 mins. The aqueous suspension was vortexed and loaded into a syringe (1 mL), after which it was coupled directly to the side-inlet of the flow reactor. Using a syringe pump, the solution was slowly added to the reactor ( $\leq 0.5 \text{ mLmin}^{-1}$ ), effectively eluting excess aqueous solvent. This procedure was repeated 3  $\times$  after which the reactor was sealed before the catalysis experiments. After the indicated time intervals (Table S1) the reaction mixture was separately collected for 10 min (3  $\times$ ). The samples were concentrated *in vacuo* and the conversion determined using  $^1\text{H}$  NMR in  $\text{D}_2\text{O}$ .

**NAL- *c-CLEnA* stability test in a membrane in-flow reactor:** The MikroKros<sup>®</sup> reactor was loaded with *c-CLEnA* enzyme dispersion (containing up to 18 mg NAL) according to the aforementioned procedure. An HPLC pump was loaded with a solution of ManNAc (**1**, 500 mM) and sodium pyruvate (**2**, 100 mM) and the pH was adjusted to 7.0 using 1 M aqueous NaOH or HCl. The MikroKros reactor was connected directly to the HPLC pump. The reactor has a filter module: ID (mm) 0.5, pore size 10 kDa of poly(ether sulfone) (mPES Effective Length (cm) 20.0, Total Length (cm) 23.0, surface area 28.0  $\text{cm}^2$  and was purchased from Spectrum Lab<sup>®</sup>. The reactor was submerged in a 35  $^\circ\text{C}$  water bath for 10 minutes before starting the experiment. The flow rate was set to 25  $\mu\text{Lmin}^{-1}$ , and the substrate solution was continuously pumped through the reactor. After the indicated time intervals, the reaction mixture was separately collected for 10 min (3  $\times$ ). The samples were concentrated *in vacuo* and the conversions were determined using  $^1\text{H}$  NMR in  $\text{D}_2\text{O}$ .

**Enzymatic assay:** the enzymatic activity of 7 $\alpha$ -HSDH and 7 $\beta$ -HSDH (on purified enzyme, encapsulated and co-encapsulated) was determined at room temperature (25  $^\circ\text{C}$ ) using 2.0 mM CDCA or UDCA respectively, 1.0 mM  $\text{NAD}^+$ , in 50 mM KPi buffer and 10% methanol (v/v), pH 8.0. The 7 $\alpha$ -HSDH activity was measured using the conversion of CDCA into the intermediate 7-oxo-LCA. The activity of 7 $\beta$ -HSDH was measured using the reverse reaction from UDCA to 7-oxo-LCA (as the intermediate compound 7-oxo-LCA is not commercially available). The extinction coefficients of NADH, at 340 nm is 6.220  $\text{M}^{-1}\text{cm}^{-1}$ . One unit (U) was defined as the amount of enzyme producing 1  $\mu\text{mol}$  of product per minute at 25  $^\circ\text{C}$  and at pH 8.0. Blank measurements were performed in the absence of CDCA,  $\text{NAD}^+$  and enzyme. Results are reported in Table S2.

**Epimerization of CDCA to UDCA with separately encapsulated enzymes (7 $\alpha$ -HSDH -*c-CLEnA* and 7 $\beta$ -HSDH -*c-CLEnA*):** All conversions were carried out employing 1  $U_{\text{TOT}}$  of 7 $\alpha$ -HSDH *c-CLEnA* (15  $\mu\text{L}$  of a 10x diluted stock, 2.6  $\mu\text{g}$ ) and 0.8  $U_{\text{TOT}}$  of 7 $\beta$ -HSDH *c-CLEnA* (333  $\mu\text{L}$ , 133  $\mu\text{g}$ ) on 10 mM CDCA, using 1 or 0.5 mM  $\text{NAD}^+$ . As a general procedure, 1 mL of reaction mixture containing 10% MeOH and 50 mM of KPi buffer, pH 8.0 was incubated at 25  $^\circ\text{C}$  on a rotatory wheel. At fixed times of incubation 50  $\mu\text{L}$  of reaction mixture were diluted with 200  $\mu\text{L}$  of mobile phased centrifuged in order to separate the nanoreactors from the mixture (14000 rpm, 2 min). The supernatant was filtered (syringe filter 0.2  $\mu\text{m}$ ) and 10  $\mu\text{L}$  of these preparations were analyzed by HPLC.

**Epimerization of CDCA to UDCA with co-encapsulated enzymes (7 $\alpha$ /7 $\beta$ -HSDH stomatocytes and 7 $\alpha$ /7 $\beta$ -HSDH -c-CLEnA):** All conversions were carried out employing different amounts of 7 $\alpha$ /7 $\beta$ -HSDH c-CLEnA (300  $\mu$ L of different dilution, Table S3) on 10 mM CDCA, using 1 or 0.5 mM NAD<sup>+</sup>. As a general procedure, 1 mL of reaction mixture containing 10% MeOH and 50 mM of KPi buffer, pH 8.0 was incubated at 25 °C on a rotatory wheel. At fixed times of incubation 50  $\mu$ L of reaction mixture were diluted with 200  $\mu$ L of mobile phase and centrifuged in order to separate the nanoreactors from the mixture (14000 rpm, 2 min). The supernatant was filtered (syringe filter 0.2  $\mu$ m) and 10  $\mu$ L of these preparations were analyzed by HPLC.

**Bradford assay:** The Bradford method was used to quantify the enzyme loading. Pierce™ Coomassie Plus (Bradford) assay kit was used as described in the protocol of the assay, Table S1 reports the amount of enzyme used in all the experiments.

## 5.5. Experimental procedures

### 5.5.1. Synthesis of poly(ethylene glycol)<sub>44</sub>-polystyrene (PEG<sub>44</sub>-*b*-PS<sub>200</sub>) block copolymer

PEG-*b*-PS was synthesized using atom-transfer controlled radical polymerization (ATRP), according to previously reported literature procedures. For the macro initiator synthesis, poly(ethylene glycol) methyl ether (5.0 g, 2.5 mmol), was twice dried by co-evaporation with toluene. In a flame-dried Schlenk tube, the poly(ethylene glycol) methyl ether was then dissolved in dry THF (2.0 mL) and triethylamine (1.04 mL, 7.5 mmol) was added to the solution. The Schlenk tube was placed on an ice bath, followed by the dropwise addition of  $\alpha$ -bromoisobutyryl bromide (616  $\mu$ L, 5.0 mmol) while stirring. The solution was then stirred for a further 24 h, while slowly warming to room temperature, to form a white solid due to the amine salt in the colorless solution. The amine salt was filtered off and the solution was concentrated in vacuum. The precipitation of macro-initiator poly(ethylene glycol)<sub>44</sub> methyl ether 2-bromoisobutyrate was induced by ice-cold diethyl ether.

For the PEG<sub>44</sub>-*b*-PS<sub>200</sub> synthesis, copper bromide (CuBr) (45.0 mg, 0.32 mmol) was first added to a flame dried Schlenk tube equipped with a stirring bar under argon atmosphere. The Schlenk tube was sealed with a septum, and evacuated for 15 min, after which argon was filled back into the flask. PMDETA (66.0  $\mu$ L, 0.32 mmol) was dissolved in toluene (0.5 mL) and added to the CuBr powder. The mixture was left stirring for 15 min with argon for oxygen removal. Poly(ethylene glycol) macroinitiator (215 mg, 0.10 mmol), dissolved in toluene (1 mL), was added into the Schlenk tube. The solution was degassed for 15 min while cooling in an ice bath. Distilled styrene (5.0 mL, 43.6 mmol) was added to the reaction mixture. The mixture was then degassed and the Schlenk tube was inserted into a preheated 70 °C oil bath, overnight. At the end of the reaction, dichloromethane (DCM) (75 mL) was added to the polymer solution and the mixture was filtered over an alumina column to remove the CuBr. The final solution was then concentrated and the polymer was precipitated in cold methanol, filtered, and dried overnight in vacuum. The amphiphilic polymer obtained, PEG<sub>44</sub>-*b*-PS<sub>200</sub> had a number average molecular weight ( $M_n$ ) of 29.1 kg mol<sup>-1</sup> and  $\bar{D}$ = 1.08.

### 5.5.2. General procedure for polymersome preparation

The polymersomes were self-assembled using a slightly modified variation of a previously reported solvent switch method.

In short, 20.0 mg synthesized PEG<sub>44</sub>-*b*-PS<sub>200</sub> polymer was dissolved in a 2 mL mixture of THF: dioxane (4:1 v/v), to which 1.0 mL MilliQ was added via a syringe pump with a flow rate of 1.0 mL h<sup>-1</sup>, resulting in the formation of a cloudy solution. The assembly was performed inside a 5.0 mL vial which contained a magnetic stirring bar and which was capped with a septum. The cloudy solution was then dialyzed against MilliQ water for 24 h, with the MilliQ frequently refreshed.

### 5.5.3. General procedure for stomatocyte preparation and enzyme loading

Stomatocytes were prepared using the previously reported solvent addition methodology as described in Chapter IV. Next, 1 mL of a 10 mg mL<sup>-1</sup> NAL solution in 50 mM sodium phosphate buffer (50 mM pH 7.5), was added to the stomatocytes and mixed vigorously at 7000 rpm for 30 mins. To narrow the neck of the stomatocytes 150  $\mu$ L THF: dioxane (4 : 1 v/v) at 150  $\mu$ L h<sup>-1</sup> flow rate was added to the solution. To remove the THF, samples were purified using spin filtration (15 mins, 13523 rcf) two times with Amicon 3 kDa filters. To remove non-encapsulated enzymes, stomatocytes were purified from the solution mixture using size exclusion chromatography (SEC). After SEC, the stomatocytes were concentrated again to a final volume of 500  $\mu$ L (10 mg mL<sup>-1</sup>). The same procedure was used for the 7 $\alpha$ -HSDH and 7 $\beta$ -HSDH stomatocytes, using 8 mg mL<sup>-1</sup> of 7 $\alpha$ -HSDH and 8 mg mL<sup>-1</sup> of 7 $\beta$ -HSDH or a solution of [7 $\alpha$ -HSDH +7 $\beta$ -HSDH]=8 mg mL<sup>-1</sup> with both enzymes. In the case of 7 $\alpha$ -HSDH and 7 $\beta$ -HSDH, the samples were re-dispersed in PKi (50mM pH = 8).

### 5.5.4. General procedure for the formation of compartmentalized cross-linked enzyme nano aggregates (c-CLEnA) with glutaraldehyde

Having ensured complete removal of free enzyme from the previously prepared stomatocyte nanoreactors, glutaraldehyde (100  $\mu$ L, at different concentrations varying between 100 mM and 300 mM) was slowly added, at a rate of 100  $\mu$ L h<sup>-1</sup>, to a 500  $\mu$ L solution of enzyme loaded stomatocytes (10 mg mL<sup>-1</sup>) while stirring. In the case of NAL samples, the cross-linking reaction was quenched with 1mL of sodium phosphate buffer (1M, pH = 7.5) solution, and in the case of 7 $\alpha$ -HSDH and 7 $\beta$ -HSDH, the reaction was quenched with 1mL of PKi (50 mM pH = 8). To remove the excess of buffer and cross-linker glutaraldehyde, all resulting c-CLEnAs were concentrated via spin filtration (15 mins, 13523 rcf) two times with Amicon 3 kDa filters and then were re-dispersed in sodium phosphate buffer (50 mM, pH = 7.4). In the case of 7 $\alpha$ -HSDH and 7 $\beta$ -HSDH, the c-CLEnA was re-dispersed in PKi (50mM pH = 8).

### 5.5.5. General procedure for the formation of compartmentalized cross-linked enzyme nano aggregates (c-CLEnA) with genipin

500  $\mu$ L of genipin solution (1wt%-1.6wt%-0.75wt%) was added to 500  $\mu$ L of stomatocyte sample (10 mg mL<sup>-1</sup>) in an Eppendorf tube. The solutions were kept for 24h at RT under gentle stirring.



The optimal procedure for NAL *c-CLEnA* formation, employed a dispersion of 500  $\mu\text{L}$  of NAL-stomatocytes ( $10 \text{ mg mL}^{-1}$ ) with a 14% loading efficiency (EE%) (corresponding to 1.4 mg of NAL encapsulated in 500  $\mu\text{L}$  sample, determined by Bradford), which was mixed with 500  $\mu\text{L}$  genipin 1wt%.

The optimal procedure for the formation of  $7\alpha$ -HSDH and  $7\beta$ -HSD- *c-CLEnAs* employed 500  $\mu\text{L}$  stomatocytes ( $10 \text{ mg mL}^{-1}$ ) with a 25% loading efficiency (2 mg of enzyme loaded in 500  $\mu\text{L}$  sample, determined by Bradford) of either  $7\alpha$ -HSDH or  $7\beta$ -HSDH, which were mixed with 500  $\mu\text{L}$  of genipin solution (1wt%). The co-encapsulated sample was prepared in the same way starting from 500  $\mu\text{L}$  of  $7\alpha/7\beta$ -HSDH stomatocytes ( $10 \text{ mg mL}^{-1}$ ) with a loading efficiency of 25% (2 mg total enzymes loaded in the 500  $\mu\text{L}$  sample, determined by Bradford).

After 24h genipin was removed from the solution, by using 10 kDa filters in a centrifuge at 12000 rpm for 15 min, the final concentration was adjusted to  $10 \text{ mg mL}^{-1}$  with sodium phosphate buffer for the NAL sample or with 50mM PKi buffer (pH 8) for the  $7\alpha$ -HSDH and  $7\beta$ -HSDH samples.

### 5.5.6. Quantification of enzyme loading

The Bradford assay was used to quantify the amount of enzyme loaded in the stomatocytes and in the *c-CLEnAs*. All the samples were treated with  $\text{CH}_2\text{Cl}_2$  to completely remove the polymeric membrane, which would alter the absorbance measured in the test. 150  $\mu\text{L}$  of enzyme loaded stomatocytes were mixed with 500  $\mu\text{L}$  of  $\text{CH}_2\text{Cl}_2$  for 30 mins. The final solution was then spin filtered with a centrifugal filter Unit 3 kDa (Millipore) to remove the organic solvent. The fraction collected was adjusted with buffer to the final volume of 150  $\mu\text{L}$ . The measurements were performed in triplicate using 50  $\mu\text{L}$  aliquots. For protein quantification, the Coomassie Plus (Bradford) assay kit was used (Pierce™) according to the manufacturer's instructions. In each cuvette both 1.5 mL of Coomassie reagent and 50  $\mu\text{L}$  of sample were added. Before measuring the absorbance at 595 nm, all samples and the standard solutions were incubated for 5 mins at room temperature and the spectrophotometer was calibrated with a cuvette containing a blank solution.

Using the protein concentrations that were measured, the encapsulation efficiency (E.E. %) was determined by considering the protein concentration in the initial feed solution.

$$\text{E.E. (\%)} = \frac{\text{Protein concentration measured with the Bradford assay (mg mL}^{-1}\text{)}}{\text{Lowest value of protein concentration used in the feed (mg mL}^{-1}\text{)}} \times 100$$

## References

- 1 M. P. Thompson, I. Peñafiel, S. C. Cosgrove and N. J. Turner, *Org. Process Res. Dev.*, 2019, 23, 9–18.
- 2 S. Budžaki, G. Miljić, S. Sundaram and V. Hessel, *Appl. Ener.* 2017, 201, 124–134.
- 3 M. Miyazaki and H. Maeda, *Trends Biotechnol.*, 2006, 24, 463–470.
- 4 L. Schober, S. Ratnam, Y. Yamashita, N. Adebar, M. Pieper, A. Berkessel, V. Hessel H. Gröger *Synthesis* (Germany), 2019, 51 (5), 1178–1184.
- 5 R. A. Sheldon and S. van Pelt, *Chem. Soc. Rev.*, 2013, 42, 6223–6235.

- 6 U. Hanefeld, *Chem. Soc. Rev.*, 2013, **42**, 6308.
- 7 J. Britton, S. Majumdar and G. A. Weiss, *Chem. Soc. Rev.*, 2018, **47**, 5891–5918.
- 8 D. M. Vriezema, P. M. L. Garcia, N. Sancho Oltra, N. S. Hatzakis, S. M. Kuiper, R. J. M. Nolte, A. E. Rowan and J. C. M. Van Hest, *Angew. Chem. Int. Ed.*, 2007, **46**, 7378–7382.
- 9 M. van Oers, F. Rutjes and J. van Hest, *Curr. Opin. Biotechnol.*, 2014, **28**, 10–16.
- 10 A. Küchler, M. Yoshimoto, S. Luginbühl, F. Mavelli and P. Walde, *Nat. Nanotechnol.*, 2016, **11**, 409–420.
- 11 M. T. De Martino, L. K. E. A. E. A. Abdelmohsen, F. P. J. T. J. T. Rutjes and J. C. M. M. van Hest, *Beilstein J. Org. Chem.*, 2018, **14**, 716–733.
- 12 M. T. De Martino, F. Tonin, N. A. Yewdall, M. Abdelghani, D. S. Williams, U. Hanefeld, F. P. J. T. Rutjes, L. K. E. A. Abdelmohsen and J. C. M. Van Hest, *Chem. Sci.*, 2020, **11**, 2765–2769.
- 13 C. Cui, H. Chen, B. Chen and T. Tan, *Appl. Biochem. Biotechnol.*, DOI:10.1007/s12010-016-2228-z.
- 14 Q. Ji, B. Wang, J. Tan, L. Zhu and L. Li, *Process Biochem.*, 2016, **51**, 1193–1203.
- 15 V. R. L. J. Bloemendal, S. J. Moons, J. J. A. Heming, M. Chayoua, O. Niesink, J. C. M. van Hest, T. J. Boltje and F. P. J. T. Rutjes, *Adv. Synth. Catal.*, DOI:10.1002/adsc.201900146.
- 16 X. Zhou, G. Yang and F. Guan, *Cells*, 2020, **9**, 273.
- 17 A. Bianco, M. Brufani, R. Ciabatti, C. Melchioni and V. Pasquali, *Mol. Online*, 1998, **2**, 129–136.
- 18 F. Tao, Y. Zhang, C. Ma and P. Xu, DOI:10.1038/srep00142.
- 19 M. I. García-García, A. Sola-Carvajal, G. Sánchez-Carrón, F. García-Carmona and Á. Sánchez-Ferrer, *Bioresour. Technol.*, 2011, **102**, 6186–6191.
- 20 J. Nahálka, A. Vikartovská and E. Hrabárová, *J. Biotechnol.*, 2008, **134**, 146–153.
- 21 M. I. García García, A. Sola Carvajal, F. García Carmona and Á. Sánchez Ferrer, *Process Biochem.*, 2014, **49**, 90–94.
- 22 V. R. L. J. L. J. Bloemendal, S. J. Moons, J. J. A. A. Heming, M. Chayoua, O. Niesink, J. C. M. van Hest, T. J. Boltje, F. P. J. T. J. T. Rutjes, J. C. M. van Hest, T. J. Boltje and F. P. J. T. J. T. Rutjes, *Adv. Synth. Catal.*, 2019, **361**, 2443–2447.
- 23 F. Tonin, L. G. Otten and I. W. C. E. Arends, *ChemSusChem*, 2019, **12**, 3192–3203.
- 24 J. L. Thistle, *Semin. Liver Dis.*, 1983, **3**, 146–156.
- 25 T. Ikegami and Y. Matsuzaki, *Hepatol. Res.*, 2008, **38**, 123–131.
- 26 F. Tonin and I. W. C. E. Arends, *Beilstein J. Org. Chem.*, 2018, **14**, 470–483.
- 27 O. Barbosa, C. Ortiz, Á. Berenguer-Murcia, R. Torres, R. C. Rodrigues and R. Fernandez-Lafuente, *RSC Adv.*, 2014, **4**, 1583–1600.
- 28 F. Tonin, L. G. Otten and I. W. C. E. Arends, *ChemSusChem*, 2019, **12**, 3192–3203.

## 5.6. Supplementary Figures and Tables

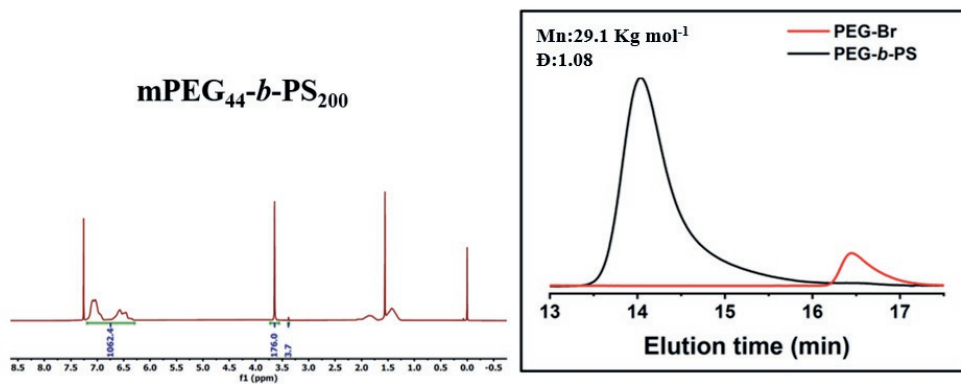


**Figure S1**— $^1\text{H-NMR}$  and GPC spectra of block copolymer ( $\text{PEG}_{44}\text{-}b\text{-PS}_{200}$ ) prepared by ATRP polymerization,  $M_n: 29.1 \text{ kg mol}^{-1}$  and  $\text{Đ}: 1.08$ .

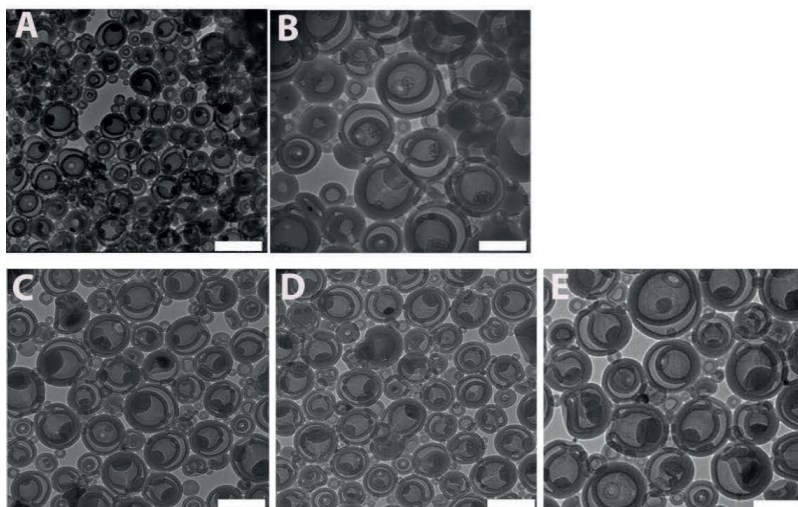


**Figure S2**—TEM pictures of (A-B): NAL-*c*-CLEnA formed with 1%wt of genipin. Scalebars are 500nm and 200nm respectively. (C-E) combined  $7\alpha\text{-HSDS}/7\beta\text{-HSDS}$  *c*-CLEnAs formed with 1%wt genipin. Scalebars are 500nm in C,D and 200nm in E.

**TableS1-** Optimisation of the formation of Neu5Ac using genipin cross-linked NAL-*c*-CLEnA in a microporous flow reactor. ME= Mixed Cellulose Ester; mPES= modified poly(ether sulfone). $t_R$  = residence time; <sup>a</sup> conversion toward Neu5Ac measured by <sup>1</sup>H NMR spectroscopy of the crude reaction mixture.

Entry	Flow ( $\mu\text{Lmin}^{-1}$ )	$t_R$ (min)	T ( $^{\circ}\text{C}$ )	Conversion (%) <sup>a</sup>	Membrane type
1	50	30	50	37	ME (0.1 $\mu\text{m}$ , 1.5 mL)
2	25	60	50	41	
3	100	15	35	35	
4	75	20	35	41	mPES (10kDa, 1.5 mL)
5	50	30	35	47	
6	40	37.5	35	52	
7	30	50	35	60	
8	20	75	35	69	
9	20	75	50	50	
10	50	30	60	48	
11	50	30	70	22	
12	60	75	35	13	mPES (10kDa, 4.5 mL)
13	60	75	45	10	
14	75	60	50	16	

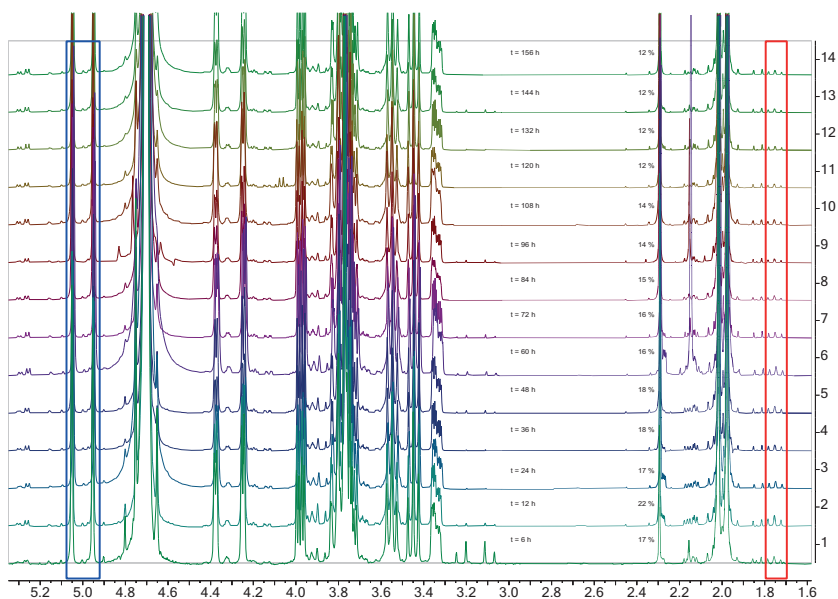


**Figure S3-** Stacked NMR plots of the continuous experiment described in Table S1. A gradual decrease in conversion of Neu5Ac is observed over time. Yields were determined using the integral sum of 5 distinct NMR signals: Blue box: H-1<sub>ax</sub> and H-1<sub>eq</sub> of *N*-acetyl-D-mannosamine. Red box: H-3<sub>ax</sub> of *N*-acetylneuraminic acid

**Table S2-** Specific activity of 7 $\alpha$ -HSDH and 7 $\beta$ -HSDH after cross-linking with different crosslinking agents. The initial activity of the purified enzymes was: 7 $\alpha$ -HSDH 432.8  $\pm$  18.5 U mg<sup>-1</sup>; 7 $\beta$ -HSDH 2.38  $\pm$  0.6. U mg<sup>-1</sup>. Results are averages of triplicate measurements performed on three different samples. Glutaraldehyde= GA; Genipin= GP.

[cross-linker]	7 $\alpha$ -HSDH <i>c</i> -CLEnA U mg <sup>-1</sup>	7 $\beta$ -HSDH <i>c</i> -CLEnA U mg <sup>-1</sup>
GP 1% wt.	382.66 $\pm$ 46.3	6.0 $\pm$ 1.4
GP 1.6 % wt	26.5 $\pm$ 2.2	nd
GP 0.75 % wt	16.8 $\pm$ 2.1	nd
GA 100mM	nd	nd

**Table S3-**One-pot conversion using different dilutions (x10, x100,x1000) of the combined *c*-CLEnAs and stomatocyte samples and different concentrations of NAD<sup>+</sup> (0.5 mM and 1mM). The conditions are given in 5.4.1.

7 $\alpha$ /7 $\beta$ -HSDH-stomatocytes 202.2 $\mu$ g/mL, 1 mM NAD <sup>+</sup>				7 $\alpha$ /7 $\beta$ -HSDH-stomatocytes 202.2 $\mu$ g/mL, 0.5 mM NAD <sup>+</sup>			
Time(min)	[hydroxysteroid] (mM)			Time(min)	[hydroxysteroid] (mM)		
	UDCA	7-oxo-LCA	CDCA		UDCA	7-oxo-LCA	CDCA
0	0.0	0.0	10.0	0	0.0	0.0	10.0
20	1.7	0.5	7.8	20	0.5	0.2	9.3
80	5.0	0.4	4.6	80	2.4	0.2	7.4
160	8.0	0.3	1.7	160	5.3	0.1	4.6
240	8.6	0.2	1.2	240	6.6	0.1	3.3
1440	9.0	0.3	0.7	1440	9.3	0.2	0.9

7 $\alpha$ /7 $\beta$ -HSDH-stomatocytes 20.2 $\mu$ g/mL, 1 mM NAD <sup>+</sup>				7 $\alpha$ /7 $\beta$ -HSDH-stomatocytes 20.2 $\mu$ g/mL, 0.5 mM NAD <sup>+</sup>			
Time(min)	[hydroxysteroid] (mM)			Time(min)	[hydroxysteroid] (mM)		
	UDCA	7-oxo-LCA	CDCA		UDCA	7-oxo-LCA	CDCA
0	0.0	0.0	10.0	0	0.0	0.0	10.0
20	0.1	0.5	9.4	20	0.0	0.1	9.8
80	0.4	0.4	9.2	80	0.1	0.1	9.8
160	0.9	0.4	8.7	160	0.3	0.1	9.6
240	1.4	0.4	8.2	240	0.5	0.1	9.4
1440	6.2	0.4	3.4	1440	2.8	0.2	7.0

7 $\alpha$ /7 $\beta$ -HSDH-stomatocytes

7 $\alpha$ /7 $\beta$ -HSDH-stomatocytes

Time(min)	2.0 µg/mL, 1 mM NAD <sup>+</sup>			Time(min)	2.0 µg/mL, 0.5 mM NAD <sup>+</sup>		
	[hydroxysteroid] (mM)				[hydroxysteroid] (mM)		
	UDCA	7-oxo-LCA	CDCA		UDCA	7-oxo-LCA	CDCA
0	0.0	0.0	10.0	0	0.0	0.0	10.0
20	0.0	0.4	9.6	20	0.0	0.1	9.9
80	0.0	0.4	9.6	80	0.0	0.1	9.9
160	0.0	0.3	9.7	160	0.0	0.1	9.9
240	0.0	0.4	9.5	240	0.1	0.2	9.7
1440	0.3	0.4	9.3	1440	0.1	0.1	9.8

7α/7β-HSDH-c-CLEnA				7α/7β-HSDH-c-CLEnA			
284.7 µg/mL, 1 mM NAD <sup>+</sup>				284.7 µg/mL, 0.5 mM NAD <sup>+</sup>			
Time(min)	[hydroxysteroid] (mM)			Time(min)	[hydroxysteroid] (mM)		
	UDCA	7-oxo-LCA	CDCA		UDCA	7-oxo-LCA	CDCA
0	0.0	0.0	10.0	0	0.0	0.0	10.0
20	2.4	0.4	7.1	20	0.5	0.1	9.4
80	5.7	0.5	3.9	80	2.8	0.2	7.0
160	8.1	0.4	1.5	160	4.8	0.2	5.0
240	8.7	0.4	1.0	240	5.7	0.2	4.2
1440	9.0	0.3	0.7	1440	9.3	0.1	0.7

7α/7β-HSDH-c-CLEnA				7α/7β-HSDH-c-CLEnA			
28.5 µg/mL, 1 mM NAD <sup>+</sup>				28.5 µg/mL, 0.5 mM NAD <sup>+</sup>			
Time(min)	[hydroxysteroid] (mM)			Time(min)	[hydroxysteroid] (mM)		
	UDCA	7-oxo-LCA	CDCA		UDCA	7-oxo-LCA	CDCA
0	0.0	0.0	10.0	0	0.0	0.0	10.0
20	0.1	0.4	9.5	20	0.1	0.2	9.8
80	0.4	0.4	9.2	80	0.1	0.2	9.7
160	1.2	0.4	8.4	160	0.4	0.1	9.5
240	1.7	0.4	7.8	240	0.6	0.1	9.3
1440	7.2	0.3	2.5	1440	3.5	0.1	6.4

7α/7β-HSDH-c-CLEnA				7α/7β-HSDH-c-CLEnA			
2.8 µg/mL, 1 mM NAD <sup>+</sup>				2.8 µg/mL, 0.5 mM NAD <sup>+</sup>			
Time(min)	[hydroxysteroid] (mM)			Time(min)	[hydroxysteroid] (mM)		
	UDCA	7-oxo-LCA	CDCA		UDCA	7-oxo-LCA	CDCA
0	0.0	0.0	10.0	0	0.0	0.0	10.0
20	0.0	0.4	9.6	20	0.0	0.1	9.9
80	0.0	0.0	10.0	80	0.0	0.1	9.9
160	0.0	0.4	9.6	160	0.0	0.1	9.9
240	0.1	0.4	9.6	240	0.0	0.2	9.8
1440	0.5	0.4	9.1	1440	0.1	0.1	9.8

7α-HSDSH-c-CLEnA + 7β-HSDH-c-CLEnA

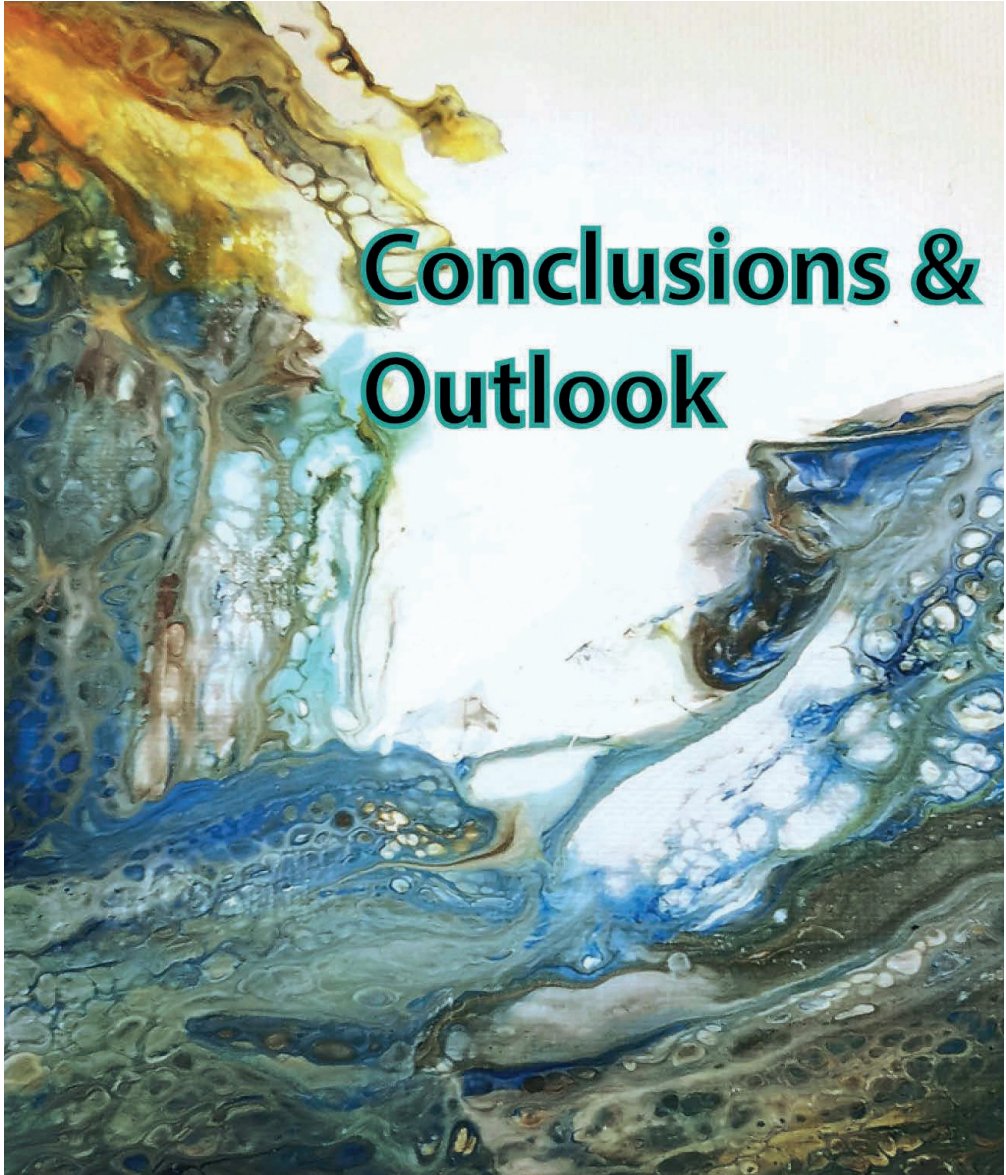
7α-HSDSH-c-CLEnA + 7β-HSDH-c-CLEnA

2.6 µg/mL and 133 µg/mL respectively, 1 mM NAD<sup>+</sup>

Time(min)	[hydroxysteroid] (mM)		
	UDCA	7-oxo-LCA	CDCA
0	0.0	0.0	10.0
60	4.0	0.4	5.6
120	5.4	0.4	4.2
200	6.2	0.3	3.5
1440	6.8	0.4	2.8

2.6 µg/mL and 133 µg/mL respectively, 0.5 mM NAD<sup>+</sup>

Time(min)	[hydroxysteroid] (mM)		
	UDCA	7-oxo-LCA	CDCA
0	0.0	0.0	10.0
60	0.9	0.1	8.9
120	1.1	0.2	8.7
200	1.4	0.1	8.5
1440	2.2	0.1	7.7





## Summary & Conclusions

Studying new immobilization strategies for metal and bio-catalysts is an interesting field of research where different branches of chemistry and engineering are integrated. Having the catalyst anchored to a support allows minimizing the time for workup operations and confers stability to the catalytic material, all parameters that are crucial for continuous flow processes. Polymeric nanoreactors have been explored over the years as effective catalytic carrier systems, which accommodate the catalytic species in a benign microenvironment. This not only enables catalysis in more environmentally friendly conditions, but also enhances an easier separation and faster recovery of the catalytic materials compared to many traditional strategies developed. We hypothesized that compartmentalizing the catalyst into polymeric vesicles based on PEG-*b*-PS block copolymers would significantly improve flow processes by 1) reducing the mass transfer limitations and the formation of gradients at different substrate concentrations, often experienced when using heterogeneous supports (resulting in better conversions); 2) minimizing the interactions between the catalyst and the external environment, especially important when side reactions compete in the selectivity of the desired product or when the catalyst can be poisoned by the surrounding species (resulting in higher yields of the desired product); and 3) due to their good mechanical stability, enabling faster recovery and recycling of the catalyst together with improved selectivity and conversion. These specific aspects would make these nanoreactors ideal candidates for supporting catalysts in flow setups. In this thesis we focused on two specific nanoreactor types, namely: catalyst-loaded membrane cross-linked polymersomes and bowl-shaped polymersomes loaded with crosslinked enzymes (*c*-CLEnAs), with the scope to enable cascade reactions in a ONE-FLOW fashion. As ONE-FLOW aims to perform multiple reactions in continuous way without intermediate work-up processes, the usage of nanoreactors to separate and compatibilize different catalytic species is of great importance.

In **Chapter I** an overview of the current most used catalyst compartmentalization methodologies involving polymeric platforms was provided. Four nanoreactor platforms and their properties were described, together with their application potential to allow catalysis to proceed in water rather than in organic solvents. From this review it was clear that this compartmentalization strategy was still underexplored in continuous flow applications. As such many opportunities can still be investigated for their usage in the ONE-FLOW concept.

**Chapter II** presents cross-linked polymersomes and micelles in which a Cu-bis-oxazoline catalyst complex was incorporated for usage in the asymmetric cyclopropanation of styrene with EDA. Previously, it was reported that the shielding of the Cu catalyst in the hydrophobic environment of a polymersome membrane allowed the reaction to proceed unperturbed even when water was used as medium. In this chapter a comparison was made between polymersomal and micellar immobilization platforms with respect to catalyst performance and stability. The reaction was performed both in water and a biphasic Pickering emulsion, with the nanoparticles as stabilizing agents. With regard to initial reaction rate and conversion no large differences were observed. However, in water the micellar system proved to have better colloidal stability, which allowed the reaction to continue to higher conversions. Regarding Cu leaching, the vesicular system was preferred in a continuous flow set-up.

**Chapter III** describes a ONE-FLOW approach for the multi-step synthesis of Rufinamide. Two compartmentalization strategies were combined, the first being a functional solvent system. With the help of computational solvent selection, acetonitrile was identified as reaction medium in which at elevated temperatures all reagents were in solution, while at room temperature the product selectively crystallized out. The second compartment were cross-linked polymersomes which accommodated a Cu(I) catalyst in their membrane for the execution of the second step. In this process, polymersomes not only functioned as catalytic nanoreactors but also allowed for catalyst recycling; After cooling down and separation of the crystallized product, the acetonitrile layer containing the polymersomes could be directly used in a second passage through the flow reactor. All passages yielded Rufinamide with high conversions. This chapter is a clear example of how the smart combination of different compartmentalization strategies can enhance a continuous process with industrial potential.

**Chapter IV** introduces a novel class of nanoreactors named *c-CLEnAs*. In previous research we showed that polymeric vesicles can be shape-changed in bowl-shaped structures (stomatocytes) with an internal cavity that is in direct contact with the outside environment. The cavity can be loaded during this process with enzymes. Although this system was proven to be catalytically active, upon prolonged usage enzymes leached out and the catalytic activity was diminished. To stabilize the nanoreactors and make them suitable for flow processes, the enzymes were crosslinked inside the cavity, thereby yielding compartmentalized crosslinked enzyme nano aggregates, or *c-CLEnAs*. *c-CLEnAs* showed to preserve their catalytic activity after 10 cycles in-flow with minimal leaching of bio-catalyst. The *c-CLEnA* preparation proved to be generally applicable and could also be used for the incorporation of two enzymes to realize a two-step cascade process.

In **Chapter V** the use of *c-CLEnAs* was extended to pharmaceutically more relevant processes. These entailed the in-flow aldol condensation to Neu5Ac and the batch two-step cascade reaction from CDCA to UDCA. For the former transformation *N*-acetylneuraminase lyase (NAL) was encapsulated and crosslinked in stomatocytes, while for the latter reaction the hydroxysteroid dehydrogenases 7 $\alpha$  HSDH and 7 $\beta$  HSDH were separately co-encapsulated to form *c-CLEnAs*. NAL-*c-CLEnAs* were active and stable under continuous operation for at least a week, showing only 30% of loss in their activity. The cascade was realized successfully using co-encapsulated nanoreactors, which resulted in superior yields compared to the use of two separated nanoreactors. Using these cross-linked polymersomes for in-flow processes allowed catalysis to be performed even in organic solvents without any sample instability issues. Key to efficient crosslinking was the use of the mild agent genipin which in all cases preserved the catalytic activity. The polymersome nanoreactors developed in this thesis can therefore be regarded as a useful tool for implementation in the ONE-FLOW concept as they protect and stabilize different catalytic species in either their lumen or membrane, which solves compatibility issues, facilitates catalyst recycling and prolongs their usage in a flow process.

## Outlook

In this thesis it has been demonstrated that nanoreactors can be successfully applied for industrially relevant conversions. Cross-linked polymersomes show good colloidal stability even at elevated temperatures and in organic solvents. It is to be expected that other catalysts than Cu can be incorporated in the membrane, to allow other types of reactions to be catalyzed. Although catalyst leaching is not severe, it cannot be ignored. For prolonged catalyst usage this issue should be solved. This can for example be done by using non-leachable catalysts, such as organocatalysts, as was shown before. It is worth to point out that recycling and reuse of Cu-cross-linked polymersomes was realized by using membrane systems, which are a greener alternative to the usual extraction methods in which large amount of solvents are needed, although they might be more expensive especially in large scale applications. Therefore, there are a number of considerations that have to be taken into account before actual implementation can be achieved. Two of the main challenges are the cost of the overall manufacturing process and the feasibility of large-scale production of the nanoreactors. Furthermore, the environmental impact of the use of nanoreactors as catalytic tools in chemistry should be addressed. Life Cycle Cost and Life Cycle Assessment are useful instruments in providing answers to these open questions. In a preliminary study we identified that the most expensive part of the *c-CLEnA* production process is the usage of filter systems for the purification of the nanoreactors. Other parameters that could be optimized to minimize costs are related to the preparation of the polymer building blocks.

The *c-CLEnA* nanoreactors until now have only been constructed from PEG-*b*-PS polymers. This is very useful for most catalytic applications. However, if one wants to extend the applicability to other fields, such as biomedicine, the composition should be altered to biodegradable components. These could be, in analogy with stomatocytes, PEG-pol(D,L-lactic acid) block copolymers. Furthermore, *c-CLEnAs* could not only be employed for catalytic transformations, their catalytic activity can also be explored for nanomotor applications. In previous research in our group, enzyme-loaded stomatocytes were already reported. The use of their asymmetric shape with the specific aperture, as well as the effective loading capacity with catalytic species make stomatocytes versatile nanomotor systems. In this thesis we have already shown *c-CLEnAs* to have superior performance compared to stomatocytes, regarding catalyst entrapment and stability. We therefore investigated if this feature could also be translated to nanomotors. For this purpose, we constructed catalase-*c-CLEnAs*. Catalase is a well-known enzyme in the nanomotor field, as it effectively converts hydrogen peroxide into oxygen. The oxygen formed can propel the particles either via bubble formation at higher concentrations, or via self-diffusiophoresis. Motion performance of catalase-*c-CLEnAs* was measured with nanoparticle-tracking analysis (NTA) under real-time conditions by determining their mean square displacement (MSD), and compared to the motion of catalase-stomatocytes (Figure- A). Directional motion was observed which showed a linear relationship with the concentration of hydrogen peroxide (Figure- B,C).

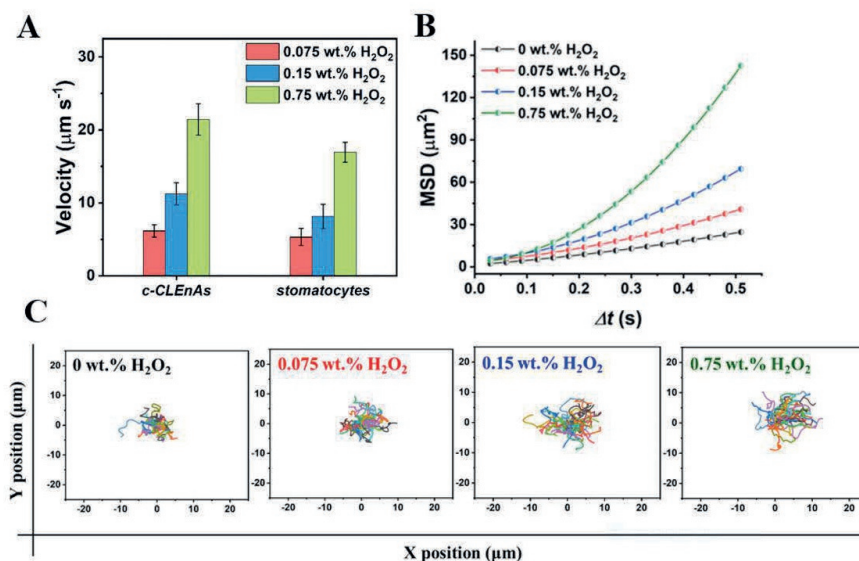


**Figure- A)** Average speed of catalase-*c*-CLEnAs and uncrosslinked catalase-stomatocytes **B)** Mean square displacement (MSD) and velocity of *c*-CLEnAs in presence of  $\text{H}_2\text{O}_2$  with a range of concentrations (0 wt.%  $\text{H}_2\text{O}_2$ , 0.15 wt.%  $\text{H}_2\text{O}_2$ , and 0.75 wt.%  $\text{H}_2\text{O}_2$ .) **C)** Motion trajectory of *c*-CLEnAs as a function of  $\text{H}_2\text{O}_2$  concentration.

This preliminary investigation shows that *c*-CLEnA nanomotors can be effectively created and that their performance is at least equal to regular stomatocytes. The improved stability still needs to be investigated. However, it is to be expected that *c*-CLEnA nanomotors will retain enzymes more effectively, even when structures are used with wider necks and when multiple enzymes are combined to install motile behavior.

## List of Symbols and Abbreviations

**E-factor:** Environmental Factor  
**CMC:** Critical Micellar Concentration  
**p:** Packing parameter:  
 **$a_0$ :** Area of the head groups  
 **$l_c$ :** Length of the hydrophobic chain  
 **$\rho$ :** Shape factor  
 **$R_g$ :** Radius of gyration  
 **$R_h$ :** Hydrodynamic radius  
 **$V_{\text{hydrophobic}}$ :** Hydrophobic Volume  
 **$S_{\text{hydrophobic}}$ :** Hydrophobic Surface Area  
 **$M_n$ :** polymer molecular weight  
 **$\mathcal{D}$ :** polymer polydispersity index  
 **$\varphi^o$ :** Volumetric oil fraction  
**E.E. %:** Encapsulation Efficiency (%)  
**EF:** Effective Length (cm)  
**TL:** Total Length (cm)  
**O/W:** oil in water emulsion  
**W/O:** water in oil emulsion  
**LCST:** Lower Critical Solution Temperature  
**RAFT:** Reversible Addition Fragmentation chain Transfer polymerization  
**ATRP:** Atomic Transfer Radical Polymerization  
**ROP:** Ring Opening Polymerization  
**CuAAC:** Cu-catalyzed azide-alkyne cycloaddition  
**TPGS-750-M:** dl- $\alpha$ -tocopherol methoxypolyethylene glycol succinate  
**PTS:** Polyoxyethanyl  $\alpha$ -tocopheryl sebacate  
**DPEphos:** Bis[[2-diphenylphosphino)phenyl] ether DPEphos  
**TMEDA:** Tetramethyl ethylene diamine  
**SCS:** Sulfur-Carbon-Sulfur  
**TRITC:** Tetramethylrhodamine Isothiocyanate  
**Cy3:** Cyanine 3 Alkyne  
**CaIB:** *Candida Antarctica* lipase B  
**GOx:** Glucose oxidase  
**HRP:** Horseradish peroxidase  
**PLE:** Porcine Liver Esterase  
**Myo:** Myoglobin  
**DSN:** Dendrimer-Stabilized Nanoparticles  
**PAA:** Poly(acrylic acid)  
**PEG-*b*-PS:** Poly(ethylene glycol)-*b*-polystyrene  
**PEG-*b*-P(S-4-VBC):** Poly(ethylene glycol)-*b*-poly(styrene-4-vinylbenzylchloride)  
**PEG-*b*-P(S-4-VBA):** Poly(ethylene glycol)-*b*-poly(styrene-4-vinylbenzylazide)  
**PS-*b*-PIAT:** Polystyrene-*b*-polyisocyanopeptide  
**PNIPAM-*b*-PEO:** Poly(N-isopropylacrylamide) –*b*-poly(ethylene oxide)  
**PDEAEM:** Poly(diethyl aminoethyl methacrylate)

**PDMIBM:** Poly(3,4-dimethyl maleic imido butyl methacrylate)

**PAMAM:** Polyamidoamine

**PNIPAM:** Poly(*N*-isopropylacrylamide)

**PVCL:** Poly(*N*-vinylcaprolactam)

**PNIPAM:** Poly (*N*-isopropylacrylamide)

**Poly(AAm-co-AAc):** poly(acrylamide-co-acryl acid)

**PMDETA:** N,N,N',N'',N''-Pentamethyldiethylenetriamine

**CDCA:** Chenodeoxycholic acid

**UDCA:** Ursodeoxycholic acid

**CLEA:** Cross-linked enzyme aggregates

**c-CLEnA:** *Compartmentalized*- cross-linked- enzymes *nano*-aggregate

**BOX:** (4*S*,4'*S*)-2,2'-(Hepta-1,6-diyne-4,4-diyl)bis(4-phenyl-4,5-dihydrooxazole); bisoxazoline

**Cu(I)-BOX:** [(4*S*,4'*S*)-2,2'-(hepta-1,6-diyne-4,4-diyl)bis(4-phenyl-4,5-dihydrooxazole)]-copper(I)iodide; Cu(I) bis(oxazoline)

**Cu(I)-PLs:** Cu(I)-bis(oxazoline) cross-linked polymersomes

**Cu-BOX:** [(4*S*,4'*S*)-2,2'-(hepta-1,6-diyne-4,4-diyl)bis(4-phenyl-4,5-dihydrooxazole)]-copper(II) triflate

**THF:** Tetrahydrofuran

**ACN:** Acetonitrile

**DMSO:** Dimethylsulfoxide

**DCM:** Dichloromethane

**EDA:** Ethyldiazoacetate

**<sup>1</sup>H-NMR:** Proton nuclear magnetic resonance spectroscopy

**GPC:** Gel permeation chromatography

**FTIR:** Fourier transform infrared

**TEM:** Transmission Electron Microscopy

**SEM:** Scanning Electron Microscopy

**DLS:** Dynamic Light Scattering

**XPS:** X-Ray Photoelectron Spectroscopy

**ICP-MS:** Inductively Coupled Plasma Mass-Spectroscopy

**AF4-LS:** Asymmetric flow field flow fractionation – light scattering

**NTA:** Nanoparticle Tracking Analysis

**SDS-PAGE:** Sodium Dodecyl Sulphate - PolyAcrylamide Gel Electrophoresis

# Curriculum Vitae

M. Teresa received her BSc. and her MSc. in Science and Technology of Industrial Chemistry, working in the Naples Industrial Chemistry Laboratories (NICL) at the University of Napoli Federico II (Naples, Italy). Her BSc. in 2012 was obtained with a project in collaboration with Conser SPA named "Side Reactions Investigation HPPO Process: Kinetic Studies for the Hydrogen Peroxide decomposition and Methylformate formation". While in 2014 she finished her master project entitled "Synthesis and Characterization of heterogeneous catalyst Niobium based for 5-HMF formation". In January 2015 she moved to Eindhoven where she started working in the Chemical Reactor Engineering laboratories of TU/e on "open-microstructured random packing in Gas-Liquid-Solid catalytic reactor for Fischer-Tropsch Synthesis", this project was part of the MCEC (the Netherlands Center for Multiscale Catalytic Energy Conversion).

In 2017, she started her PhD in the Bio-Organic Chemistry Group of TU/e as part of ONE-FLOW project.

During her PhD she experienced the teaching for the OGO Molecules & Materials and coaching in 2019 for the ICMS industrial challenge (in collaboration with Sabic).

Her PhD project turned into several collaborations with TU/e Delft, Radboud University, and University of Hull (UK). The main achievements of her research are summarized in this thesis. Since March 2021 she is employed in Elstar Dynamics as R&D Chemical Engineer.

# List of publications

- **M.T. De Martino** et al. "Nanoreactors for green catalysis". *Beilstein J. Org. Chem.* **2018**, *14*, 716–733. [doi:10.3762/bjoc.14.61](https://doi.org/10.3762/bjoc.14.61)
- J. Passaro, P. Russo, A. Bifulco, **M.T. De Martino** et al. "Water Resistant Self-Extinguishing Low Frequency Soundproofing Polyvinylpyrrolidone Based Electrospun Blankets". *Polymers*, **2019**, *11*(7), 1205, [doi.org/10.3390/polym11071205](https://doi.org/10.3390/polym11071205)
- **M.T. De Martino** et al. "Compartmentalized cross-linked enzymatic nano-aggregates (c-CLEnA) for efficient in-flow biocatalysis" *Chem. Sci.*, **2020**, *11*, 2765-2769. <https://doi.org/10.1039/C9SC05420K>
- Nicosia, F. Vento, G. Marletta, G.M.L. Messina, C. Satriano, V. Villani, N. Micali, **M.T. De Martino** et al., "Supramolecular Flags in the Thermal Gradients' Wind: Correlation Between Aggregates Features and Thermal-Induced Symmetry Breaking" **(Manuscript Submitted)**
- C. Zhang (\*), **M. T. De Martino**(\*) et.al., "Designed ONE-FLOW System for the Synthesis of Rufinamide". **(Manuscript Submitted)**
- **M. T. De Martino** (\*), Fabio Tonin (\*) V. R.L.J. Bloemendal (\*) et al., " Extending the scope of compartmentalized cross-linked enzyme nano aggregates (c-CLEnAs) toward pharmaceutically relevant transformations" **(Manuscript Submitted)**
- O. M. Morales-Gonzalez, **M. T. De Martino** et al., *Techno-economic Analysis of Compartmentalized Cross-linked Enzymatic nano-Aggregates (c-CLEnA)* **(Manuscript in preparation)**
- J. Shao, **M.T. De Martino** et al., *Biomimetic Micro-and Nano swimmers: working together via Enzymatic cascade* **(Manuscript in preparation)**
- S. Cao, J. Shao, S. Song, **M.T. De Martino** et. al, "Photoactivated Nanomotors via Aggregation Induced Emission for enhanced Phototherapy". **(Manuscript Accepted in Nat. Comm.)**
- S. Cao, J. Shao, **M.T. De Martino** et al., "Engineering Asymmetrical Biodegradable Fluorescent Polymersomes with Aggregation-Induced Emission". **(Manuscript Submitted)**



## Acknowledgments

More than six years have passed since the first day I started my journey in TU/e.

I would like to express my gratitude to Prof. Jan van Hest for his supervision and support during these four years of PhD and for giving me the opportunity to be part of the Bio-Organic Chemistry group. Many thanks to dr. Loai Abdelmohsen for his constant help and his encouraging enthusiasm which guided me through my work. Thank you Marjo for your sweetness and patience, and thanks to all the colleagues of the van Hest's group for the nice and friendly environment, especially thanks to the people in Lab 6 for tolerating my panic attacks and my "abuse" of glassware. Thanks to Mona, Amy, Imke, Pascal, Shoupeng, Jingxin, Chenyue, many thanks to Alex&Chiara miei compatrioti, and to my officemates and all the people that have been helping me in my work. Thanks to Bastiaan, Hailong and Joost Opsteen for the guidance in the lab during my first months in the group, your kindness and knowledge helped me to find my own path for the rest of my PhD research.

Thanks to the SMG group for letting me use the EMs (also as a hobby in my weekends), I became very passionate about SEM and TEM; thanks to Rick, Paul and Ingeborg.

I am very grateful to Prof. John van der Schaaf and dr. Fernanda Neira D'Angelo for all the things I have learned from them and for the nice time together in Grenoble and at the ICOSCAR conference in San Sebastian. Thanks to all the people in the SCR group for the great two years I spent there. Many thanks to Shamayita, Akaterini, Smitha, Elnaz I hope we are going to see each other soon again. Thanks to Carlo Bruijs, Marlies Coolen and Eric Herk I have learned so many things from you and I will never forget that amazing feeling to have my first reactor setup up and running thanks to our work together.

Thanks to the people of the NIOK school 2015, to prof. Johan Padding and all the friends from MCEC.

Thanks to my colleagues and friends in Helix. **Pia**... friend, colleague, and neighbor. Thanks for the constant presence in my life even now from the UK you painted my thesis cover, you sent me cookies... and it still feels like when you were living just next door. **Jasper** my very first Dutch friend and officemate... time really runs fast... I remember those happy days in office, singing and playing videogames while matlab was doing the rest of the job, often sharing frustration when the code was not right. All the jokes you made about me and my accent...especially when I try to spell names of some Dutch city. **Amin**, **Maurilio** and **Alejo** thanks for the funny moments and for always finding the time for a cigarette and a walk. Thanks for the beautiful time at NCCC, also to **Fabio Tonin** amico and co-author, grazie per gli esperimenti insieme a Delft e per i bei momenti durante i ONE-FLOW meetings. A special thought goes to **Victor** my ONE-FLOW team-mate, we started the PhD together and I have enjoyed so much working with you, talking with you, your positive attitude and encouraging words when things were not working as we were hoping, thank you for always having faith in our science and I wish you all the best for your future. Thanks to **Dario Balice**, friends since the bachelor in Naples and later in the PhD in TU/e.

My years in Eindhoven would not have been the same without **Carmine**, **Daniela**, **Alberto** since 2015 I never walked alone, thank you for your constant presence in my life, for our adventures, for the binladone, for the carnivals; you are the best. Madam, Bibi also from distance you are always part of the game and the concilium. Carmine, il mio

paraninfo, quante ne abbiamo passate... finalmente siamo alla fine del tunnel, e soprattutto siamo sopravvissuti ai nostri 30 anni. **Luca, Morena, Ema, Zandra, Pasquale, Humberto, Gianluca, Gianmarco, Fernando, Federica, Paolotto, Nacho, Antonio** (my favorite), you gave me so much since I met you that I would never be able to compensate... thank you for your love and for the happy moments with me. **Oscar, Alok, Nrupa, Janly, Raj, Alessia S., Marianna, Tommaso, Alice, Rishi, Tarek, Marta, Christian, Davide, Demetrio, Simone, Matias** thank you for sharing this journey with me and for the support and fun moments, for the parties, the science, the karaoke, the poetry, the dreams and for being my friends. **Maria e Sasa** grazie per il tempo insieme, per riportarmi con la mente in Italia al mare, per il cibo buono, e per l'affetto dimostrato da quando vi conosco, e grazie anche al resto del gruppo per i bei momenti assieme.

Thanks to all the people I have met in Eindhoven, the random people in the bars, the Irish fellows, the Americans, the Latinos, the Greeks, the Mexicans.

Grazie ai miei amici in Italia, **Ester e Jessica** per credere in me ed essere le mie supporters da sempre. Non sarei la persona che sono oggi se non avessi amiche come voi e non vi ringrazierò mai abbastanza.

Thanks to **Francesco** for his love and patience, ASML and I would be lost without you.

Thanks to my **mom**, her dedication to work, her love for the knowledge, her passion for teaching and studying guided me since always and were inspiring for me through all my life. I hope I can make her proud of me every day. You are the light in all my days. Sei la cosa più bella del mondo.

Thanks to my **brother**, I cannot find the words to express how I feel about him and everything he has done for me. He is my rock, my safe castle, my best friend. I will never compensate enough for all the things he has been giving me since I was born. Non ce l'avrei mai fatta senza te.





